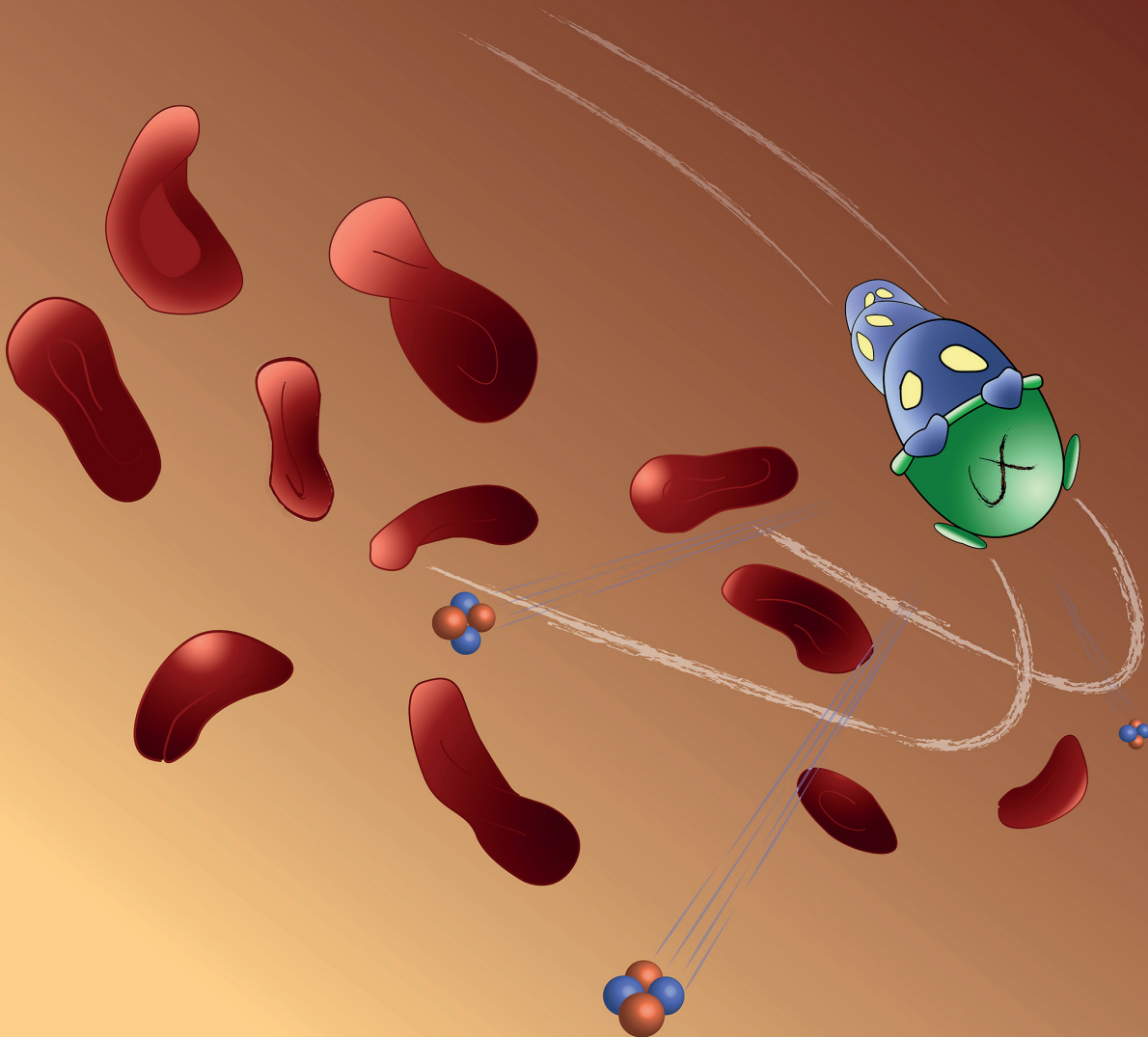


^{213}Bi -DOTATATE for Targeted Alpha Therapy in Neuroendocrine Tumours



Ho Sze Chan

**²¹³Bi-DOTATATE FOR TARGETED ALPHA THERAPY
IN NEUROENDOCRINE TUMOURS**

Ho Sze Chan

© Ho Sze Chan 2017

All rights reserved. No parts of this thesis may be reproduced, stored in retrieval system or transmitted in any form or by means, without prior written permission of the author, or when appropriate, of the publishers of the publications included in this thesis.

ISBN: 978-94-6299-742-4

Lay-out by: Ridderprint BV, Ridderkerk, the Netherlands

Cover by: Stuart Koelewijn

Printed by: Ridderprint BV, Ridderkerk, the Netherlands

**²¹³Bi-DOTATATE for Targeted Alpha Therapy in Neuroendocrine
Tumours**

²¹³Bi-DOTATATE voor doelgerichte alfa-therapie voor neuroendocriene tumoren

Proefschrift

ter verkrijgen van de graad van doctor
aan de Erasmus Universiteit Rotterdam

op gezag van rector magnificus
Prof.dr. H.A.P. Pols
en volgens besluit van College voor Promoties.

De openbare verdediging zal plaatsvinden op
dinsdag 31 oktober 2017 om 11:30 uur

door
Ho Sze Chan
geboren te Hong Kong

Promotiecommissie

Promotor: Prof.dr.ir. M. de Jong

Overige leden: Prof.dr. J.F. Verzijlbergen
Prof.dr. J.P. Norenberg
Prof.dr. P.M. van Hagen

Copromotoren: Dr. W.A.P. Breeman
Dr. M.W. Konijnenberg

TABLE OF CONTENTS

Chapter 1	General introduction	7
Chapter 2	Optimizing labelling conditions of ^{213}Bi -DOTATATE for preclinical applications of peptide receptor targeted alpha therapy <i>EJNMMI Radiopharmacy and Chemistry. 2016; 1:9</i>	31
Chapter 3	Improved safety and efficacy of ^{213}Bi -DOTATATE-targeted alpha therapy of somatostatin receptor-expressing neuroendocrine tumors in mice pre-treated with L-lysine <i>EJNMMI Research. 2016; 6:83</i>	49
Chapter 4	Influence of tumour size on the efficacy of targeted alpha therapy with ^{213}Bi -DOTATATE <i>EJNMMI Research. 2016; 6(1):6</i>	73
Chapter 5	<i>In vitro</i> comparison of ^{213}Bi - and ^{177}Lu -radiation for peptide receptor radionuclide therapy <i>PLoS One. 2017;12(7)</i>	95
Chapter 6	Utilizing high-energy gamma photons for high-resolution ^{213}Bi SPECT in mice <i>JNM. 2016; 57,3, 486–492</i>	115
	Summary and Concluding Remarks, Samenvatting	135
	List of publications	145
	PhD portfolio	147
	Acknowledgements	149
	Curriculum vitae	153

1

Chapter 1

General Introduction

GENERAL INTRODUCTION

α -Particles can be used to deliver a highly efficacious targeted therapy of (metastasized) cancer with an α -emitting radionuclide stably labelled to a cancer-specific targeting ligand. Such ligands like somatostatin-derived peptides have a proven track record of stable labelling with γ -ray and β -particle emitting radionuclides for diagnostic and therapeutic applications in patients with neuroendocrine tumours (NETs), respectively. Stabilized somatostatin-based peptides with radiometal-bifunctional chelators form ideal experimental model systems to test aspects of radiochemistry, *in vitro* cell irradiation and *in vivo* therapy using α -emitter labelled peptides.

NEUROENDOCRINE TUMOURS AND SOMATOSTATIN ANALOGUES

The neuroendocrine system produces hormones e.g. somatostatin and dopamine, which are released in the bloodstream to regulate body functions. Tumour cells originating from this system often (over)express somatostatin receptors to which the peptide somatostatin can bind with high, i.e. nanomolar, affinity. Native somatostatin consists in two forms, one containing 14 amino acids (somatostatin-14) and the other 28 amino acids (somatostatin-28). Both target somatostatin receptors (SSTRs) through specific receptor-mediated processes [1]. Five subtypes of SSTRs are known; SSTR₁, SSTR₂, SSTR₃, SSTR₄ and SSTR₅ [2]. Upon binding to the receptor, receptor agonistic somatostatin analogues inhibit the secretion of a wide range of hormones from the neuroendocrine system [3, 4]. Somatostatin can also inhibit proliferation of tumour cells that overexpress SSTRs, including various NETs. Several studies have been performed to evaluate the inhibition of NET growth by native somatostatin, but unfortunately the results obtained were not promising [5–7]. One of the reasons was believed to be the poor biological stability of native somatostatin after release into the bloodstream, due to rapid enzymatic degradation (within 2–3 minutes) [8, 9]. Therefore, stabilized somatostatin analogues, such as octreotide, have been developed with shortened peptide length and the introduction of D-amino acids. Radiolabelled somatostatin analogues have become very attractive for visualization of NETs. ¹²³I-Tyr³-octreotide was the first radioactive somatostatin analog developed for *in vivo* imaging [10–12]. Tumour lesions could be visualized with this radioactive somatostatin analog, however, the radiolabelled analog was not stable due to dehalogenation of ¹²³I-Tyr³ causing undesired uptake in thyroid and gastro-intestinal tract. Therefore, alternative methods have been explored to increase the stability of radioactive somatostatin analogues.

CHELATORS AND CHOICE OF RADIONUCLIDES

Chelators can bind metals through ionic interaction and are attractive for labelling of radiometals. Somatostatin analogues can be radiolabelled with clinically attractive radiometals via bifunctional chelators, such as DTPA (diethylenetriaminepentaacetic acid), DOTA (1,4,7,10-tetraazacyclododecane-1,4,7,10-tetraacetic acid), CHX-A''DTPA [(R)-2-Amino-3-(p-isothiocyanatophenyl)propyl]-trans-(S,S)-cyclohexane-1,2-diamine-pentaacetic acid) and NOTA (1,4,7-triazacyclononane-N,N',N''-triacetic acid) [13], see Fig. 1. The choice of radionuclides depends on physical and biochemical characteristics and the effective half-life. The physical characteristics include the physical half-life with an attractive half-life between 6h-7d [14], type of emission, energy of the radiation and decay chain. Biochemical characteristics include the pharmacokinetics within the patient, *in vivo* stability, efficacy and toxicity [13, 15, 16]. The effective half-life is considered to be the most important factor. The effective half-life is the net half-life derived from both the physical half-life

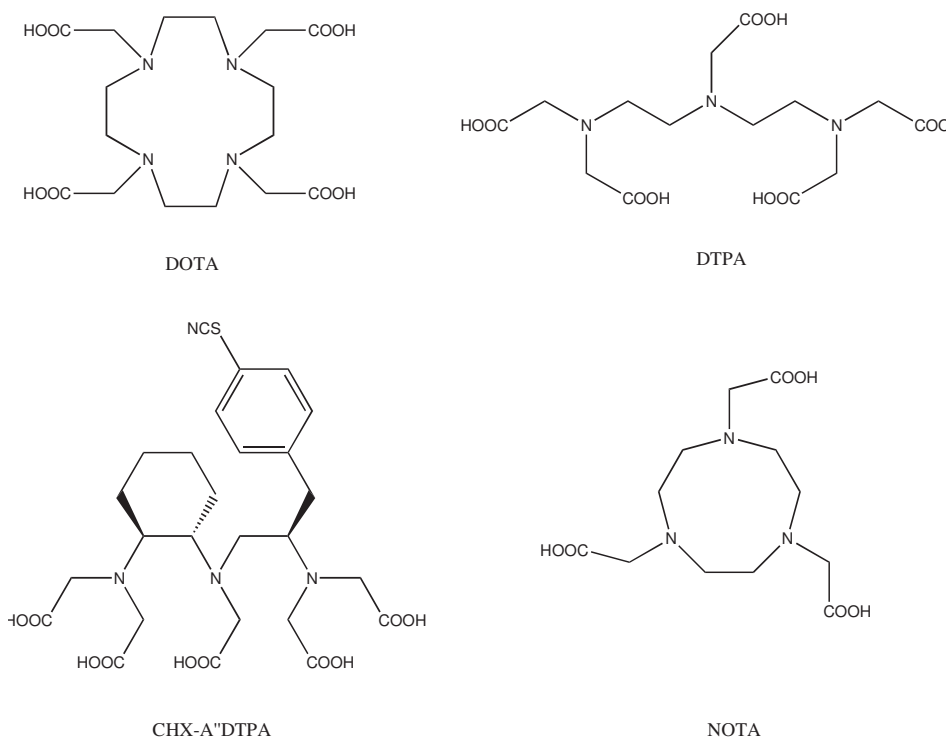


Figure 1, Chelators used in targeted radionuclide therapy with radiometals, DOTA = 1,4,7,10-tetraazacyclododecane-1,4,7,10-tetraacetic acid, CHX-A''DTPA=[(R)-2-Amino-3-(p-isothiocyanatophenyl)propyl]-trans-(S,S)-cyclohexane-1,2-diamine-pentaacetic acid, DTPA= diethylenetriaminepentaacetic acid and NOTA = 1,4,7-triazacyclononane-N,N',N''-triacetic acid.

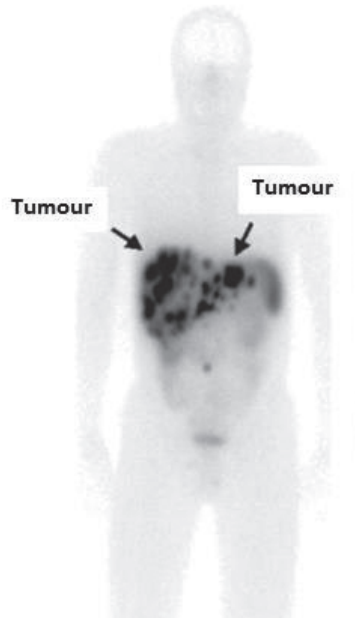


Figure 2, SPECT imaging in a patient after injection with ^{111}In -DTPA-DPhe¹-octreotide (Octreoscan[®]). Dark spots indicate accumulation of radioactivity.

and the biological half-life of the radionuclide within a patient's body or organs [16]. Other important parameters related to the choice of radionuclide are availability, production and the chemical properties to bind to a biofunctional ligand [15, 16].

After successful modification and *in vivo* stabilization of somatostatin analogues, the concept to use radiolabelled somatostatin analogues, e.g. DTPA-DPhe¹octreotide, DOTA-Tyr³-octreotide (DOTATOC) or DOTA-Tyr³-octreotate (DOTATATE) radiolabelled with ^{111}In to visualize NETs *in vivo*, was born and introduced as peptide receptor scintigraphy (PRS). Since then, ^{111}In -DTPA-DPhe¹-octreotide (Octreoscan[®]) has been routinely applied in the clinical setting as a diagnostic tool in patients with NETs and their metastases with SSTR₂ expression, see Fig. 2. Nowadays ^{68}Ga -DOTATATE is considered to be a better diagnostic radiolabelled peptide than Octreoscan[®], since the consensus is that ^{68}Ga -DOTATATE offers diagnostic images with greater sensitivity and specificity [17, 18], although evidence in large multi-centre trials is missing.

PEPTIDE RECEPTOR SCINTIGRAPHY AND PEPTIDE RECEPTOR RADIONUCLIDE THERAPY (PRRT)

PRS applies radiolabelled peptides to visualize and localize tumour lesions with Positron Emission Tomography (PET) or Single Photon Emission Computed Tomography (SPECT) techniques. Besides visualization and localization in combination with Computed Tomography (CT), PET and SPECT imaging can provide information on tumour staging. Based on the characteristics of the radionuclide, PET or SPECT can be applied.

Radionuclides for imaging

SPECT cameras can measure γ -rays emitted by radionuclides. A collimator is placed in front of the scintillation crystal and only γ -rays traversing through the holes of the collimator can reach the scintillation crystal. Collimators are generally made of tungsten or lead. Several collimators are available: low-, medium- or high-energy and high-resolution, all-purpose and high-sensitivity, each with a specific thickness, hole shape, hole diameter and septal thickness. The resolution obtained depends on the size of the holes in the collimator used. Through several reconstruction algorithms, a three-dimensional image can be obtained via a series of two-dimensional projections images obtained from SPECT. Most commonly used radionuclides for SPECT are ^{111}In (half-life = 2.8 days) and $^{99\text{m}}\text{Tc}$ ($T_{1/2}$ = 6.0 hours). Table 1 lists other commonly used radionuclides for SPECT imaging. SPECT cameras for clinical applications mostly use parallel collimators and preclinical applications pinhole collimators. Pinhole collimators allow high magnification to achieve submillimeter resolution [19].

The concept of PET is similar to that of SPECT, but one of the major differences being that for PET β^+ (positron)-emitting radionuclides are applied. Commonly applied radionuclides are ^{18}F (half-life = 109.8 min), ^{68}Ga (half-life = 67.7 min), and ^{11}C (half-life = 20.3 min).

Table 1, Physical characteristics of commonly applied radionuclides for SPECT

Radionuclide	Half-life	Decay mode (%)	E_{np} (keV)	E_{γ} (keV)	Abundance (%)	Production
^{123}I	13.3 h	ϵ (100%)	Auger L (3.2)	159.0	83.3	Cyclotron
			Auger K (22.7)	529.0	1.4	
			CE-K (127.2)			
^{111}In	2.8 d	ϵ (100%)	Auger L (2.3)	171.3	90.7	Cyclotron
			Auger K (19.3)	245.4	94.1	
			CE-K (144.6)			
			CE-K (218.6)			
$^{99\text{m}}\text{Tc}$	6.0 h	β^- (0.004)	Auger L (2.2)	140.5	89.1	$^{99}\text{Mo}/^{99\text{m}}\text{Tc}$ Generator
		IT (99.9963)	CE-K (1.6)			

d=days, h=hours, ϵ =electron capture, IT=internal transmission, E_{np} = energy of neutron converts to proton, E_{γ} = γ energy

Table 2, Physical characteristics of commonly applied radionuclides for PET

Radionuclide	Half-life	Decay mode (%)	E_{β^+} (keV)	Abundance (%)	Production
^{11}C	20.4 m	β^+	385.6	99.8	Cyclotron
^{13}N	10.0 m	β^+	491.8	99.8	Cyclotron
^{15}O	2.0 m	β^+	735.3	99.9	Cyclotron
^{18}F	109.8 m	β^+	249.8	96.7	Cyclotron
^{64}Cu	12.7 h	ε (61.5%) β^+ (17.6%) β^- (38.5%)	278.2	17.4	Reactor or Cyclotron
^{68}Ga	67.7 m	ε (10%) β^+ (90%)	836.0	88.9	$^{68}\text{Ge}/^{68}\text{Ga}$ Generator

m=minutes, h=hours, ε =electron capture, E_{β^+} = mean β^+ energy

These radionuclides can be covalently bound or linked via a bifunctional chelator to a pharmaceutical. β^+ -Emitters emit positrons, which collide with electrons and undergo annihilation. After annihilation, two γ -rays with energies of 511 keV will be emitted in opposite directions. PET camera detectors can detect both annihilation photons without a collimator and after mathematical processing and reconstruction, PET images can be generated. Due to the physical properties of the PET camera, PET can offer higher sensitivity and higher spatial resolution images than SPECT. Table 2 lists some commonly used radionuclides for PET imaging.

Radionuclides for therapy

PRRT uses the same targeting concept as PRS. Through a receptor-mediated process, the radiolabelled peptide can bind to receptors on tumour cells; this way radioactivity and consequently radiation exposure can be delivered to the cells. β^- -Emitters like ^{177}Lu and ^{90}Y are the most commonly used radionuclides for PRRT. These radionuclides are suitable candidates for therapy in large solid tumours rather than in small clusters of tumour and small metastases, due to their relative large penetration depth in tissue: 1–12 mm [20]. Radiation exposure by β^- -particles can eradicate tumour cells.

Development of next generation somatostatin analogues

In nuclear medicine, PRRT has been applied in patients with NETs since more than 25 years, mostly with ^{177}Lu -DOTA-Tyr³-octreotate (DOTATATE) or ^{90}Y -DOTA-Tyr³-octreotide (DOTATOC), both radiolabelled somatostatin analogs, see Fig. 3.

In most studies, applied in > 10.000 patients with NET, good clinical outcome with low toxicity and an improvement in quality of life was found in patients treated with PRRT [21, 22]. In a phase 3 study, ^{177}Lu -DOTATATE resulted in markedly longer progression-free survival in patients with well-differentiated, metastatic midgut NET. A progression-free

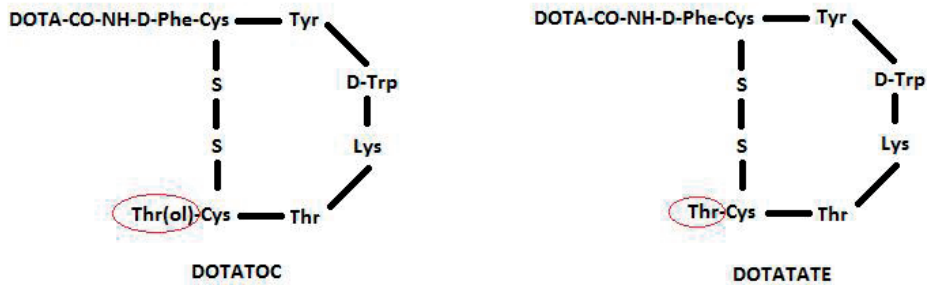


Figure 3, Chemical sequences of DOTATOC and DOTATATE, red circles indicating the chemical difference between DOTATOC and DOTATATE.

survival of 20 months was found compared to that in patients treated with high dose octreotide, with no evidence of renal toxicity during this time-frame [23]. However, complete remission of the disease, once metastasized, is still rare. Therefore continuation of the research aiming at safe and more powerful treatment for NET patients is still ongoing.

Linear Energy Transfer and relative biological effect

A promising approach radionuclide therapy is the use of exposure to particle radiation with high Linear Energy Transfer (LET), because of its high cytotoxic capabilities [24–26]. LET refers to the number of ionizations per unit of path length and is often expressed as keV/ μm . Particles with a LET > 100 keV/ μm are classified as high LET [27]. Absorbed dose and the induced biological effects are dependent on the LET-nature of the radiation, see Fig. 4.

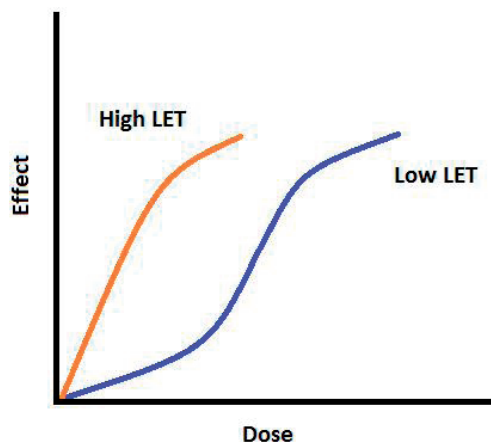


Figure 4, Principle of dose related effects of low and high LET, adapted from Strauma et al. [28]. LET= Linear energy transfer.

Dosimetry is an important tool to judge the probability of tumour reduction against the probability of normal organ toxicity after targeted radionuclide therapy. The MIRD formalism is a well-established method for calculating absorbed doses in normal organs and tumours for low-LET β^- and γ -emitters. The absorbed dose is the average absorbed energy in the target volume (normal organ or tumour) from radiation emitted from a source volume. α -Particles with their short path length and high LET might not be well represented by the average energy absorption assumption. A single α -particle track can lead to cell death when traversing the cell nucleus and its DNA, while the average absorbed dose to the cell is low. Single cell dosimetry should therefore be based on the micro-dosimetric approach (microdosimetry), taking into account the stochastic variation of energy deposition and probability of cell nucleus hits. Multi-cellular dosimetry can be based on the average absorbed energy macrodosimetry model with source and target equivalent, assuming that crossfire doses from source to other target volumes are limited and healthy tissue surrounding the target will not be affected. This approach is used to calculate the absorbed dose for β^- and γ -emitters, stochastic variation of energy deposition caused by short path length, inhomogeneous distribution and small size of target volume are neglected [29, 30]. The calculated absorbed dose can also be used to determine the relative biological effect (RBE). The relative biological effectiveness of radiation indicates the ratio of macroscopic absorbed doses for a certain type of ionizing radiation compared to a reference type of radiation, usually X-rays, both causing the same biological effect endpoint. Typical RBE-values of α -particles range from 3–7 in comparison to irradiation with photons or electrons at the same endpoint [30]. According to the International Commission on Radiological Protection (ICRP Publication 92), the current weighting factor is set to be 20 for α -particles and 1 for β -emitters, for late stochastic effects (cancer induction). The weighting factor is used to estimate the effective absorbed dose (in Sv, Sievert), which is related to the stochastic effect endpoint caused by different types of radiation [30, 31].

TARGETED ALPHA THERAPY (TAT)

α -Particle emitting radionuclides (α -emitters) emit high energy α -particles (positively double-charged helium nuclei) that have a higher LET compared to β -particles and γ -radiation. Typically energies of the α -particles emitted are in the range of 5–8 MeV. Due to these physical properties, α -particles show more potent cytotoxic effects than β -particles; α -particles cause more irreparable DNA clusters and double-strand breaks in cells than low LET radiation types [32]. The penetration depth in tissue of an α -particle is relatively short (50–100 μm). Therefore, α -particles are thought to be most suitable for treatment of small clusters of tumours and/or metastases. Inhomogeneous uptake of α -emitter labelled radio-

Table 3, Overview of the radioactivity characteristics of α versus β^- -radiation

Properties	α	β^-
Particle mass in (u)	4.00	5.49×10^{-4}
Penetration depth in tissues	50-100 μm	1–12 mm
LET (keV/ μm)	60-230	0.1–1.0
Ion pair/ μm	2000-7000	5-20
DNA hits cell kill	1-4	> 1000
Example	^{213}Bi , ^{225}Ac	^{177}Lu , ^{90}Y

pharmaceuticals in larger tumours may seriously jeopardize the therapeutic advantages. Table 3 shows typical physical characteristics of α -emitters versus β^- -emitters.

By linking α -emitters through covalent binding or through a bifunctional chelator to biologically functional molecules with a selectively binding ligand, α -emitters can reach their target; this process is defined as targeted alpha therapy (TAT). High LET α -particles might lead to severe damage of the DNA of tumour cells, leading to cell death.

The first introduction of α -emitters as candidates for clinical application as brachytherapy [33] or external therapy [34] dates back to the early 1900 [35]. The first phase I clinical study in patients with leukemia treated with ^{213}Bi -HuM195mAb as TAT dates back to 1997, patients treated with ^{213}Bi -HuM195mAb showed remarkable results [36], since then various (pre)clinical studies have been performed on the use of α -emitters, but also potential limitations for clinical application, including toxicity, have been investigated. ^{213}Bi Bismuth (^{213}Bi , half-life 46 min) has been applied in several (pre)clinical studies on TAT. ^{213}Bi is a decay product of ^{225}Ac Actinium (^{225}Ac), with a $T_{1/2}$ of 45.6 min, emitting α -particles of 8.4 MeV and γ -rays of 440 keV. Figure 5 demonstrates the decay scheme of ^{225}Ac to ^{209}Bi , ^{213}Bi decays via ^{213}Po Polonium (^{213}Po) or ^{209}Tl Thallium (^{209}Tl) to stable ^{209}Bi . ^{213}Po emits α -particles with 8.38 MeV energy and by its short half-life of 3.7 μs ^{213}Po decays in equilibrium with the parent ^{213}Bi .

^{213}Bi -DOTATOC showed dose-related anti-tumour efficacies in rats, without acute or chronic hematological toxicity and tolerated nephrotoxicity [37]. Kratochwil et al. published the first clinical study with ^{213}Bi -DOTATOC [38]. After treatment using ^{213}Bi -DOTATOC in 7 patients with progressive advanced neuroendocrine liver metastases, refractory to treatment with $^{90}\text{Y}/^{177}\text{Lu}$ -DOTATOC, tumour response was observed. An overview of clinical applications with ^{213}Bi conjugated ligands is shown in Table 4. Recently, ^{225}Ac was applied; ^{225}Ac -PMSA inhibitor demonstrated to be effective in treatment of two patients with metastatic castration-resistant prostate cancer (mCRPC) in a pilot study without relevant hematological toxicity [39]. In a study that followed, 11 patients were treated with ^{225}Ac -PSMA-617. Xerostomia was found to be the dose-limiting factor in this study. Overall, a

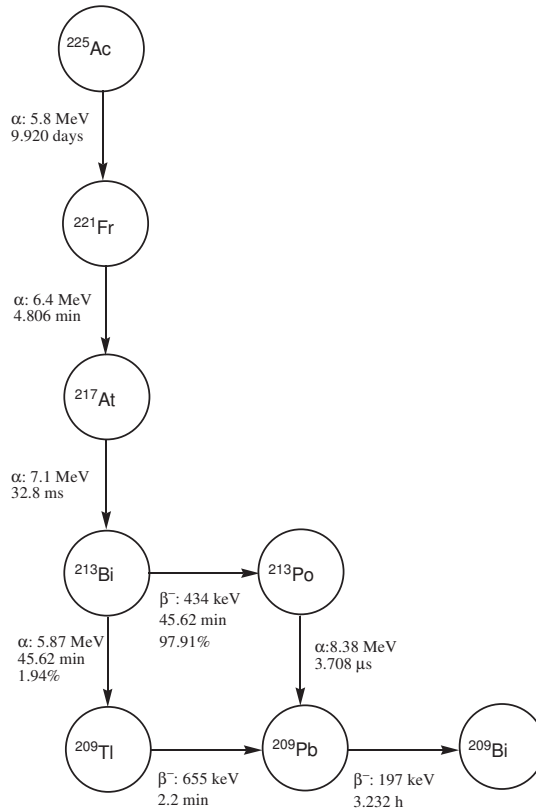


Figure 5, Decay scheme of ^{225}Ac to ^{209}Bi , including half-lives of the daughters and energy of particles emitted by the daughters.

Table 4, Overview clinical applications of ^{213}Bi

^{213}Bi conjugate	Cancer Type	Phase	Reference
HuM195mAb	Leukemia	Phase I/II	[36, 41]
9.2.27mAb	Melanoma	Phase I	[42–44]
Substance-P	Glioma	Pilot Phase I	[45]
DOTATOC	NETs	Pilot	[38]

treatment of 100 kBq/kg with a re-treatment interval of 8 weeks was found to be promising for anti-tumour effect with tolerable side-effects [40].

Only a limited number of α -emitting radionuclides is suitable for TAT and has been investigated in humans or animal models. In this next paragraph we will discuss the potential, the availability and the feasibility of some of these radionuclides.

²²⁵Actinium (²²⁵Ac)

²²⁵Ac (half-life, 10.0 days) decays via a cascade of six daughters to ²⁰⁹Bi. ²²⁵Ac emits a net of 4 α -emitting particles with a cumulative energy of 28 MeV and two β -disintegrations with a maximum energy of 1.6 and 0.6 MeV, see Fig. 5. ²²⁵Ac is produced via radiochemical extraction from a decay product of ²²⁹Th ($T_{1/2} = 7340$ y), ²²⁹Th being a natural decay product of ²³³U. Another route to produce ²²⁵Ac is by irradiation of ²²⁶Ra through accelerator-based methods using the ²²⁶Ra (p,n) reaction [46, 47]. ²²⁵Ac has been used to construct ²¹³Bi producing generators. Molecules labelled or drug carriers encapsulated with ²²⁵Ac are very attractive for application in theranostic radiopharmaceuticals [48, 49]. γ -Ray detection of ²²⁵Ac is also possible, due to γ -emissions of decay daughters ²²¹Fr (218 keV, abundance 11.6%) and ²¹³Bi (440 keV, abundance 26.1%). Conjugated ²²⁵Ac can act as an atomic nanogenerator due to the cascade of emitted α -particles, making ²²⁵Ac even much more potent than its daughter ²¹³Bi. Despite and due to the fact that ²²⁵Ac seems to be more cytotoxic than other α -emitters, concerns were raised about potential toxicity caused by free daughters, released into the circulation, by recoil effects during the decay of ²²⁵Ac [50]. Therefore, the search for the ideal “carrier/chelator” for ²²⁵Ac is still ongoing. Although DOTA is not the ideal chelator for ²²⁵Ac, due to the recoil effect, it is as yet the most often used chelator for ²²⁵Ac.

²¹³Bismuth (²¹³Bi)

²¹³Bi is obtained from the decay of ²²⁵Ac. ²¹³Bi can be eluted from a generator with ²²⁵Ac entrapped on a cation-exchange resin column [51]. With its relative short half-life (46 min), ²¹³Bi has been a commonly used α -emitter for TAT. ²¹³Bi decays to ²⁰⁹Bi by emitting one α -particle per disintegration. A γ -photon of 440 keV enables visualization/calculation of biodistribution, pharmacokinetics studies and dosimetry calculations for preclinical applications. After eluting ²¹³Bi from the generator, ²¹³Bi can be labelled by conjugation to a peptide [37, 52], nanobody, liposome or antibody [53] through bifunctional chelators e.g. DOTA, or CHX-A”DTPA [54].

²¹²Bismuth (²¹²Bi)

²¹²Bi with a half-life of 60.6 min can be eluted from a generator containing ²²⁴Ra as parent radionuclide. ²¹²Bi emits an α -particle with a mean energy of 7.8 MeV per decay and finally decays to stable ²⁰⁸Pb. Emission of a γ of 2.6 MeV along with other medium to high γ -radiation by the daughter ²⁰⁸Tl, requires heavy shielding for radiation exposure, limiting the use of ²¹²Bi in clinical as well as in preclinical settings. Chelators suitable for ²¹³Bi labelling can be used for the labelling of ²¹²Bi as well, since the chemical properties of these radionuclides are equal.

²¹¹Astatine (²¹¹At)

²¹¹At (half-life 7.3 hr) is produced in a cyclotron. The reaction occurs by bombardment of ²⁰⁹Bi with α -particles, via an (α , 2n) reaction. ²¹¹At has more a halogenic character than metallic, therefore the labelling methods of ²¹¹At are different from α -emitting radiometals. ²¹¹At is often covalently linked to the target biomolecule through labelling methods with e.g. electrophilic demetallation with stannyl or silyl precursors [55, 56]. ²¹¹At-labelled radiopharmaceuticals have been applied in several preclinical studies for treatment of ovarian cancer, glioma, leukemia, lymphoma and prostate cancer. Clinical trials have been performed in patients with primary brain tumour and ovarian carcinoma using ²¹¹At-antibodies [57–59].

²²³Radium (²²³Ra)

²²³Ra in the form of ²²³RaCl₂ is the first FDA approved α -emitting radiopharmaceutical for clinical use in patients with castration-resistant prostate cancer and symptomatic bone metastases. ²²³Ra has a half-life of 11.4 d. ²²³Ra is actually a byproduct produced during neutron irradiation of ²²⁶Ra to produce ²²⁷Ac, which decays to ²²³Ra through ²²⁷Th. ²²³Ra acts like a calcium mimetic and targets the bone area undergoing changes induced by tumour lesions. ²²³Ra emits four α -emitting particles per desintegration and is considered to be potent for therapeutic applications in tumours. However, there are currently no chelators which can form stable complex with ²²³Ra, it can therefore not be conjugated to tumour targeting molecules for TAT [57].

²²⁷Thorium (²²⁷Th)

²²⁷Th (half-life = 18.7 d) is one of the decay daughters from natural ²³⁵U. ²²⁷Th can also be obtained from decay of ²²⁷Ac, as indicated above. ²²⁷Th decays to ²²³Ra by emission of an α -particle with an average energy of 5.9 MeV. In the 1990s, ²²⁷Th was mainly used as a generator for ²²³Ra. ²²⁷Th binds stably to DOTA-derivative chelators and can therefore conjugated to e.g. antibodies. Conjugated ²²⁷Th-antibodies have been used in several preclinical studies to evaluate their therapeutic potential in TAT [60–63].

CHALLENGES AND LIMITATIONS OF TAT WITH ²¹³Bi IN (PRE) CLINICAL APPLICATIONS

¹⁷⁷Lu-DOTATATE has been applied in our department for decades in patients with NETs, complete cure in patients with metastasized NETs is however rarely achieved. ²¹³Bi might improve PRRT by eradicating small metastases, which have escaped from e.g. ¹⁷⁷Lu therapy. This thesis focuses on ²¹³Bi-labelled DOTATATE application in preclinical models of NETs. In general, to deliver an absorbed dose to the tumour through receptor-mediated uptake that is therapeutically efficacious *in vivo* can be challenging. Several factors can

influence the delivered absorbed dose e.g. the limited number of available binding sites, distribution patterns, tumour perfusion and elimination from the tumour. Apart from these *in vivo* challenges, the chemical and physical properties of ^{213}Bi can also provide hurdles. In the following paragraphs, several of these limitations will be discussed.

Chemical and physical challenges

In general for PRRT and especially in small animals, a labelled peptide with a relatively high molar activity (MA, expressed as MBq/nmol peptide) with high *in vivo* stability is required to deliver sufficient dose to the tumour. MA is expressed as the maximum amount of radioactivity per nmol of peptide [64–66]. For the labelling of ^{213}Bi , the MA is dependent on the interaction between chelator and ^{213}Bi , whereas the electric charge, stereometric hindrance, thermodynamic stability and kinetic stability play a major role in the chemical stability of the labelled peptide as described below. The most commonly used chelator for ^{213}Bi is DOTA, with a thermodynamic stability constant of Log K 30.3. DOTA conjugated ligands demonstrate high *in vitro* and *in vivo* stability with $^{213}\text{Bi}^{3+}$. Impurities in the labelling process may however often lead to a lower MA obtained. These impurities can be formed during from the production of the ^{225}Ac , decay products of ^{213}Bi , derived from the solvent used for elution, or buffers and quenchers used for the labelling reaction. In general, these impurities have no influence on the labelling when they have no affinity for the chelator. However, when these impurities do show affinity for the chelator, the MA might decrease, the effect being dependent on the stability of this complex. During labelling of ^{213}Bi the resulting radiopeptide can be damaged by radicals ($\cdot\text{OH}$) or directly by high LET α -particle tracks in the labelling reaction mixture, potentially resulting in decrease of chemical purity and (partial) loss of affinity to the target. The extent of radical formation in the labelling is dependent on the type of radionuclide, the duration of exposure and also on the energy release by the radionuclide. Addition of quenchers or scavengers during radiolabelling will limit the damage to the peptide due to radicals, thus maintaining the stability of the radiopeptide when the damage is mainly indirect due to radicals. De Blois et al. demonstrated the importance of quenchers e.g. addition of ascorbic acid, gentisic acid, ethanol, to minimize the damaging effects of radicals to the radio-peptide with ^{177}Lu and ^{111}In [67].

The most commonly applied methods used to determine the quality and stability of radioligands in the field of nuclear medicine are by instant thin layer chromatography or high performance liquid chromatography (HPLC). HPLC can also be used to determine the radiochemical purity (RCP) of the labelled compounds.

(Pre)clinical challenges of PRRT and TAT

For receptor-mediated processes the most challenging aspect is to deliver a therapeutic dose to the tumour with acceptable toxicity, so the ideal radiolabelled peptide combines low a-specific binding to normal tissues with high specific binding to tumour lesions. Since

the numbers of receptors available for binding of radiopeptides are limited and the injected amount of peptide can therefore influence tumour uptake, administration of a radioligand with high MA is highly recommended, to avoid saturation of the receptors. (Partial) saturation of the receptors by unlabelled peptide will result in lower uptake of the radiolabelled peptide in the tumour cells, potentially leading to insufficient absorbed dose delivered to the tumour cells in the case of e.g. β -emitters. As mentioned before, α -emitters are more cytotoxic than β -emitters. Only 1–4 hits are required for cell death, provided the high LET α -particles traverse the nucleus of the tumour cell, causing irreparable complex DNA damage, leading to cell death.

Off-targeting or binding to healthy organs is a major issue in receptor-mediated processes, either by the labelled peptide itself, by its metabolites or de-chelated radionuclide. Especially α -emitters have a high risk to cause undesirable radiation damage to healthy organs and tissues when used for therapeutic applications. This effect could be minimized several ways; most often modification of the radio-peptide is applied, by e.g. selecting the most suitable chelator or changing the peptide sequence of the radiopeptide. Other options to improve *in vivo* stability are to reduce the enzymatic degradation by co-injection of peptidase inhibitors [68] or by saturating the receptors on healthy organs and tissue by unlabelled peptides to decrease uptake [69]. The latter can have a negative influence on the tumour uptake, since tumour uptake for somatostatine analogues is dependent on the peptide amount injected [70].

PRRT with the β -particle emitter ^{177}Lu coupled to DOTATATE is generally well tolerated by patients with NETs, if necessary precautions are taken, e.g. co-administration of amino acids, without severe side effect. Kidneys and bone marrow are critical organs, although kidney it is not dose-limiting with ^{177}Lu in contrast to ^{90}Y -labelled peptides [71–73]. The most common subacute side effect of bone marrow irradiation is haematological toxicity, which occurs 4–6 weeks after PRRT. This toxicity is often mild and reverses within weeks after treatment cessation [74]. Renal retention of radiopeptides remains a problem in PRRT, in particularly for TAT [75]. The partial retention of the radioactivity in the kidneys is mainly caused by tubular reabsorption caused by the interaction between the radiopeptide with the receptor complex of megalin/or cubulin [76]. Megalin and cubulin work in close interaction with each other and are situated in the proximal tubules in the renal cortex and their function is to reabsorb glomerular filtered substances through mediated endocytosis. Beside megalin and cubilin, ^{213}Bi -conjugated complexes can also have strong interaction with a metallothionein in the kidney [77], which might result in a higher absorbed dose and leading to loss of renal function and nephrotoxicity. Retention of radio-peptides in kidneys can be reduced by co-administration of kidney protectants like lysine/arginine during PRRT [78]. The technique to use lysine/arginine to compete with the ligand binding site cluster of megalin and cubilin is routinely applied during PRRT application with ^{177}Lu -DOTATATE and ^{90}Y -DOTATOC.

Renal function during and after PRRT can be monitored using renal biomarkers e.g. creatinine clearance/EGFR and biomarkers like ^{99m}Tc -dimercaptosuccinic acid (^{99m}Tc -DMSA) or ^{99m}Tc -mercaptoacetyltriglycine (^{99m}Tc -MAG3) [79]. ^{99m}Tc -DMSA is used as renal cortical imaging agent [80] and ^{99m}Tc -MAG3 is typically used to determine renal tubular function. ^{99m}Tc -MAG3 however, has shown to have limited value for the prediction of late radiation induced nephropathy by ^{177}Lu -DOTATATE or ^{177}Lu -DOTATOC [81]. Permanent renal toxicity normally appears 6–12 months after PRRT [72, 74]. The threshold dose for late-stage kidney radiation damage was set to be 23 Gy, this was according to the dose obtained from external beam radiation therapy [82]. Bergsma et al. found that a threshold dose for kidney of 28 Gy was more a conservative value for therapy with ^{177}Lu -DOTATATE [73]. To investigate long-term nephrotoxicity after PRRT, classical approach is often used; creatinine clearance [83]. Creatinine is filtered through the glomeruli. However, the level of serum creatinine is generally not sufficiently accurate for analytical measurement. Due to several factors such as age, diet, and muscle mass can influence creatinine levels in serum [84]. Nowadays, novel renal markers e.g. Neutrophil Gelatinase-Associated Lipocalin (NGAL) [85, 86] can be used to evaluate renal dysfunction at early events. This biomarker has shown to be sensitive and specific as renal marker for acute kidney injury [86].

One of the most challenging issues regarding application of conjugated ^{213}Bi for TAT is the relatively short half-life. For clinical purposes, generators with ^{225}Ac activity of 4 GBq and more are produced. However, for preclinical applications, typical generators are produced containing less than 222 MBq, due to the limited availability of ^{225}Ac ; studies with these low activity generators are even more challenging. Apart from using the low activity generator, ^{213}Bi has to be eluted from the generator in an acidic environment containing 0.1 M/0.1M HCl/NaI in a relative large volume (> 600 μL). ^{213}Bi conjugates are labelled generally at pH 3.5 or higher, and highly concentrated buffers are to be used to adjust the pH of the labelling. Addition of quenchers or scavengers to protect the labelled peptide from radicals during labelling, increases the osmolarity (Osmol/L) of the labelling reaction even further than 0.3 Osmol/L. Direct administration of the ^{213}Bi -labelled conjugated is impossible in small animals such as mice, since the maximum volume for intravenous injection in mice is 200 μL , at pH 7.4 with a osmolarity close to 0.3 Osmol/L, to avoid e.g. loss of venous endothelial cells and inflammatory cell infiltration, and to maintain homeostasis [87]. The requirements for (pre)clinical applications with PRRT or TAT are again summarized below.

The following requirements are typically required for PRRT or TAT in (pre)clinical applications:

- High molar activity radioligand with high tumour affinity and fast clearance from kidney and circulation
- Stable radioligand *in vitro* and *in vivo*
- Small injected volume (~ 200 μL) for small animals
- Physiological conditions of the drug ($\sim \text{pH } 7.4$, 0.3 Osmol/L)
- Renal protection

OUTLINE OF THIS THESIS

In this thesis we describe research on applications, limitations, and problems regarding ^{213}Bi for TAT in preclinical studies. DOTATATE was used as a model peptide, being a peptide analogue widely applied in NET patients. The objectives of this thesis were:

1. Optimizing ^{213}Bi DOTA-peptide labelling for applications in mice
2. Determine the maximum tolerated dose and reduce nephrotoxicity using the kidney protectant L-lysine in mice
3. Pharmacokinetic and pharmacodynamics studies of ^{213}Bi -DOTATATE in different NET models in mice
4. Comparison of the therapeutic effects of the α -emitter ^{213}Bi , the β -emitter ^{177}Lu and external beam radiation in *in vitro* studies
5. ^{213}Bi -SPECT imaging *in vivo* in mice.

In our research we focused on ^{213}Bi for PRRT/TAT in SSTR-expressing NET mouse models. In this first chapter the concept of PRS and PRRT and advantages of the use of α -emitters for TAT are explained. Moreover, the requirements for the labelling procedure and preclinical applications of TAT are presented in Chapter 1.

Chapter 2 describes the optimized labelling procedure required for preclinical applications. The labelling conditions were adapted to meet the requirements for preclinical studies and to preserve the stability of ^{213}Bi -DOTATATE.

In Chapter 3, peptide amount-dependent uptake in tumour tissue is described. L-Lysine, an amino acid to inhibit renal uptake, was applied during TAT with ^{213}Bi -DOTATATE to decrease renal radioactivity and prolong survival. Furthermore, the maximum tolerated dose was estimated for renal tissue with and without renal protection. Acute kidney injury after TAT with ^{213}Bi -DOTATATE was investigated to determine its dose-dependency by using NGAL, as renal marker of acute nephrotoxicity.

Chapter 4 describes the therapeutic efficacy of ^{213}Bi -DOTATATE in different somatostatin receptor positive tumour models: CA20948 (rat pancreatic tumour) and H69 (human small lung carcinoma). Besides different tumour models, investigation of different tumour sizes was performed in tumours with sizes of 50 mm^3 – 200 mm^3 , this to answer the question whether TAT with ^{213}Bi -DOTATATE is suitable for therapy of larger tumours as well. Renal function was monitored by SPECT/CT after administration of $^{99\text{m}}\text{Tc}$ -DMSA.

In Chapter 5, a comparison of cytotoxic effects induced by ^{213}Bi -conjugates, ^{177}Lu -conjugates and external radiation was performed in CA20948 and BON (human carcinoid) cell lines. In addition, the absorbed dose was calculated using a small-scale dosimetry model to compare the relative biological effects of these radiation types.

Chapter 6 describes the feasibility of imaging ^{213}Bi with a dedicated small animal SPECT imaging device. Settings were tested related to the energy windows and image reconstruc-

tion methods for 440 keV γ -rays and the lower energy X-rays. SPECT imaging of tumour uptake and physiological distribution was investigated. Ultimately dynamics scan was performed and the absorbed dose to the kidneys was calculated based on dynamic imaging data obtained with this SPECT system.

Chapter 7 provides the summary and concluding remarks.

REFERENCES:

1. Gatto, F. and L.J. Hofland, *The role of somatostatin and dopamine D2 receptors in endocrine tumors*. *Endocr Relat Cancer*, 2011. 18(6): p. R233-51.
2. Patel, Y.C. and C.B. Srikant, *Somatostatin receptors*. *Trends Endocrinol Metab*, 1997. 8(10): p. 398-405.
3. Patel, Y.C., *Somatostatin and its receptor family*. *Front Neuroendocrinol*, 1999. 20(3): p. 157-98.
4. Bell, G.I., et al., *Molecular biology of somatostatin receptors*. *Ciba Found Symp*, 1995. 190: p. 65-79; discussion 80-8.
5. Choi, T.K., et al., *Somatostatin in the treatment of acute pancreatitis: a prospective randomised controlled trial*. *Gut*, 1989. 30(2): p. 223-7.
6. Gjorup, I., et al., *A double-blinded multicenter trial of somatostatin in the treatment of acute pancreatitis*. *Surg Gynecol Obstet*, 1992. 175(5): p. 397-400.
7. McKay, C.J., C.W. Imrie, and J.N. Baxter, *Somatostatin and somatostatin analogues—are they indicated in the management of acute pancreatitis?* *Gut*, 1993. 34(11): p. 1622-6.
8. Patel, Y.C., *Somatostatin-receptor imaging for the detection of tumors*. *N Engl J Med*, 1990. 323(18): p. 1274-6.
9. Patel, Y.C. and T. Wheatley, *In vivo and in vitro plasma disappearance and metabolism of somatostatin-28 and somatostatin-14 in the rat*. *Endocrinology*, 1983. 112(1): p. 220-5.
10. Krenning, E.P., et al., *Localisation of endocrine-related tumours with radioiodinated analogue of somatostatin*. *Lancet*, 1989. 1(8632): p. 242-4.
11. Nocaudie-Calzada, M., et al., *Iodine-123-Tyr-3-octreotide uptake in pancreatic endocrine tumors and in carcinoids in relation to hormonal inhibition by octreotide*. *J Nucl Med*, 1994. 35(1): p. 57-62.
12. Bakker, W.H., et al., *[111In-DTPA-D-Phe1]-octreotide, a potential radiopharmaceutical for imaging of somatostatin receptor-positive tumors: synthesis, radiolabeling and in vitro validation*. *Life Sci*, 1991. 49(22): p. 1583-91.
13. Brechbiel, M.W., *Bifunctional chelates for metal nuclides*. *Q J Nucl Med Mol Imaging*, 2008. 52(2): p. 166-73.
14. Qaim, S.M., *Therapeutic radionuclides and nuclear data*. *Radiochimica Acta*, 2001. 89.
15. Kassis, A.I., *Therapeutic radionuclides: biophysical and radiobiologic principles*. *Semin Nucl Med*, 2008. 38(5): p. 358-66.
16. Yeong, C.H., M.H. Cheng, and K.H. Ng, *Therapeutic radionuclides in nuclear medicine: current and future prospects*. *J Zhejiang Univ Sci B*, 2014. 15(10): p. 845-63.
17. El-Maouche, D., et al., *68Ga-DOTATATE for Tumor Localization in Tumor-Induced Osteomalacia*. *J Clin Endocrinol Metab*, 2016. 101(10): p. 3575-3581.
18. Virgolini, I., et al., *Procedure guidelines for PET/CT tumour imaging with 68Ga-DOTA-conjugated peptides: 68Ga-DOTA-TOC, 68Ga-DOTA-NOC, 68Ga-DOTA-TATE*. *Eur J Nucl Med Mol Imaging*, 2010. 37(10): p. 2004-10.
19. Van Audenhaege, K., et al., *Review of SPECT collimator selection, optimization, and fabrication for clinical and preclinical imaging*. *Med Phys*, 2015. 42(8): p. 4796-813.
20. O'Donoghue, J.A., M. Bardies, and T.E. Wheldon, *Relationships between tumor size and curability for uniformly targeted therapy with beta-emitting radionuclides*. *J Nucl Med*, 1995. 36(10): p. 1902-9.

21. van der Zwan, W.A., et al., *GEPNETs UPDATE: Radionuclide therapy in neuroendocrine tumors*. Eur J Endocrinol, 2015. 172(1): p. R1-R8.
22. Bodei, L., et al., *PRRT: Defining the paradigm shift to achieve standardization and individualization*. J Nucl Med, 2014. 55(11): p. 1753-6.
23. Strosberg, J., et al., *Phase 3 Trial of 177Lu-Dotatate for Midgut Neuroendocrine Tumors*. N Engl J Med, 2017. 376(2): p. 125-135.
24. Nayak, T., et al., *A comparison of high- versus low-linear energy transfer somatostatin receptor targeted radionuclide therapy in vitro*. Cancer Biother Radiopharm, 2005. 20(1): p. 52-7.
25. Imam, S.K., *Advancements in cancer therapy with alpha-emitters: a review*. Int J Radiat Oncol Biol Phys, 2001. 51(1): p. 271-8.
26. Dash, A., et al., *Peptide receptor radionuclide therapy: an overview*. Cancer Biother Radiopharm, 2015. 30(2): p. 47-71.
27. Allen, C., et al., *Heavy charged particle radiobiology: using enhanced biological effectiveness and improved beam focusing to advance cancer therapy*. Mutat Res, 2011. 711(1-2): p. 150-7.
28. Straume, T., R.L. Dobson, and T.C. Kwan, *Neutron RBEs and the radiosensitive target for mouse immature oocyte killing*. Radiat Res, 1987. 111(1): p. 47-57.
29. Huang, C.Y., et al., *Microdosimetry for targeted alpha therapy of cancer*. Comput Math Methods Med, 2012. 2012: p. 153212.
30. Elgqvist, J., et al., *The potential and hurdles of targeted alpha therapy - clinical trials and beyond*. Front Oncol, 2014. 3: p. 324.
31. Sgouros, G., et al., *MIRD Pamphlet No. 22 (abridged): radiobiology and dosimetry of alpha-particle emitters for targeted radionuclide therapy*. J Nucl Med, 2010. 51(2): p. 311-28.
32. Graf, F., et al., *DNA double strand breaks as predictor of efficacy of the alpha-particle emitter Ac-225 and the electron emitter Lu-177 for somatostatin receptor targeted radiotherapy*. PLoS One, 2014. 9(2): p. e88239.
33. Sorbe, B., O. Kjellgren, and S. Stenson, *Prognosis of endometrial carcinoma stage I in two Swedish regions. A study with special regard to the effects of intracavitary irradiation with high dose-rate afterloading technique or with low dose-rate radium*. Acta Oncol, 1990. 29(1): p. 29-37.
34. Carling, E.R. and F.M. Allchin, *The Present and Future of Radium Teletherapy: (Section of Radiology)*. Proc R Soc Med, 1935. 28(8): p. 1145-56.
35. Mould, R.F., *Priority for radium therapy of benign conditions and cancer*. Curr Oncol, 2007. 14(3): p. 118-22.
36. Jurcic, J.G., et al., *Targeted alpha particle immunotherapy for myeloid leukemia*. Blood, 2002. 100(4): p. 1233-9.
37. Norenberg, J.P., et al., *213Bi-[DOTA0, Tyr3]octreotide peptide receptor radionuclide therapy of pancreatic tumors in a preclinical animal model*. Clin Cancer Res, 2006. 12(3 Pt 1): p. 897-903.
38. Kratochwil, C., et al., *(2)(1)(3)Bi-DOTATOC receptor-targeted alpha-radionuclide therapy induces remission in neuroendocrine tumours refractory to beta radiation: a first-in-human experience*. Eur J Nucl Med Mol Imaging, 2014. 41(11): p. 2106-19.
39. Kratochwil, C., et al., *225Ac-PSMA-617 for PSMA-Targeted alpha-Radiation Therapy of Metastatic Castration-Resistant Prostate Cancer*. J Nucl Med, 2016. 57(12): p. 1941-1944.
40. Kratochwil, C., et al., *Targeted Alpha Therapy of mCRPC with 225Actinium-PSMA-617: Dosimetry estimate and empirical dose finding*. J Nucl Med, 2017.
41. Rosenblat, T.L., et al., *Sequential cytarabine and alpha-particle immunotherapy with bismuth-213-lintuzumab (HuM195) for acute myeloid leukemia*. Clin Cancer Res, 2010. 16(21): p. 5303-11.

42. Allen, B.J., et al., *Intralesional targeted alpha therapy for metastatic melanoma*. *Cancer Biol Ther*, 2005. 4(12): p. 1318-24.
43. Allen, B.J., et al., *Analysis of patient survival in a Phase I trial of systemic targeted alpha-therapy for metastatic melanoma*. *Immunotherapy*, 2011. 3(9): p. 1041-50.
44. Raja, C., et al., *Interim analysis of toxicity and response in phase I trial of systemic targeted alpha therapy for metastatic melanoma*. *Cancer Biol Ther*, 2007. 6(6): p. 846-52.
45. Cordier, D., et al., *Targeted alpha-radionuclide therapy of functionally critically located gliomas with ^{213}Bi -DOTA-[Thi8,Mei(O2)11]-substance P: a pilot trial*. *Eur J Nucl Med Mol Imaging*, 2010. 37(7): p. 1335-44.
46. Boll, R.A., D. Malkemus, and S. Mirzadeh, *Production of actinium-225 for alpha particle mediated radioimmunotherapy*. *Appl Radiat Isot*, 2005. 62(5): p. 667-79.
47. Apostolidis, C., et al., *Production of Ac-225 from Th-229 for targeted alpha therapy*. *Anal Chem*, 2005. 77(19): p. 6288-91.
48. Wang, G., et al., *Retention studies of recoiling daughter nuclides of ^{225}Ac in polymer vesicles*. *Appl Radiat Isot*, 2014. 85: p. 45-53.
49. McDevitt, M.R., et al., *Tumor therapy with targeted atomic nanogenerators*. *Science*, 2001. 294(5546): p. 1537-40.
50. Jaggi, J.S., et al., *Mitigation of radiation nephropathy after internal alpha-particle irradiation of kidneys*. *Int J Radiat Oncol Biol Phys*, 2006. 64(5): p. 1503-12.
51. Morgenstern, A., F. Bruchertseifer, and C. Apostolidis, *Bismuth-213 and actinium-225 — generator performance and evolving therapeutic applications of two generator-derived alpha-emitting radioisotopes*. *Curr Radiopharm*, 2012. 5(3): p. 221-7.
52. Wild, D., et al., *Alpha- versus beta-particle radiopeptide therapy in a human prostate cancer model (^{213}Bi -DOTA-PESIN and ^{213}Bi -AMBA versus ^{177}Lu -DOTA-PESIN)*. *Cancer Res*, 2011. 71(3): p. 1009-18.
53. Ma, D., et al., *Rapid preparation of short-lived alpha particle emitting radioimmunopharmaceuticals*. *Appl Radiat Isot*, 2001. 55(4): p. 463-70.
54. Wu, C., et al., *Stereochemical influence on the stability of radio-metal complexes in vivo. Synthesis and evaluation of the four stereoisomers of 2-(p-nitrobenzyl)-trans-CyDTPA*. *Bioorg Med Chem*, 1997. 5(10): p. 1925-34.
55. Zalutsky, M.R. and M. Pruszynski, *Astatine-211: production and availability*. *Curr Radiopharm*, 2011. 4(3): p. 177-85.
56. Pozzi, O.R. and M.R. Zalutsky, *Radiopharmaceutical chemistry of targeted radiotherapeutics, part 4: Strategies for ^{211}At labeling at high activities and radiation doses of ^{211}At alpha-particles*. *Nucl Med Biol*, 2017. 46: p. 43-49.
57. Vaidyanathan, G. and M.R. Zalutsky, *Applications of ^{211}At and ^{223}Ra in targeted alpha-particle radiotherapy*. *Curr Radiopharm*, 2011. 4(4): p. 283-94.
58. Andersson, H., et al., *Intraperitoneal alpha-particle radioimmunotherapy of ovarian cancer patients: pharmacokinetics and dosimetry of (^{211}At -MX35 F(ab')₂—a phase I study*. *J Nucl Med*, 2009. 50(7): p. 1153-60.
59. Zalutsky, M.R., et al., *Clinical experience with alpha-particle emitting ^{211}At : treatment of recurrent brain tumor patients with ^{211}At -labeled chimeric antitenascin monoclonal antibody 81C6*. *J Nucl Med*, 2008. 49(1): p. 30-8.
60. Abbas, N., et al., *Comparing high LET ^{227}Th - and low LET ^{177}Lu -trastuzumab in mice with HER-2 positive SKBR-3 xenografts*. *Curr Radiopharm*, 2013. 6(2): p. 78-86.

61. Hagemann, U.B., et al., *In Vitro and In Vivo Efficacy of a Novel CD33-Targeted Thorium-227 Conjugate for the Treatment of Acute Myeloid Leukemia*. *Mol Cancer Ther*, 2016. 15(10): p. 2422-2431.
62. Heyerdahl, H., et al., *Targeted alpha therapy with 227Th-trastuzumab of intraperitoneal ovarian cancer in nude mice*. *Curr Radiopharm*, 2013. 6(2): p. 106-16.
63. Staudacher, A.H., et al., *Targeted alpha-therapy using 227Th-APOMAB and cross-fire antitumour effects: preliminary in-vivo evaluation*. *Nucl Med Commun*, 2014. 35(12): p. 1284-90.
64. Breeman, W.A., et al., *Effect of dose and specific activity on tissue distribution of indium-111-pentetreotide in rats*. *J Nucl Med*, 1995. 36(4): p. 623-7.
65. Breeman, W.A., et al., *Optimising conditions for radiolabelling of DOTA-peptides with 90Y, 111In and 177Lu at high specific activities*. *Eur J Nucl Med Mol Imaging*, 2003. 30(6): p. 917-20.
66. Breeman, W.A., et al., *Somatostatin receptor-mediated imaging and therapy: basic science, current knowledge, limitations and future perspectives*. *Eur J Nucl Med*, 2001. 28(9): p. 1421-9.
67. de Blois, E., et al., *Effectiveness of quenchers to reduce radiolysis of (111)In- or (177)Lu-labelled methionine-containing regulatory peptides. Maintaining radiochemical purity as measured by HPLC*. *Curr Top Med Chem*, 2012. 12(23): p. 2677-85.
68. Kaloudi, A., et al., *Impact of clinically tested NEP/ACE inhibitors on tumor uptake of [(111)In-DOTA]MG11-first estimates for clinical translation*. *EJNMMI Res*, 2016. 6(1): p. 15.
69. Kletting, P., et al., *Investigating the Effect of Ligand Amount and Injected Therapeutic Activity: A Simulation Study for 177Lu-Labeled PSMA-Targeting Peptides*. *PLoS One*, 2016. 11(9): p. e0162303.
70. de Jong, M., et al., *Tumour uptake of the radiolabelled somatostatin analogue [DOTA0, TYR3] octreotide is dependent on the peptide amount*. *Eur J Nucl Med*, 1999. 26(7): p. 693-8.
71. Bergsma, H., et al., *Subacute haematotoxicity after PRRT with (177)Lu-DOTA-octreotate: prognostic factors, incidence and course*. *Eur J Nucl Med Mol Imaging*, 2016. 43(3): p. 453-63.
72. Bodei, L., et al., *Long-term evaluation of renal toxicity after peptide receptor radionuclide therapy with 90Y-DOTATOC and 177Lu-DOTATATE: the role of associated risk factors*. *Eur J Nucl Med Mol Imaging*, 2008. 35(10): p. 1847-56.
73. Bergsma, H., et al., *Nephrotoxicity after PRRT with (177)Lu-DOTA-octreotate*. *Eur J Nucl Med Mol Imaging*, 2016. 43(10): p. 1802-11.
74. Bodei, L., et al., *Long-term tolerability of PRRT in 807 patients with neuroendocrine tumours: the value and limitations of clinical factors*. *Eur J Nucl Med Mol Imaging*, 2015. 42(1): p. 5-19.
75. Szymanska, J.A., E.M. Mogilnicka, and B.W. Kaszper, *Binding of bismuth in the kidneys of the rat: the role of metallothionein-like proteins*. *Biochem Pharmacol*, 1977. 26(3): p. 257-8.
76. Verroust, P.J. and E.I. Christensen, *Megalyn and cubilin—the story of two multipurpose receptors unfolds*. *Nephrol Dial Transplant*, 2002. 17(11): p. 1867-71.
77. Sun, H., et al., *Interactions of bismuth complexes with metallothionein(II)*. *J Biol Chem*, 1999. 274(41): p. 29094-101.
78. Rolleman, E.J., et al., *Molecular imaging of reduced renal uptake of radiolabelled [DOTA0,Tyr3] octreotate by the combination of lysine and Gelofusine in rats*. *Nuklearmedizin*, 2008. 47(3): p. 110-5.
79. Ritchie, G., A.G. Wilkinson, and R.J. Prescott, *Comparison of differential renal function using technetium-99m mercaptoacetyl triglycine (MAG3) and technetium-99m dimercaptosuccinic acid (DMSA) renography in a paediatric population*. *Pediatr Radiol*, 2008. 38(8): p. 857-62.
80. Weyer, K., et al., *Renal uptake of 99mTc-dimercaptosuccinic acid is dependent on normal proximal tubule receptor-mediated endocytosis*. *J Nucl Med*, 2013. 54(1): p. 159-65.

81. Werner, R.A., et al., *The impact of 177Lu-octreotide therapy on 99mTc-MAG3 clearance is not predictive for late nephropathy*. *Oncotarget*, 2016. 7(27): p. 41233-41241.
82. Cremonesi, M., et al., *Dosimetry in Peptide radionuclide receptor therapy: a review*. *J Nucl Med*, 2006. 47(9): p. 1467-75.
83. Valkema, R., et al., *Long-term follow-up of renal function after peptide receptor radiation therapy with (90)Y-DOTA(0), Tyr(3)-octreotide and (177)Lu-DOTA(0), Tyr(3)-octreotate*. *J Nucl Med*, 2005. 46 Suppl 1: p. 83S-91S.
84. Erbas, B. and M. Tuncel, *Renal Function Assessment During Peptide Receptor Radionuclide Therapy*. *Semin Nucl Med*, 2016. 46(5): p. 462-78.
85. Devarajan, P., *Neutrophil gelatinase-associated lipocalin—an emerging troponin for kidney injury*. *Nephrol Dial Transplant*, 2008. 23(12): p. 3737-43.
86. Bolignano, D., et al., *Neutrophil gelatinase-associated lipocalin (NGAL) as a marker of kidney damage*. *Am J Kidney Dis*, 2008. 52(3): p. 595-605.
87. Turner, P.V., et al., *Administration of substances to laboratory animals: equipment considerations, vehicle selection, and solute preparation*. *J Am Assoc Lab Anim Sci*, 2011. 50(5): p. 614-27.



Chapter 2

Optimizing labelling conditions of ²¹³Bi-DOTATATE for preclinical applications of peptide receptor targeted alpha therapy

Ho Sze Chan, Erik de Blois, Mark W. Konijnenberg, Alfred Morgenstern,
Frank Bruchertseifer, Jeffrey P. Norenberg, Fred J. Verzijlbergen, Marion de Jong,
Wouter A. P. Breeman

EJNMMI Radiopharmacy and Chemistry (2016) 1:9

ABSTRACT

Background:

^{213}Bi (^{213}Bi , $T_{1/2} = 45.6$ min) is one of the most frequently used α -emitters in cancer research. High specific activity radioligands are required for peptide receptor radionuclide therapy. The use of generators containing less than 222 MBq ^{225}Ac (actinium), due to limited availability and the high cost to produce large-scale $^{225}\text{Ac}/^{213}\text{Bi}$ generators, might complicate *in vitro* and *in vivo* applications though.

Here we present optimized labelling conditions of a DOTA-peptide with an $^{225}\text{Ac}/^{213}\text{Bi}$ generator (< 222 MBq) for preclinical applications using DOTA-Tyr³-octreotate (DOTATATE), a somatostatin analogue. The following labelling conditions of DOTATATE with ^{213}Bi were investigated; peptide mass was varied from 1.7–7.0 nmol, concentration of TRIS buffer from 0.15 mol.L⁻¹ to 0.34 mol.L⁻¹, and ascorbic acid from 0 to 71 mmol.L⁻¹ in 800 μL . All reactions were performed at 95°C for 5 min. After incubation, DTPA (50 nmol) was added to stop the labelling reaction. Besides optimizing the labelling conditions, incorporation yield was determined by ITLC-SG and radiochemical purity (RCP) was monitored by RP-HPLC up to 120 min after labelling. Dosimetry studies in the reaction vial were performed using Monte Carlo and *in vitro* clonogenic assay was performed with a rat pancreatic tumour cell line, CA20948.

Results:

At least 3.5 nmol DOTATATE was required to obtain incorporation $\geq 99\%$ with 100 MBq ^{213}Bi (at optimized pH conditions, pH 8.3 with 0.15 mol.L⁻¹ TRIS) in a reaction volume of 800 μL . The cumulative absorbed dose in the reaction vial was 230 Gy/100 MBq in 30 min. A minimal final concentration of 0.9 mmol.L⁻¹ ascorbic acid was required for ~ 100 MBq ($t = 0$) to minimize radiation damage of DOTATATE. The osmolarity was decreased to 0.45 Osmol/L.

Under optimized labelling conditions, ^{213}Bi -DOTATATE remained stable up to 2 h after labelling, RCP was $\geq 85\%$. *In vitro* showed a negative correlation between ascorbic acid concentration and cell survival.

Conclusion:

^{213}Bi -DOTA-peptide labelling conditions including peptide amount, quencher and pH were optimized to meet the requirements needed for preclinical applications in peptide receptor radionuclide therapy.

BACKGROUND

Peptide receptor radionuclide therapy (PRRT) is an effective treatment for metastatic and inoperable neuroendocrine tumours [1–3]. The most common radionuclides used for PRRT include ^{177}Lu (β^- -emitter, $T_{1/2} = 6.71$ days, 149 and 497 keV) and ^{90}Y (β^- -emitter, $T_{1/2} = 64.1$ h, 935 and 2284 keV).

α -Emitters have been demonstrated to offer an additional treatment option for patients refractory to standard PRRT with β^- -emitters or chemotherapy [4–6]. Moreover, α -particles have short path length in tissue (~ 80 μm), sparing non-target tissues from radiation. ^{213}Bi ($T_{1/2} = 45.6$ min) is an α -emitter and has been applied in several (pre)clinical research studies of targeted alpha therapy (TAT) [4, 5, 7–9].

PRRT is based on receptor-mediated processes. In order to achieve treatment success, a sufficient cytotoxic dose of radio-peptide must be delivered to the targeted cells [10]. Moreover, the number of receptors available on the cell membrane is limited, so high specific activity (SA, expressed in MBq per nmol of peptide) of labelled peptides is advantageous for administration in small animals e.g. mice (~ 25 g) [11–13]. Besides high SA, other requirements for preclinical applications include high stability of the radio-peptide at physiological conditions *in vitro* (~ 0.3 Osmol.L $^{-1}$, pH ~ 7.4) and *in vivo*. In addition, a high osmolarity of the drug-containing solution is inconsistent with maintenance of physiological conditions for *in vitro* and *in vivo* applications.

Due to the limited availability and the high cost to produce large-scale $^{225}\text{Ac}/^{213}\text{Bi}$ generators, preclinical studies with ^{213}Bi are often being performed using relatively low activity generators (e.g. 222 MBq ^{225}Ac). Under these conditions, the standard clinical labelling procedure for ^{213}Bi , which was designed for high activity generators (up to 4 GBq) with a reaction volume of 2 mL at > 0.7 Osmol.L $^{-1}$ [14], probably needs to be adjusted. Therefore, the labelling conditions for preclinical applications required modifications.

In this study, we systematically studied the consequences using the somatostatin analogue [DOTA 0 , Tyr 3]-octreotate (DOTATATE) as a model for optimizing labelling conditions of ^{213}Bi for preclinical applications, starting from the standard labelling protocol.

Herein we varied the labelling conditions such as peptide amount, quenchers and pH. The stability of the labelled peptide and the radiochemical purity (RCP) was monitored up to 2 h after labelling. The absorbed dose rates of ^{213}Bi , ^{213}Po , ^{209}Tl and ^{209}Pb (mGy.s $^{-1}$) as function of reaction volume were calculated. The use of the absorbed dose rate is investigated as a possible surrogate indicator for the ionization probability and consequential radiolysis to the peptide in the reaction vial. And lastly, *in vitro* clonogenic assay was performed to investigate the influence caused by labelling conditions used.

The objective of this study was to establish a practical, ready to use, and reproducible labelling procedure of ^{213}Bi -DOTATATE to meet the constraint for the use of peptide as radiopharmaceutical for preclinical applications.

METHODS

²¹³Bi-elution

The ²²⁵Ac/²¹³Bi generator (222 MBq) was supplied by the Institute for Transuranium Elements (ITU), Germany. Prior to elution, the column was rinsed with diluted HCl (0.01 mol.L⁻¹). ²¹³Bi was eluted from the ²²⁵Ac/²¹³Bi generator by NaI/HCl (0.1 mol.L⁻¹/0.1 mol.L⁻¹) in a volume of 600 µL. After elution the column was rinsed and stored with diluted HCl (0.01 mol.L⁻¹) [15].

Standard protocol radiolabelling of ²¹³Bi-DOTATATE

DOTATATE (DOTA-DPhe-Cys-Tyr-DTrp-Lys-Thr-Cys-Thr, *M_w* 1436 g/mol) was purchased from BioSynthema (St. Louis, MO, USA). All chemicals were purchased from Sigma-Aldrich (Zwijndrecht, the Netherlands).

The following standard labelling protocol was applied: ²¹³Bi (600 µL) was added to DOTATATE (7.0 nmol), TRIS buffer (0.34 mol.L⁻¹), ascorbic acid (71 mmol.L⁻¹) and MilliQ water in a final volume 800 µL at pH 8.7. The reaction was incubated for 5 min at 95°C. The radionuclide incorporation reaction was halted by cooling the mixture for 2 min in ice and through the addition of 50 nmol diethylenetriaminepentaacetic acid (DTPA, Erasmus MC Pharmacy) to chelate any unbound or “free” ²¹³Bi.

Labelling optimization for preclinical studies

Standard labelling protocol was used as described above, while varying the following conditions:

1. Peptide mass; labelling was performed with 1.7, 3.5 and 7.0 nmol DOTATATE.
2. pH dependence study; 7.0 nmol DOTATATE was labelled in a reaction containing 71 mmol.L⁻¹ ascorbic acid and 0.15 mol.L⁻¹ and 0.34 mol.L⁻¹ TRIS buffer.
3. Quencher dependence study; in absence of ascorbic acid and 0.1, 0.3, 0.9, 2.6, 7.9, 24 and 71 mmol.L⁻¹ ascorbic acid.

Quality control of radiolabelled peptide

The quality control of labelled peptides was determined by ITLC-SG (instant thin layer chromatography silica gel, Varian) and HPLC (high performance liquid chromatography). Incorporation yield (expressed as mean ± SD) was determined by ITLC using sodium citrate (0.1 mol.L⁻¹, pH 5) as mobile phase. The ²¹³Bi activity was determined by HPGe detector with a pulse height multichannel analysis (MetorX, Goedereede, The Netherlands and Software Genie 2000 Canberra) at fixed geometry, all measurements were performed for the 440 keV γ-emission by ²¹³Bi with a yield of 0.261 per decay. The counting efficiency of the HPGe detector at 440 keV γ-emission was determined using a known amount of ²²⁵Ac activity provided and calibrated by ITU, Germany [15–17].

The RCP (expressed as percentage \pm SD intact radio-peptide of interest, compared to other detectable radioactive compounds in the same analysis) and stability of the labelled peptide as function of time were determined by HPLC. HPLC-grade methanol and trifluoroacetic acid (TFA) were purchased from Mallinckrodt Baker (Deventer, the Netherlands). The HPLC system (Waters 2695 separation module, Alliance, Waters, Etten-Leur, The Netherlands) consisted of a quaternary pump and an autosampler, Waters 2996 photodiode array detector (Waters, Etten-Leur, The Netherlands), radiometric sodium iodide detector (Canberra, Canberra, Genie 2000) and symmetry C_{18} $5\mu\text{m}$ column, $4.6\text{ mm}\times 250\text{ mm}$ (Waters, Etten-Leur, The Netherlands). The mobile phase consisted of buffer A (0.1% TFA in water) and buffer B (Methanol). The gradient used for the analysis was as described earlier [18]. The retention times of the unlabelled DOTATATE and ^{213}Bi -DOTATATE were 12.0 ± 0.3 min and 13.0 ± 0.3 min, respectively.

Dosimetry model of ^{213}Bi exposure in reaction vials

The degradation of radiopharmaceuticals by radiolysis is dependent on the amount of energy absorbed within the ligand. Most of the α -particle energy emitted by ^{213}Bi and its daughter ^{213}Po will be absorbed within the reaction vial with the ^{213}Bi -labelled compound, as their particle ranges in water are smaller than the vial dimensions. The energy emitted by the α - and β -particles from ^{213}Bi itself and its daughters ^{209}Tl and ^{209}Pb , however, will not be completely absorbed within the small vials. The activity as a function of time for ^{213}Bi , ^{213}Po , ^{209}Tl and ^{209}Pb was calculated by the Bateman equations, see Equation 1. The β -emission spectra are summarized in Table 1 together with their ranges in water, from the NIST Star database (<http://www.nist.gov/pml/data/star/>; assessed 27–11-15). The α -particle energies from ^{213}Bi and ^{213}Po are also indicated with their projected ranges as calculated with the Stopping and Range of Ions in Matter (SRIM version 2013.00 software; www.SRIM.org). The recoil energies from the α -particle emissions are 112 keV (^{213}Bi) and 160 keV (^{213}Po) [19].

Table 1, α - and β -particle emissions by ^{213}Bi and its daughters, emission abundances per decay of ^{213}Bi or daughter nuclide and energies are from the MIRD Radionuclide data and decay schemes book (Eckerman, 2008). Particle ranges (mm) in water were determined from the NIST Star database (electrons) and with the SRIM code (α -particles). Abundance (Ab.) is expressed in % decay and energy (E) in MeV

α -particles	Ab. (%/decay)	E (MeV)	range (μm)		
^{213}Bi	1.94	5.87	46.47		
^{213}Po	100	8.38	81.75		
β -particles	Ab. (%/decay)	E_{mean} (MeV)	range (mm)	E_{max} (MeV)	range (mm)
^{213}Bi	97.91	0.434	1.45	1.422	6.65
^{209}Tl	100	0.655	2.55	1.944	9.48
^{209}Pb	100	0.197	0.44	0.644	2.49

Equation 1.

$$\begin{aligned}
A_{Bi}(t) &= A_{Bi}(0) \exp(\lambda_{Bi} t) \\
A_{Po}(t) &= \frac{BR_{Po} \lambda_{Po} A_{Bi}(0)}{\lambda_{Bi} - \lambda_{Po}} (\exp(-\lambda_{Po} t) - \exp(-\lambda_{Bi} t)) \approx BR_{Po} A_{Bi}(0) \exp(-\lambda_{Bi} t) \\
A_{Tl}(t) &= \frac{BR_{Tl} \lambda_{Tl}}{\lambda_{Bi} - \lambda_{Tl}} A_{Bi}(0) (\exp(-\lambda_{Tl} t) - \exp(-\lambda_{Bi} t)) \\
A_{Pb}(t) &= \\
&\frac{BR_{Po} \lambda_{Pb}}{\lambda_{Bi} - \lambda_{Pb}} A_{Bi}(0) \left(\frac{\exp(-\lambda_{Pb} t) - \exp(-\lambda_{Po} t)}{\lambda_{Po} - \lambda_{Pb}} - \frac{\exp(-\lambda_{Pb} t) - \exp(-\lambda_{Bi} t)}{\lambda_{Bi} - \lambda_{Pb}} \right) \\
&- \frac{BR_{Tl} \lambda_{Tl} \lambda_{Pb}}{\lambda_{Bi} - \lambda_{Tl}} A_{Bi}(0) \left(\frac{\exp(-\lambda_{Pb} t) - \exp(-\lambda_{Tl} t)}{\lambda_{Tl} - \lambda_{Pb}} - \frac{\exp(-\lambda_{Pb} t) - \exp(-\lambda_{Bi} t)}{\lambda_{Bi} - \lambda_{Pb}} \right)
\end{aligned}$$

Radiation transport was calculated for ^{213}Bi containing liquid inside reaction vials to determine the absorbed energy and absorbed dose to the hot liquid. The Monte Carlo codes MCNP5 [20] and MCNPX [21] were used for the calculations. Calculations for the α -particles from ^{213}Bi and ^{213}Po were performed with MCNPX using the α -particle energies listed in Table 1. The β -spectra and low-energy internal conversion and Auger electron spectra for ^{213}Bi , ^{209}Tl and ^{209}Pb from MIRD Radionuclide data and decay schemes book [19] were used in MCNP5. Particulate radiation emissions with the given energy spectra were simulated so as to be uniformly distributed within a conical reaction vial with isotropic direction emission. All physics processes were taken into account by choosing either the α (MODE A) or the photon–electron mode (MODE P E) and the default PHYS cards with the default cut-off energy at 1 keV for electrons and photons and 4 MeV for α -particles. The *F8 tally determined energy absorption within the hot reaction fluid. Sufficient particle histories (NPS) were used to reduce the variation in the data to be less than 5% for most cases; NPS was set to 1×10^7 particles. A conically shaped 1 mL reaction vial was modelled with various volumes of radioactive fluid inside the vial. The MCNP-model geometry for a vial containing 0.8 mL liquid is shown in Fig. 1. The labelling volumes were modelled: 10, 50, 100, 200, 400 and 800 μL by adjusting the reaction fluid level accordingly. Average dose rates were determined in the vial volume.

***In vitro* clonogenic assay**

For *in vitro* clonogenic assays the CA20948 cell line (derived from a rat pancreas tumour at our institute Erasmus MC) was used. CA20948 is a rat pancreatic tumour cell line

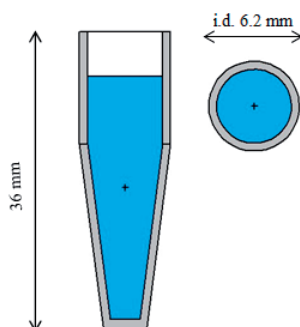


Figure 1, MCNP geometry input for 1 mL reaction vial with 0.8 mL radioactive fluid (in blue), water with density 1 g/mL. The vial wall (in grey) had a thickness of 0.65 mm and was polyethylene with density 0.9 g/mL.

with relative high expression of somatostatin receptor type 2 (SSTR₂), and was cultured in DMEM supplemented with 10% fetal calf serum (FBS, Gibco, Life technologies). Cells (500 cells/well) were seeded in 6-wellplates pre-coated with poly-l-lysine 24 h before exposure to the compounds used for labelling, except for peptide and ^{213}Bi . For clonogenic assay, 400 μL of standard labelling procedure was used, and diluted in 8 mL incubation medium containing 30 mmol.L^{-1} HEPES and 0.25% BSA. The concentration of TRIS, ascorbic acid, NaI, HCl and DTPA corresponded to 16, 3.4, 3.6, 3.6, and 6.1×10^{-3} mmol.L^{-1} , respectively. Cells were incubated with compounds for 1 h at 37°C in a humidified atmosphere of 5% CO_2 and 95% air. Untreated CA20948 cells were used as control. After 1 h, incubation medium containing labelling compounds was removed from cells, cells were washed twice with PBS and incubated with culture medium containing 10% FBS for 12 days. Every 2 or 3 days, culture medium was replaced by fresh medium. At day 12, colonies were fixed with 100% ethanol and stained with hematoxyline. Survival colonies were counted and the survival CA20948 was determined. Clonogenic assay with CA20948 as function of ascorbic acid was also performed with the method described above.

RESULTS

Labelling

The standard labelling protocol ^{213}Bi -DOTATATE resulted in an incorporation > 99% and a RCP > 85% at pH 8.7 for up to 2 h after labelling. The calculated osmolality of the labelling using the standard procedure was 0.7 Osmol.L^{-1} .

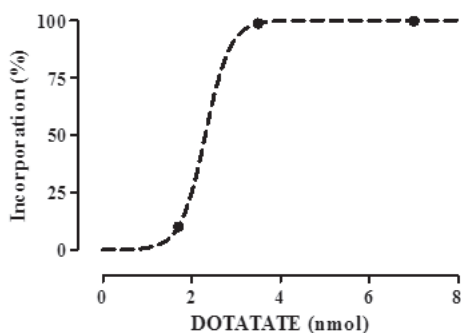


Figure 2, The incorporation (%) of ^{213}Bi -DOTATATE 71 ± 28 MBq determined by ITLC analysis as function of peptide amount in a reaction volume of $800 \mu\text{L}$. An S-shaped curve has been fitted through the data with an incorporation of 50% at 2.4 ± 0.09 nmol and a slope of 0.25 ± 0.03 nmol peptide, $n \geq 3$.

Labelling with 1.7 nmol DOTATATE in $800 \mu\text{L}$ resulted in low incorporation of $6 \pm 4\%$ and poor RCP of $5 \pm 5\%$ (median: 6.9% (range: $0 - 8.6\%$)), see Fig. 2. A high incorporation and high RCP were found when labelled with 3.5 nmol (incorporation was $99 \pm 1\%$, RCP was $89 \pm 4\%$) and 7.0 nmol peptide (incorporation was $99 \pm 1\%$, RCP was $88 \pm 6\%$).

Reducing the amount of TRIS buffer in the labelling did not show an effect on the incorporation of the labelled compound, incorporation of $> 99\%$ and a RCP of $> 85\%$ were found for labelling with 0.15 mol.L^{-1} and 0.34 mol.L^{-1} TRIS, corresponding to pH 8.3 and 8.7, respectively.

After labelling in the presence of ascorbic acid under the standard procedure, an incorporation of $> 99\%$ and a RCP of $> 85\%$ were found, Fig. 3A. Labelling in absence of ascorbic acid however showed a high incorporation of $99 \pm 1\%$ but at poor RCP, $< 5\%$ ^{213}Bi -DOTATATE remained intact after labelling, as shown in the HPLC chromatogram, Fig. 3B.

To decrease the osmolarity ^{213}Bi -DOTATATE labelling, labelling as function of ascorbic acid was performed, it showed that at least 0.9 mmol.L^{-1} ascorbic acid was required to maintain high incorporation and high RCP ($> 85\%$). The labelled peptide showed a RCP $> 85\%$ up to 2 h after labelling. A RCP of $75 \pm 8\%$, $83 \pm 1\%$, $87 \pm 1\%$, $86 \pm 1\%$, $86 \pm 1\%$, $87 \pm 1\%$, $88 \pm 0.4\%$ were found by addition of 0.1 mmol.L^{-1} , 0.3 mmol.L^{-1} , 0.9 mmol.L^{-1} , 2.6 mmol.L^{-1} , 7.9 mmol.L^{-1} , 24 mmol.L^{-1} and 79 mmol.L^{-1} ascorbic acid, respectively. Addition of less than 0.9 mmol.L^{-1} ascorbic acid resulted in high incorporation directly after radiolabelling, however the RCP decreased over time, see Fig. 4.

The adjusted labelling conditions in our experiment were $3.5\text{--}7.0$ nmol peptide, in 0.15 mol.L^{-1} TRIS buffer containing 2.6 mmol.L^{-1} ascorbic acid in a reaction volume of $800 \mu\text{L}$ with 71 ± 28 MBq ^{213}Bi , with a calculated osmolarity of $0.45 \text{ Osmol.L}^{-1}$.

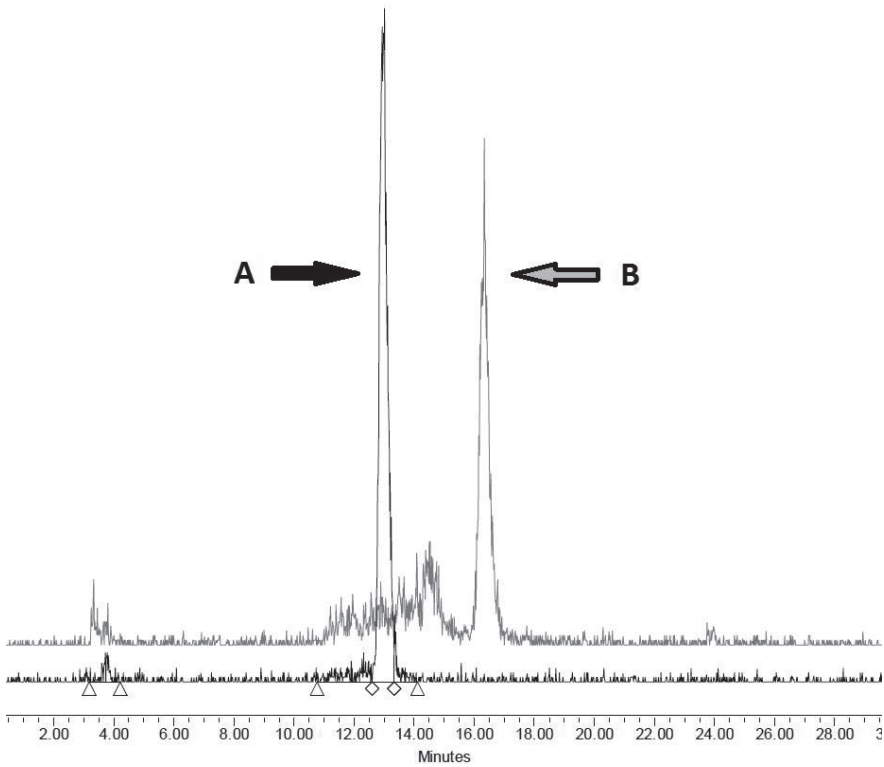


Figure 3, HPLC chromatogram of ^{213}Bi -DOTATATE in presence (A) and absence (B) of ascorbic acid during labelling ($n \geq 3$). Peak A; RT = 13.0 min and peak B; RT = 16.3 min. The y-axis represents the detected radioactive signals (mV) and x-axis represents the RT in minutes.

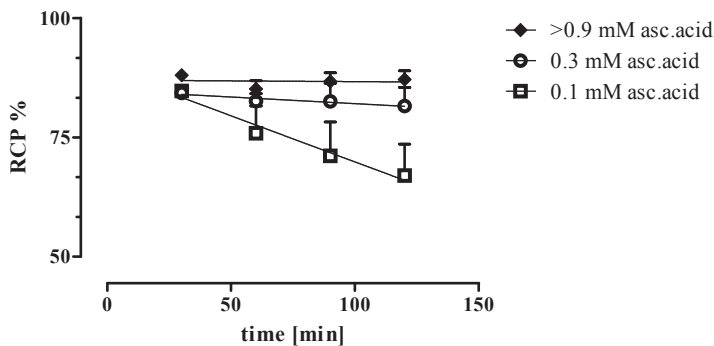


Figure 4, Stability as function of time of ^{213}Bi -DOTATATE with different concentration ascorbic acid added during labelling, y-axis is RCP expressed in mean percentage \pm SD and x-axis time in minutes after labelling ($n \geq 3$).

Dosimetry

The absorbed fraction of energy from the α -particles from ^{213}Bi was almost complete within the reaction fluids, 98.9% for the 10 μL reaction volume and further rose to 99.7% for 800 μL . The higher energy α -particles from ^{213}Po showed a little more energy transfer to the vial wall; 97.2% was absorbed in 10 μL and 99.2% in 800 μL . The absorbed dose rate caused

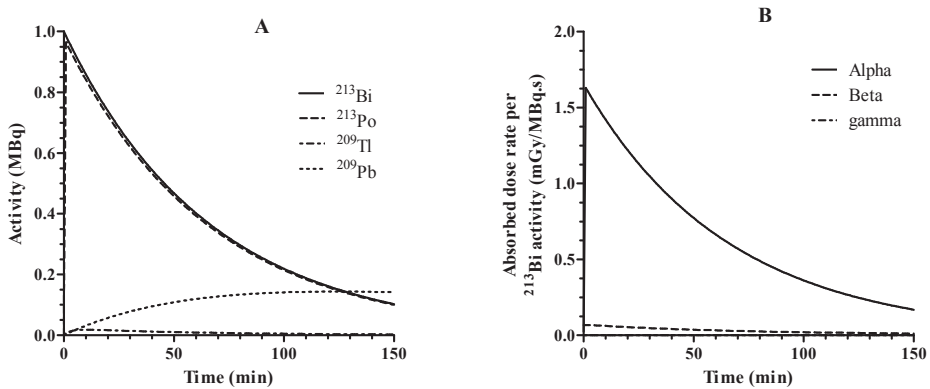


Figure 5, Time-integrated activity of ^{213}Bi , ^{213}Po , ^{209}Tl and ^{209}Pb determined by Bateman equations (A) and the resultant total absorbed dose rate (B) as a function of time, see Table 2. The majority of the absorbed dose rate (96% at 60 min) is caused by the α -particles from ^{213}Bi and ^{213}Po .

Table 2, Absorbed dose rates per unit activity (S-values, in mGy/MBq.s) in the reaction fluid for different volumes of ^{213}Bi , ^{213}Po , ^{209}Tl and ^{209}Pb . The different contributes to the S-value (α , β , low energy electrons and γ -rays) are indicated separately

^{213}Bi	10 μL	50 μL	100 μL	200 μL	400 μL	800 μL
5.97MeV α	1.94	0.39	0.19	0.097	0.049	0.024
β-particles	2.98	0.80	0.44	0.24	0.13	0.066
Auger + IC e^-	0.20	0.048	0.026	0.013	0.0067	0.0034
γ-rays	0.0054	0.0019	0.0012	0.0007	0.0005	0.0003
Total	5.12	1.24	0.67	0.35	0.18	0.094
^{213}Po						
8.38MeV α	130	26.4	13.3	6.6	3.3	1.7
^{209}Tl						
β-particles	3.17	0.94	0.55	0.30	0.17	0.08
Auger + IC e^-	0.36	0.08	0.04	0.02	0.01	0.01
γ-rays	0.04	0.02	0.01	0.01	0.00	0.00
Total	3.57	1.03	0.60	0.33	0.18	0.09
^{209}Pb						
β-particles	2.33	0.53	0.28	0.14	0.07	0.04

by ^{213}Bi , ^{213}Po , ^{209}Tl and ^{209}Pb were predominantly contributed by the α -particles from ^{213}Bi and ^{213}Po , see Fig. 5A. The β -particles and low energy electrons were less absorbed within the reaction fluid, e.g. the absorbed fraction of energy by β -particles from ^{213}Bi ranges from 44% (10 μL) to 77% (800 μL). The relative contribution of the β -particles to the total ^{213}Bi S-value thus raised from 58% to 70%. The absorbed dose rate caused by α -particles (initially 165 $\text{mGy}\cdot\text{s}^{-1}$) continued to be high compared to the absorbed dose rate of β -particles (initially 7 $\text{mGy}\cdot\text{s}^{-1}$), see Fig. 5B.

Based on the absorbed dose rate, see Table 2, the estimated absorbed dose for 100 MBq was > 230 Gy at 30 min in a reaction vial containing 800 μL hot reaction fluid. The absorbed dose was predominantly caused by the decay of α -particles, see Fig. 5B.

Clonogenic assay

In all cells treated in present of ascorbic acid (corresponding to 3.4 $\text{mmol}\cdot\text{L}^{-1}$ in incubation medium), a significant decrease of survival was found compared to control cells, $P < 0.05$, see Fig. 6. Control cell survival was 100% with a standard deviation of 12%. The mean cell survival \pm SD of CA20948 after exposure to ascorbic acid or in combination with TRIS, NaI, HCl and DTPA was listed in Table 3. The concentration of TRIS, NaI, HCl, and DTPA in incubation medium was 16 $\text{mmol}\cdot\text{L}^{-1}$, 3.6 $\text{mmol}\cdot\text{L}^{-1}$, 3.6 $\text{mmol}\cdot\text{L}^{-1}$ and 6.1×10^{-3} $\text{mmol}\cdot\text{L}^{-1}$, respectively.

Reducing the concentration of ascorbic acid during the labelling, resulted in an increase of cell survival, see Fig. 7.

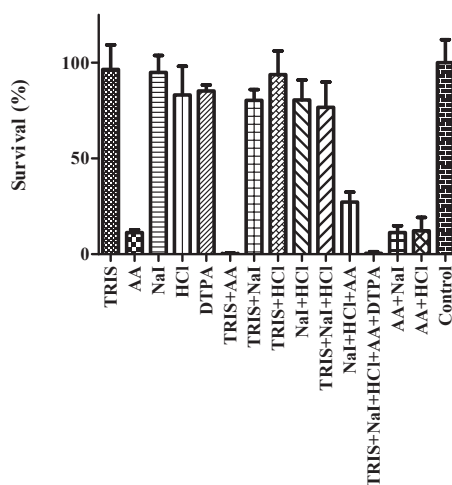


Figure 6, Survival (%) \pm SD of CA20948 after exposing to the compounds used in standard labelling procedure, $n = 3$. Concentration in incubation medium was; [TRIS] = 16 $\text{mmol}\cdot\text{L}^{-1}$, [AA]=ascorbic acid, 3.4 $\text{mmol}\cdot\text{L}^{-1}$, [NaI] = 3.6 $\text{mmol}\cdot\text{L}^{-1}$, [HCl] = 3.6 $\text{mmol}\cdot\text{L}^{-1}$ and [DTPA] = 6.1×10^{-3} $\text{mmol}\cdot\text{L}^{-1}$.

Table 3, CA20948 clonogenic survival in mean percentage \pm SD after exposing to ascorbic acid or in combination with TRIS, NaI, HCl and DTPA, $n=3$. Concentration in incubation medium was; [TRIS]= 16 mmol.L⁻¹, [AA] = ascorbic acid, 3.4 mmol.L⁻¹, [NaI] = 3.6 mmol.L⁻¹, [HCl] = 3.6 mmol.L⁻¹ and [DTPA] = 6.1×10^{-3} mmol.L⁻¹

Compounds	Survival %
AA	11 \pm 1
TRIS+AA	1 \pm 1
NaI+HCl+AA	27 \pm 5
TRIS+NaI+HCl+AA+DTPA	1 \pm 1
AA+NaI	11 \pm 4
AA+HCl	12 \pm 7

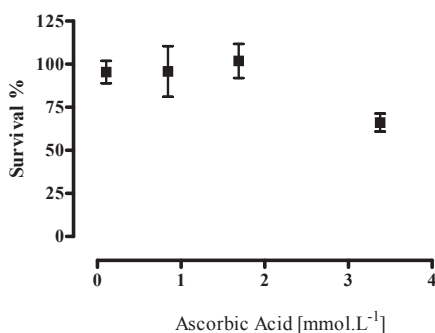


Figure 7, Survival (%) \pm SD of CA20948 as function of concentration of ascorbic acid in DMEM incubation medium containing 30 mM HEPES and 0.25% BSA (total volume was 8.4 mL), $n=3$.

DISCUSSION

A cytotoxic dose within the tumour cells is required to cause a therapeutic effect of TAT, when using a receptor-mediated process as dose delivery method. In the clinical situation using β^- -emitters, this cytotoxic dose is in the order of 200 Gy for neuroendocrine tumours [22, 23] and in the preclinical situation this dose is in the order of 70 Gy for cure of CA20948 (rat pancreatic) tumour [24]. The limited number of receptors available on the cell membrane and relative short half-life of ²¹³Bi however, require radioligands with high SA to obtain a curative tumour dose. The optimal characteristics of radioligands for TAT applications in a preclinical setting include a low injection volume, physiologic osmolarity, high SA, and suitable stability. Labelling with a radionuclide generator yielding relatively low radioactivity is a barrier for high SA radiolabelling.

The most commonly techniques used to increase the SA are purification of the elution by ion-exchange chromatography or by radiolabelling using fractionated elution to reduce the

reaction volume which may improve the reaction kinetics. This may allow high incorporation yield with lower peptide amounts and thus increase the SA of the radio-peptide. To mimic this concept, ^{213}Bi -DOTATATE labelling was performed with half of the elution volume to reach a lower reaction volume (total 400 μL), high incorporation yield was achieved even at reduced amount of peptide, e.g. 1.7 nmol (data not shown).

The most practical method to achieve high SA radiolabelling for preclinical applications is the use of a higher activity $^{225}\text{Ac}/^{213}\text{Bi}$ generator to accomplish the requirements needed for preclinical applications. Purification, e.g. by HPLC or solid phase extraction, might increase the SA. However, introduction of an extra purification step also increases the time interval prior to injection and thus reduces the ^{213}Bi radioactivity. Moreover, HPLC purification often introduces organic compounds e.g. methanol or acetonitrile into the radiolabelling, which might be harmful to animals and limit further translation to clinical studies.

We found a correlation of ascorbic acid on cell survival; at high concentration of ascorbic acid used for labelling (71 mmol.L^{-1} , corresponding to 3.4 mmol.L^{-1} in incubation medium), a significant reduction of cell survival was observed. A lower reduction of cell survival was found with only or in combination with NaI, HCl, TRIS and DTPA compared to control cells, probably caused by the high osmolarity of NaI, HCl, TRIS or Zn-depletion to cells by DTPA [25], however this reduction was not significant. Ascorbic acid, functioning as pro-oxidant, is known to be selectively toxic, especially *in vitro* to certain type of tumour cells at high concentration [26]. C_{18} solid phase extraction can be an option to prevent this by removing ascorbic acid from the labelling reaction. However, radiolysis continues to occur after labelling, and removing ascorbic acid might increase peptide damage caused by radiolysis. After optimizing the labelling conditions, the concentration of ascorbic acid used for labelling (2.6 mmol.L^{-1} , corresponding to 0.13 mmol.L^{-1} in incubation medium) did not interfere with the outcomes of *in vitro* studies, therefore direct application can be performed and no purification steps were required for further *in vitro* and *in vivo* preclinical applications.

In theory, one DOTA-peptide molecule can incorporate one atom ^{213}Bi , thus at a molar ratio of 1 metal vs DOTA, under ideal condition the maximum theoretical SA will be 155 GBq ^{213}Bi /nmol DOTA-peptide. In a study investigating the highest achievable SA, 7.0 nmol DOTATATE was labelled with different mole ratios $^{209/213}\text{Bi}$ using the standard labelling procedure. At mole ratio of 0.6 $^{209/213}\text{Bi}$ vs DOTATATE, the incorporation was $\geq 99\%$. At mole ratio > 0.6 , the incorporation started to decline, possibly caused by the presence of other cations (derived from decay product of ^{213}Bi , quencher, buffer, elution solution) in the labelling reaction which interfered with the incorporation of ^{213}Bi into DOTA-moiety [27, 28]. In theory, a SA of 93 GBq/nmol DOTATATE (at mole ratio ^{213}Bi 0.6) can be achieved under these labelling conditions.

Radiolabelling of ^{213}Bi is less pH-dependent (in the range tested) as is the case of ^{111}In and ^{177}Lu with formation of insoluble $^{111}\text{InOCl}$ or $^{177}\text{LuOCl}$ [29]. Radiolabelling with ^{213}Bi

can be performed at pH values ranging from 4.0 to 10 [7, 30, 31], due to the formation $\text{BiI}_4^-/\text{BiI}_5^{2-}$ after elution with 0.1 M/0.1 M HCl/NaI [15]. However, deprotonation of the carboxyl group of the DOTA appears faster at higher pH and resulting in more rapid radiolabelling kinetics [32, 33].

In this study, we highlighted that ITLC-SG alone as quality control is not sufficient, see labelling in absence and presence of ascorbic acid. HPLC provides beside the incorporation yield also information of peptide damage caused by α -track or radiolysis. The formation of free radicals is dependent on the type of radiation, the amount radioactivity present in the reaction mixture and on the duration of exposure, all of which have been shown to induce radiation damage of the peptide. Quenchers such as gentisic acid in combination with ascorbic acid and ethanol are often used to prevent radiolysis in radiolabelling with ^{111}In or ^{177}Lu [34]. Radiolysis leads to damage of peptide and will decrease the RCP.

With α -radiation more water radicals, such as peroxide, will be formed besides the direct radiation damage from the high LET α -particle tracks [35]. Stanton et al. observed more biological efficacy on SV40 viral DNA *in vitro* caused by low LET compared to high LET and Sugo et al. demonstrated less degradation of TODGA, a tridentate complexing agent, after irradiation with helium ion beam than that by that of γ -ray irradiation [36, 37]. Since the activated radicals are formed along the α -particle tracks and therefore decreasing the probability for damage by both the direct and the radical induced effect in the reaction solution, thus a lower amount of quenchers is required to prevent radical damage to the peptide. In our case, ascorbic acid alone showed sufficient protection capacity to prevent damage to the peptide, so no other quenchers were introduced to the labelling, also to prevent further increase of the osmolarity. Higher osmolarity would require further diluting of the injection matrix for small-animals applications, leading to lower radioactivity injections for effective TAT in small animals.

Here we present detailed results obtained with MCNP calculations of the absorbed dose of ^{213}Bi in the reaction vial. The calculated absorbed dose is an average absorbed dose estimated in a vial of 800 μL , mostly caused by α -particles, but also including doses from β^- -particles and γ -rays emitted by the decay daughters of ^{213}Bi . As shown in Fig. 4, 0.9 $\text{mmol}\cdot\text{L}^{-1}$ ascorbic acid was required to protect the peptide in a vial containing 71 ± 28 MBq in 800 μL , with an absorbed dose of ~ 200 Gy. At higher radioactivities of ^{213}Bi or smaller reaction volumes, more ascorbic acid was required to protect the peptide, since the absorbed dose in the reaction vial increased and formation of radicals also increased. These doses are much lower than the absorbed doses considered to cause radiation damage in DTPA and TODGA, which are in the order of 100 kGy [36, 37]. The main sensitive region for radiation damage will therefore be in the DOTATATE's disulfide bond and its other ionized parts, as the DOTA cage may be considered not to be damaged at the "low" absorbed doses considered.

The activation energy for the DOTA ring inversion process is in the order of 65 kJ/mol [38]. The initial dose rate by the α -radiation in the vial with 100 MBq ^{213}Bi amounts 165 mGy/s, which corresponds to an absorbed energy rate of 0.13 mJ/s in 800 μL with 7 nmol compound, or 19 kJ/mol.s. This indicative calculation shows that the momentary dose rate is on average not energetic enough to create configuration changes within the DOTA ring. The energy of 65 kJ/mol is reached within 3.5 s.

Stability, incorporation yield and SA of ^{213}Bi -labelled peptides are influenced by the affinity/stability of the metal-chelator complex, radiolysis or by the recoil effect both during and after labelling. High LET α -particles cause reactive hydrogen radicals in an aqueous environment [39]. These radicals damage the peptide, which can lead to losses of affinity of the peptide to its receptor. The relative high recoil energy of ^{213}Po , 160 keV, is a critical challenge for the choice of chelator, since complexation of metal and chelator is dependent on the binding energy. This complex should remain stable until reaching the targeted receptor. DOTA (with a Log K of 30.3) is not considered to be the most suitable chelator for ^{213}Bi , due to relative poor labelling kinetics compared to derivatives of DTPA, e.g. CHX-A-DTPA [40, 41]. Nevertheless, we demonstrated that ^{213}Bi formed a highly stable complex with DOTA in a relative short radiolabelling time of 5 min. Furthermore, under optimized radiolabelling conditions, the labelling remained stable up to 2 h after labelling.

CONCLUSION

The optimized ^{213}Bi labelling conditions demonstrated to be suitable for labelling of DOTATATE and proofed ready-to-use for preclinical applications. The labelling procedure presented herein resulted in high incorporation yield, high RCP and high stability up to 2 h after labelling. The addition of quenchers such as ascorbic acid during labelling appeared essential for the protection of the peptide, since the absorbed dose rate within the reaction was high; $> 165 \text{ mGy}\cdot\text{s}^{-1}$ with 100 MBq of ^{213}Bi .

REFERENCES

1. van der Zwan, W.A., et al., *GEPNETs UPDATE: Radionuclide therapy in neuroendocrine tumors*. Eur J Endocrinol, 2015. 172(1): p. R1-R8.
2. Bergsma, H., et al., *Peptide receptor radionuclide therapy (PRRT) for GEP-NETs*. Best Pract Res Clin Gastroenterol, 2012. 26(6): p. 867-81.
3. Bodei, L., et al., *Yttrium-labelled peptides for therapy of NET*. Eur J Nucl Med Mol Imaging, 2012. 39 Suppl 1: p. S93-102.
4. Kratochwil, C., et al., *Dose escalation study of peptide receptor alpha-therapy with arterially administered Bi-213-DOTATOC in GEP-NET patients refractory to beta-emitters*. Eur J Nucl Med Mol Imaging, 2011. 38: p. S207-S207.
5. Jurcic, J.G., et al., *Radiolabeled anti-CD33 monoclonal antibody M195 for myeloid leukemias*. Cancer Res, 1995. 55(23 Suppl): p. 5908s-5910s.
6. Cordier, D., et al., *Targeted alpha-radionuclide therapy of functionally critically located gliomas with 213Bi-DOTA-[Thi8, Met(02)11]-substance P: a pilot trial*. Eur J Nucl Med Mol Imaging, 2010. 37(7): p. 1335-44.
7. Norenberg, J.P., et al., *213Bi-[DOTA0, Tyr3]octreotide peptide receptor radionuclide therapy of pancreatic tumors in a preclinical animal model*. Clin Cancer Res, 2006. 12(3 Pt 1): p. 897-903.
8. Song, H., et al., *213Bi (alpha-emitter)-antibody targeting of breast cancer metastases in the neu-N transgenic mouse model*. Cancer Res, 2008. 68(10): p. 3873-80.
9. Wild, D., et al., *Alpha- versus beta-particle radiopeptide therapy in a human prostate cancer model (213Bi-DOTA-PESIN and 213Bi-AMBA versus 177Lu-DOTA-PESIN)*. Cancer Res, 2011. 71(3): p. 1009-18.
10. Konijnenberg, M.W., *Therapeutic application of CCK2R-targeting PP-F11: influence of particle range, activity and peptide amount*. European Journal of Nuclear Medicine & Molecular Imaging Research, 2014. 4: p. 15.
11. Breeman, W.A., et al., *Somatostatin receptor-mediated imaging and therapy: basic science, current knowledge, limitations and future perspectives*. Eur J Nucl Med, 2001. 28(9): p. 1421-9.
12. Breeman, W.A., et al., *Effect of dose and specific activity on tissue distribution of indium-111-pentetreotide in rats*. J Nucl Med, 1995. 36(4): p. 623-7.
13. de Jong, M., et al., *Tumour uptake of the radiolabelled somatostatin analogue [DOTA0, TYR3]octreotide is dependent on the peptide amount*. Eur J Nucl Med, 1999. 26(7): p. 693-8.
14. Kratochwil, C., et al., *(2)(1)(3)Bi-DOTATOC receptor-targeted alpha-radionuclide therapy induces remission in neuroendocrine tumours refractory to beta radiation: a first-in-human experience*. Eur J Nucl Med Mol Imaging, 2014. 41(11): p. 2106-19.
15. Morgenstern, A., F. Bruchertseifer, and C. Apostolidis, *Bismuth-213 and actinium-225 — generator performance and evolving therapeutic applications of two generator-derived alpha-emitting radioisotopes*. Curr Radiopharm, 2012. 5(3): p. 221-7.
16. Ma, D., et al., *Breakthrough of 225Ac and its radionuclide daughters from an 225Ac/213Bi generator: development of new methods, quantitative characterization, and implications for clinical use*. Appl Radiat Isot, 2001. 55(5): p. 667-78.
17. McDevitt, M.R., et al., *An 225Ac/213Bi generator system for therapeutic clinical applications: construction and operation*. Appl Radiat Isot, 1999. 50(5): p. 895-904.
18. de Blois, E., et al., *Characteristics of SnO2-based 68Ge/68Ga generator and aspects of radiolabelling DOTA-peptides*. Appl Radiat Isot, 2011. 69(2): p. 308-15.
19. Eckerman, K.F., *MIRD*. 2008.
20. MCNP-Team, *The Monte Carlo codes MCNP5*. MCNP5-1.40 RSiCC Release Notes. 2005.
21. Hendricks, J.S., *MCNPX Extensions Version 2.5.0*. MCNPX. Vol. LA-UR-05-2675. 2005.

22. Ilan, E., et al., *Dose response of pancreatic neuroendocrine tumors treated with peptide receptor radionuclide therapy using 177Lu-DOTATATE*. J Nucl Med, 2015. 56(2): p. 177-82.
23. Pauwels, S., et al., *Practical dosimetry of peptide receptor radionuclide therapy with (90)Y-labeled somatostatin analogs*. J Nucl Med, 2005. 46 Suppl 1: p. 92S-8S.
24. Verwijnen, S., et al., *Low-dose-rate irradiation by 131I versus high-dose-rate external-beam irradiation in the rat pancreatic tumor cell line CA20948*. Cancer Biother Radiopharm, 2004. 19(3): p. 285-92.
25. Cho, Y.E., et al., *Cellular Zn depletion by metal ion chelators (TPEN, DTPA and chelex resin) and its application to osteoblastic MC3T3-E1 cells*. Nutr Res Pract, 2007. 1(1): p. 29-35.
26. Park, S., *The effects of high concentrations of vitamin C on cancer cells*. Nutrients, 2013. 5(9): p. 3496-505.
27. Breeman, W.A., et al., *Radiolabelling DOTA-peptides with 68Ga*. Eur J Nucl Med Mol Imaging, 2005. 32(4): p. 478-85.
28. Zhernosekov, K.P., et al., *Processing of generator-produced 68Ga for medical application*. J Nucl Med, 2007. 48(10): p. 1741-8.
29. Breeman, W.A., et al., *Optimising conditions for radiolabelling of DOTA-peptides with 90Y, 111In and 177Lu at high specific activities*. Eur J Nucl Med Mol Imaging, 2003. 30(6): p. 917-20.
30. Hassfjell, S., K.O. Kongshaug, and C. Romming, *Synthesis, crystal structure and chemical stability of bismuth(III) complexed with 1,4,7,10-tetraazacyclododecane-1,4,7,10-tetramethylene phosphonic acid (H8DOTMP)*. Dalton Transactions, 2003(7): p. 1433-1437.
31. Le Gac, S., et al., *Unprecedented incorporation of alpha-emitter radioisotope 213Bi into porphyrin chelates with reference to a daughter isotope mediated assistance mechanism*. Chem Commun (Camb), 2011. 47(30): p. 8554-6.
32. Wu, S.L., K.A. Johnson, and W.D. Horrocks, *Kinetics of formation of Ca2+ complexes of acyclic and macrocyclic poly(amino carboxylate) ligands: Bimolecular rate constants for the fully-deprotonated ligands reveal the effect of macrocyclic ligand constraints on the rate-determining conversions of rapidly-formed intermediates to the final complexes*. Inorganic Chemistry, 1997. 36(9): p. 1884-1889.
33. Szilagy, E., et al., *Equilibria and formation kinetics of some cyclen derivative complexes of lanthanides*. Inorganica Chimica Acta, 2000. 298(2): p. 226-234.
34. de Blois, E., et al., *Effectiveness of quenchers to reduce radiolysis of (111)In- or (177)Lu-labelled methionine-containing regulatory peptides. Maintaining radiochemical purity as measured by HPLC*. Curr Top Med Chem, 2012. 12(23): p. 2677-85.
35. Deutsch, J.C., *Ascorbic acid oxidation by hydrogen peroxide*. Anal Biochem, 1998. 255(1): p. 1-7.
36. Sugo, Y., *Radiolysis study of actinide complexing agent by irradiation with helium ion beam*. Radiation Physics and Chemistry, 2009. 78.
37. Stanton, J., et al., *Protection of DNA from high LET radiation by two OH radical scavengers, tris (hydroxymethyl) aminomethane and 2-mercaptoethanol*. Radiat Environ Biophys, 1993. 32(1): p. 21-32.
38. Lima, L.M., et al., *Investigating the Complexation of the Pb(2+)/Bi(3+) Pair with Dipicolinate Cyclen Ligands*. Inorganic Chemistry, 2015. 54(14): p. 7045-57.
39. Bibler, N.E., *Gamma and alpha radiolysis of aqueous solutions of diethylenetriaminepenta acetic acid*. Journal of inorganic nuclear chemistry, 1972. 34: p. 8.
40. Brechbiel, M.W., *Chelated metal ions for therapeutic and diagnostic applications*. Exp Biol Med (Maywood), 2001. 226(7): p. 627-8.
41. Stavila, V., et al., *Bismuth(III) complexes with aminopolycarboxylate and polyaminopolycarboxylate ligands: Chemistry and structure*. Coordination Chemistry Reviews, 2006. 250(21-22): p. 2782-2810.



Chapter 3

Improved safety and efficacy of ^{213}Bi -DOTATATE-targeted alpha therapy of somatostatin receptor-expressing neuroendocrine tumours in mice pre-treated with L-lysine

Ho Sze Chan, Mark W. Konijnenberg, Tamara Daniels, Monique Nysus, Mehran Makvandi, Erik de Blois, Wouter A. Breeman, Robert W. Atcher, Marion de Jong and Jeffrey P. Norenberg

ABSTRACT

Background:

Targeted alpha therapy (TAT) offers advantages over current β -emitting conjugates for peptide receptor radionuclide therapy (PRRT) of neuroendocrine tumours. PRRT with ^{177}Lu -DOTATATE or ^{90}Y -DOTATOC has shown dose-limiting nephrotoxicity due to radiopeptide retention in the proximal tubules. Pharmacological protection can reduce renal uptake of radiopeptides, e.g. positively charged amino acids, to saturate in the proximal tubules, thereby enabling higher radioactivity to be safely administered. The aim of this preclinical study was to evaluate the therapeutic effect of ^{213}Bi -DOTATATE with and without renal protection using L-lysine in mice. Tumour uptake and kinetics as a function of injected mass of peptide (range: 0.03–3 nmol) were investigated using ^{111}In -DOTATATE. These results allowed estimation of the mean radiation absorbed tumour dose for ^{213}Bi -DOTATATE. Pharmacokinetics and dosimetry of ^{213}Bi -DOTATATE was determined in mice, in combination with renal protection. A dose escalation study with ^{213}Bi -DOTATATE was performed to determine the maximum tolerated dose (MTD) with and without pre-administration of L-lysine as for renal protection. Neutrophil gelatinase-associated lipocalin (NGAL) served as renal biomarker to determine kidney injury.

Results:

The maximum mean radiation absorbed tumour dose occurred at 0.03 nmol and the minimum at 3 nmol. Similar mean radiation absorbed tumour doses were determined for 0.1 nmol and 0.3 nmol with a mean radiation absorbed dose of approximately 0.5 Gy/MBq ^{213}Bi -DOTATATE. The optimal mass of injected peptide was found to be 0.3 nmol. Tumour uptake was similar for ^{111}In -DOTATATE and ^{213}Bi -DOTATATE at 0.3 nmol peptide. Lysine reduced the renal uptake of ^{213}Bi -DOTATATE by 50% with no effect on the tumour uptake. The MTD was $< 13.0 \pm 1.6$ MBq in absence of L-lysine and 21.7 ± 1.9 MBq with L-lysine renal protection, both imparting an LD_{50} mean renal radiation absorbed dose of 20 Gy. A correlation was found between the amount of injected radioactivity and NGAL levels.

Conclusion:

The therapeutic potential of ^{213}Bi -DOTATATE was illustrated by significantly decreased tumour burden and improved overall survival. Renal protection with L-lysine immediately prior to TAT with ^{213}Bi -DOTATATE prolonged survival providing substantial evidence for pharmacological nephron blockade to mitigate nephrotoxicity.

BACKGROUND

Targeted alpha therapy (TAT) has shown great promise in the treatment of both micro-metastatic [1] and large solid tumours in preclinical and clinical studies [2, 3]. Alpha-emitters emit high linear energy transfer (LET) α -particles, each causing dense ion pairs (2000–7000) within a relative short path length (50–100 μm) [3]. The radioactive decay of ^{213}Bi bismuth (^{213}Bi , $T_{1/2} = 46$ min) results in the emission of high-LET α -particles by ^{213}Bi self and by its daughter ^{213}Po around 100 keV/ μm . Due to the relative short half-life of ^{213}Bi , ^{213}Bi can deliver a high radiation dose rate to the target within a relatively short period of time. These physical characteristics make ^{213}Bi , one of the most commonly used α -emitters for medical applications, with demonstrated promise as TAT in preclinical studies, *in vivo* imaging, and in clinical treatment of cancer patients [1, 4, 5].

Peptide receptor radionuclide therapy (PRRT) with radiolabelled somatostatin analogues is commonly employed in patients with inoperable neuroendocrine tumours (NETs) overexpressing somatostatin receptors subtype 2 (SSTR₂). Current radiopeptides include; ^{177}Lu -[DOTA⁰,Tyr³]octreotate (^{177}Lu -DOTATATE) and ^{90}Y -[DOTA⁰,Tyr³]octreotide (^{90}Y -DOTATOC). Its efficacy depends on the radiation absorbed dose delivered to the tumour, which depends on SSTR₂ targeting efficiency, clearance kinetics, perfusion, distribution, and tumour mass. High-specific activity radiopeptides are required to deliver adequate radiation absorbed dose to tumours, as the mass of injected peptide is limited by the high affinity but low capacity of SSTR₂-expression systems. The mass of injected peptide influences the pharmacokinetics (PK) and absorbed doses in organs and tumours [6]. Therefore, the mass of injected peptide should be optimized to deliver efficacious tumour doses while avoiding toxic absorbed dose to organs, especially to the dose-limiting organs the kidneys and bone marrow [7, 8].

Radiolabelled somatostatin analogues are known to accumulate in the renal proximal tubules, due to their net charge, electrostatic forces, and charge distribution from metal-chelation [9, 10]. This can result in a high absorbed dose and subsequent renal dysfunction. Co-infusion of L-lysine/L-arginine has been shown to reduce renal uptake in patients receiving ^{177}Lu -DOTATATE or ^{177}Lu -DOTATOC PRRT by 30–50% [11].

Several preclinical studies showed that TAT with ^{213}Bi resulted in high renal accumulation of radioactivity [12], causing nephrotoxicity and decreased survival without renal protection compared to animals receiving protection [13, 14]. Evidence of acute or chronic interstitial nephritis was found in a previous dose escalation study in AR42J tumour-bearing rats using ^{213}Bi -DOTATOC [2]. Nephrotoxicity was observed to be moderate in a clinical trial of ^{213}Bi -DOTATOC, in combination with renal protection, in patients' refractory to ^{177}Lu -DOTATATE or ^{90}Y -DOTATOC PRRT [3]. Conventional approaches to determine kidney function use serum creatinine, or nuclear medicine imaging with $^{99\text{m}}\text{Tc}$ -MAG3 or $^{99\text{m}}\text{Tc}$ -DSMA. However, these approaches are suboptimal to detect early-stage kidney disease.

Several renal biomarkers are commercially available to determine acute or chronic kidney injury [15]. However, those biomarkers have not yet been applied in PRRT for detection of nephrotoxicity. Neutrophil gelatinase-associated lipocalin (NGAL) is among the promising renal biomarkers for detection of acute or chronic kidney injury in humans with high specificity and sensitivity [16]. Therefore, NGAL is an interesting renal biomarker to study nephrotoxicity caused by TAT with ^{213}Bi .

This study aimed to determine the suitability of ^{213}Bi -DOTATATE for TAT. Administration of ^{213}Bi -DOTATATE was optimized for *in vivo* applications in AR42J tumour-bearing mice. The rat AR42J tumour is known to express SSTR₂ at high density; this model is commonly used for investigations using somatostatin analogues and PRRT. Additionally, investigations were performed on increasing ^{213}Bi -DOTATATE's efficacy by using L-lysine as a renal protectant, radiation dosimetry to determine the mean radiation absorbed dose to the tumour and kidney, the resultant dose-effect relation, and a pilot study to evaluate NGAL as a kidney injury biomarker.

MATERIALS AND METHODS

^{213}Bi -DOTATATE labelling

^{213}Bi was eluted from a $^{225}\text{Ac}/^{213}\text{Bi}$ generator (Oak Ridge National Laboratory) with 0.1 M/0.1 M HCl/NaI. The resultant elution containing ^{213}Bi (630–740 MBq) was used for labelling with 10 μg DOTATATE (BioSynthema) in a reaction vial including 0.15 M TRIS buffer and 2.6 mM ascorbic acid at pH 8.4. The reaction was incubated for 5 min at 95°C, cooled to ambient temperature for 2 min before adding 50 mM DTPA [17]. Instant Thin-Layer Chromatography (ITLC-SG, Varian) was performed using 0.9% NaCl as mobile phase to determine the radionuclide-peptide incorporation yield. High-Performance Liquid Chromatography (HPLC, Agilent) was performed to determine the radiochemical purity (RCP) of ^{213}Bi -DOTATATE, being defined as percentage of intact radiopeptide of interest compared to other detectable radioactive compounds in the same HPLC analysis. HPLC was performed using a reverse phase C₁₈ column (JT Baker, Bakerbond®, 4.6x250 mm) eluted with 0.1% TFA and methanol [18].

^{111}In -DOTATATE labelling

$^{111}\text{InCl}_3$ (GE Healthcare) was added to a vial containing 0.03, 0.1, 0.3, 1, or 3 nmol DOTATATE. $^{115}\text{In}(\text{NO}_3)_3$ (0.01 g/L, ICP standard) was added to form a 1:1 M ratio reaction to peptide and NaOAc 4 M was used to adjust the pH to 4–5. The reaction was heated at 80°C for 20 min and cooled to ambient temperature for 5 min before addition of DTPA (50 mM) to incorporate potential free $^{111}\text{In}^{3+}$. Incorporation yields of the labelled peptide were evaluated as described previously.

Animal model

Athymic male nu/nu mice (Tachonic), 6–8 weeks old, were used in all studies. Tumour models were established by inoculating 5×10^6 rat pancreatic tumour AR42J cells (American Type Culture Collection) with high SSTR₂ expression into the right hind flank of the animals. After 3 weeks, the tumour size reached approximately 200 mm³. All animal experiments were carried out following Institutional Animal Care and Use Committee-approved protocol.

Comparison of biodistribution profiles of ¹¹¹In-DOTATATE and ²¹³Bi-DOTATATE

AR42J tumour-bearing animals were used for the comparison of the uptake of ¹¹¹In-DOTATATE versus (vs.) ²¹³Bi-DOTATATE in different organs and tumours. Biodistribution assays were performed with either ¹¹¹In-DOTATATE or ²¹³Bi-DOTATATE (0.3 nmol, n = 3/cohort). Animals were euthanized 10 and 60 min post-injection (p.i.) by CO₂ asphyxiation. Blood samples were collected and the following organs were harvested and counted in a γ -counter (Perkin Elmer): tumour, blood, heart, adrenals, kidneys, stomach without content, pancreas, liver, testicles, urinary bladder, femur, femur marrow, pituitary, and muscles. The uptake was expressed as percentage of injected activity per gram of tissue (%IA/g). The actual weight of all organs was used to calculate %IA/g.

Biodistribution ¹¹¹In-DOTATATE

Xenograft AR42J nu/nu mice were used to determine PK as a function of injected mass of peptide (n = 4/cohort). Animals were injected intravenously (i.v.) via the tail vein with 0.03, 0.1, 0.3, 1, or 3 nmol (corresponding to 2×10^{-3} , 7×10^{-3} , 0.02, 0.07, and 0.22 mg/kg, respectively) of ¹¹¹In-DOTATATE (range 0.6–2.9 MBq). Animals were euthanized by CO₂ asphyxiation at 3, 10, 30, and 60 min p.i. Blood samples, organs, and femur-containing femur marrow were harvested and counted as described previously. The uptake was expressed as percentage of injected activity per gram of tissue (%IA/g).

The effect of L-lysine on the biodistribution of ²¹³Bi-DOTATATE in tumour and nontumour-bearing mice

Twenty AR42J tumour-bearing mice, 200 mm³ tumour volume, were injected intraperitoneally (i.p.) with or without (w/wo) 35 mg/200 μ L L-lysine (L-lysine monohydrochloride) 2–10 min prior to ²¹³Bi-DOTATATE administration i.v. (1–3 MBq/0.3 nmol). Mice were euthanized at 10 min and 60 min p.i. In a parallel study, 20 nontumour-bearing mice were injected i.p. w/wo L-lysine (35 mg/200 μ L) 2–10 min prior to ²¹³Bi-DOTATATE (1–3 MBq/0.3 nmol) administration and were euthanized at 10 and 60 min p.i. (n = 5/cohort). Blood, organs, and femur-containing femur marrow were collected and counted as described previously. The uptake was expressed as percentage of injected activity per gram of tissue (%IA/g).

Toxicity and therapeutic efficacy of ^{213}Bi -DOTATATE

Toxicity and therapeutic efficacy were investigated in 18 animals ($n=6/\text{cohort}$): control, low-dose (cumulative 16.8 ± 1.3 MBq), and high-dose (cumulative 33.1 ± 3.7 MBq) cohorts. Treatment started 23 days after xenograft inoculation. Control mice received in total 4×0.3 nmol DOTATATE on two consecutive days. Two injections of 0.3 nmol DOTATATE per day were given, with a time interval of at least 6 h. The low-dose cohort received two doses of ^{213}Bi -DOTATATE on two consecutive days, one dose of 8.3 ± 1.0 MBq/0.3 nmol ^{213}Bi -DOTATATE each day. The high-dose cohort received four doses on two consecutive days, twice a day with a time interval of at least 6 h. Per dose, ^{213}Bi -DOTATATE contained 8.3 ± 1.0 MBq/0.3 nmol ^{213}Bi -DOTATATE. Animals were monitored for 30 days starting on the day of treatment. Tumours were measured by caliper, and animals were weighed at least twice weekly. The endpoints chosen were weight loss $> 15\%$ and tumour volume > 2000 mm³. At 30 days post-treatment, blood samples were obtained for hematological analysis according to the standard operating procedures for clinical laboratory samples for creatinine, CBC, WBC, RBC, Hgb, Hct, MCV, MCHC, platelets, neutrophils, lymphocytes, monocytes, eosinophils, and basophils. Survival analysis was plotted according to the Kaplan-Meier fit model.

Tumour volume $V(t)$ as a function of time was modeled according to the exponential growth function $V(t) = V_0 \times e^{kt}$, with k the growth constant, related to the doubling time T_d by $k = \frac{\ln(2)}{T_d}$. Each individual mouse $V(t)$ in the control group was fitted with the exponential growth function to enable extrapolation of the growth beyond the time when the tumour volume exceeded the maximum. An average control growth curve was obtained by using the mean of the volume data together with the extrapolated growth data to the time points of the last surviving animal. Fitting was also performed for the therapy group with an exponential growth function, where the initial growth rate k_0 slowed down or turned into shrinkage with rate $k_0 - k_1$ at onset time point T_0 of therapy effect. Regrowth was modeled by exponential growth with rate $k_0 - k_1 + k_2$, setting in after the volume nadir time point T_1 . This led to the function $V(t) = V_0 \times e^{k_0 t} \times \max_{t > T_1} e^{-k_1(t-T_1)} \times \max_{t > T_2} e^{k_2(t-T_2)}$. The regrowth doubling time T_{rd} was derived from $T_{rd} = \frac{\ln(2)}{k_0 - k_1 + k_2}$.

Maximum tolerated dose (MTD) of ^{213}Bi -DOTATATE in nontumour-bearing mice in combination of L-lysine

MTD was defined as the highest dose given to the animals allowing 100% survival with no significant weight loss $> 15\%$ throughout the experiment. Nontumour-bearing mice were randomly divided into seven cohorts used to evaluate MTD; six treatments and one control ($n=8/\text{cohort}$); see Table 1. Cohorts(+) received i.p. injections of L-lysine (35 mg/200 μL) at 2–10 min prior to ^{213}Bi -DOTATATE administration via i.v. tail vein. Control mice received DOTATATE (4×0.3 nmol) on four consecutive days. The animals were followed for 90 days. Serum was analyzed for the biomarker neutrophil gelatinase-associated lipocalin (NGAL) using ELISA (R&D Systems, 450 nm). Survival analysis was plotted according to the Kaplan-Meier fit model.

Table 1, ^{213}Bi -DOTATATE toxicity study in nontumour-bearing animals with or without pre-injection of L-lysine (35 mg), $n=8/\text{cohort}$. Control animals received 4×0.3 nmol DOTATATE ($n=8$). MTD= maximum tolerated dose

MTD study in nontumour-bearing animals in combination with L-lysine			
Cohort	^{213}Bi -DOTATATE (MBq)	L-lysine	Days of injection
low-dose(-)	13.0 ± 1.6	-	2
low-dose(+)	13.2 ± 0.9	+	2
medium-dose(-)	20.7 ± 0.8	-	3
medium-dose(+)	21.7 ± 1.9	+	3
high-dose(-)	28.7 ± 1.2	-	4
high-dose(+)	28.3 ± 0.8	+	4
control	0		4

Pharmacokinetics

Saturation of receptor-specific tumour uptake was investigated by determining the kinetics of the tumour uptake with increasing injected mass of peptide. The time-activity curves for the tumour and normal organs were fitted by single-exponential functions using Prism-5 (GraphPad). Goodness of fit was analyzed with the Pearson correlation coefficient $R^2 > 0.8$. Both F-test and the Aikake information criterion were used to decide on the complexity of the curves.

Radiation Dosimetry

Cumulated radioactivity in the tumour and normal organs were estimated by integrating the time-activity curves fitted to the ^{111}In -DOTATATE biodistribution data and folded with the decay curve of ^{213}Bi and its daughters. Dosimetry was performed according to the MIRD schema by using the spherical nodes S-factors from the Olinda/EXM software [19]. S-factors were interpolated from the actual weight of the organs and tissue. All organs and tissue were assumed to be spherical with a density of 1 kg/m^3 . Mean radiation absorbed doses were obtained as a function-injected mass of peptide, assuming a homogeneous distribution in the tumour and organs. The mean radiation absorbed dose obtained included the cumulative dose of α , β and γ from all daughters of ^{213}Bi . Owing to the short path length of α -particles, only the self-dose within each organ was included. The threshold for lethality was determined with renal absorbed dose and injected activity as indicators. Logistic regression analysis was used to determine the LD_{50} for presumed renal toxicity-related death.

Statistics

Data analyses, graphs and calculations were performed in Prism-5. Mann-Whitney t -test was used to calculate the significance. The results of statistical tests were considered significant when P was < 0.05 . Biodistribution data were expressed as mean \pm standard

deviation (SD) and tumour volume data as mean \pm standard error (SEM). Binary logistic analysis (forced entry method) was performed with SPSS software (IBM SPSS statistics, version 20).

RESULTS

Radiolabelling

The radiolabelling incorporation yield of ^{213}Bi -DOTATATE was $\geq 95\%$ and RCP was $\geq 85\%$; the incorporation yield of ^{111}In -DOTATATE was $\geq 95\%$.

Biodistribution of ^{111}In -DOTATATE as function of injected mass of peptide and time

In animals injected with < 0.3 nmol ^{111}In -DOTATATE, higher tumour uptake was observed than in animals injected with > 0.3 nmol, Fig. 1A-1F. At lower injected mass of peptide (0.03, 0.1 and 0.3 nmol), tumour uptake increased as function of time. At > 0.3 nmol of injected peptide, the uptake of ^{111}In -DOTATATE was more uniform and low compared to < 0.3 nmol of injected peptide, indicating the receptors on the tumours were partially saturated by the injected masses of unlabelled peptide. Renal uptake was higher compared to other organs for all injected mass of peptide at all time points, except for tumour. Organs uptake of 0.03–3 nmol mass of injected peptide are indicated in supplemental data, Table S1–5.

Decreased absorbed tumour doses from ^{213}Bi -DOTATATE as a function of increased of injected mass of peptide was predicted based on the ^{111}In -DOTATATE uptake data. The mean radiation absorbed tumour dose ranged between, 0.66 Gy/MBq ^{213}Bi -DOTATATE at 0.03 nmol peptide and 0.19 Gy/MBq ^{213}Bi -DOTATATE at 3 nmol peptide; see Fig. 1F. A comparable mean radiation absorbed dose of 0.50 Gy/MBq was found for 0.1 and 0.3 nmol peptide.

Biodistribution of ^{111}In -DOTATATE vs. ^{213}Bi -DOTATATE

Tumour uptake of ^{213}Bi -DOTATATE compared to ^{111}In -DOTATATE was $5.3 \pm 2.8\%$ IA/g vs. $6.3 \pm 1.3\%$ IA/g at 10 min p.i., respectively ($P=0.70$). Similar results were observed at 60 min p.i.: $6.5 \pm 2.3\%$ IA/g vs. $6.0 \pm 1.2\%$ IA/g, respectively ($P=1.0$).

Renal activity at 60 min p.i. for ^{213}Bi -DOTATATE was significantly higher than that of ^{111}In -DOTATATE: $17.4 \pm 2.2\%$ IA/g and $10.9 \pm 0.6\%$ IA/g, respectively ($P=0.0022$). ^{111}In -DOTATATE was retained in the pancreas at 10 and 60 min p.i., whereas ^{213}Bi -DOTATATE radioactivity in plasma was higher at 60 min p.i. and uptake in pituitary was higher at 10 and 60 min p.i. All other organs showed similar uptakes for ^{111}In -DOTATATE and ^{213}Bi -DOTATATE at 10 min and 60 min p.i., see Fig. 2.

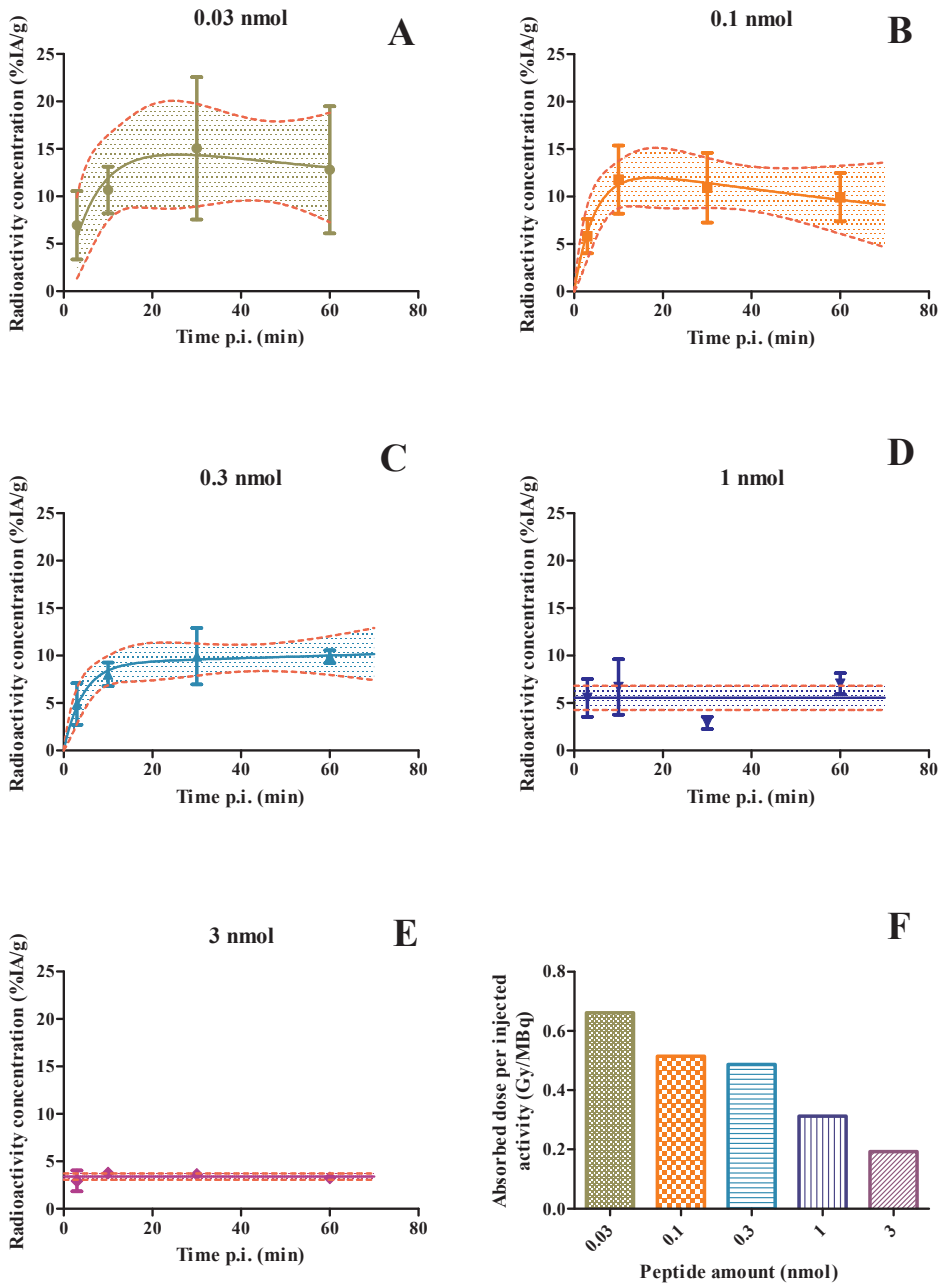


Figure 1A-E, Tumour uptake of ^{111}In -DOTATATE as function of time and injected mass of peptide (0.03–3 nmol, $n=4$ /cohort). The uptake was expressed as percentage of injected activity per gram of tissue (%IA/g). 1F, Predicted absorbed tumour dose of ^{213}Bi -DOTATATE was based on ^{111}In -DOTATATE tumour biodistribution results.

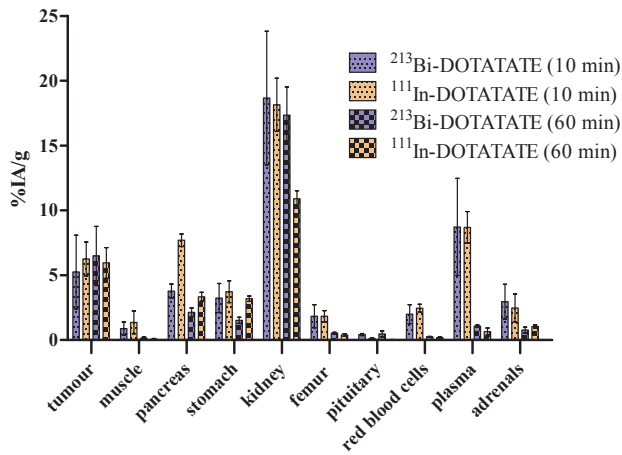


Figure 2, Comparative biodistributions (%IA/g±SD) after i.v. administration of ^{213}Bi -DOTATATE vs. ^{111}In -DOTATATE (0.3 nmol peptide, $n=3/\text{cohort}$) at 10 min and 60 min p.i. in AR42J tumour-bearing mice. The uptake was expressed as percentage of injected activity per gram of tissue (%IA/g).

Biodistribution of ^{213}Bi -DOTATATE; influence of L-lysine

Figure 3 shows the uptake of ^{213}Bi -DOTATATE with or without L-lysine pre-injection in different organs and tissues in tumour-bearing and nontumour-bearing animals. Lower renal uptake was observed in tumour-bearing mice receiving L-lysine prior to administration of ^{213}Bi -DOTATATE versus mice without L-lysine (10 min p.i.; $21.3 \pm 8.1\% \text{IA/g}$ vs. $30.8 \pm 5.8\% \text{IA/g}$ and 60 min p.i.; $5.7 \pm 1.1\% \text{IA/g}$ vs. $18.4 \pm 1.8\% \text{IA/g}$ ($P < 0.0001$)).

No differences in tumour uptake were found in animals w/wo L-lysine pretreatment. However, at 60 min p.i., a significant difference in stomach uptake was found in tumour-bearing animals with and without L-lysine; $0.9 \pm 0.1\% \text{IA/g}$ versus $1.6 \pm 0.5\% \text{IA/g}$, $P=0.0079$. Figure 3 shows the uptake of ^{213}Bi -DOTATATE w/wo L-lysine pre-injection in different organs in tumour- and nontumour-bearing animals.

In tumour-bearing animals receiving L-lysine, the renal absorbed dose was 0.56 Gy/MBq vs. 1.1 Gy/MBq without L-lysine. In nontumour-bearing animals, the renal absorbed dose was 0.50 Gy/MBq with L-lysine versus 1.0 Gy/MBq without L-lysine, see estimated mean radiation absorbed dose in supplemental data Table S6.

Pharmacodynamics of ^{213}Bi -DOTATATE in AR42J tumour-bearing animals

Tumour volumes significantly decreased in mice treated with low-dose ($16.8 \pm 1.3 \text{ MBq}$) and high-dose ($33.1 \pm 3.7 \text{ MBq}$) ^{213}Bi -DOTATATE. Tumour regression was observed in both ^{213}Bi -DOTATATE cohorts. Tumour regrowth was delayed until 21 ± 9 days p.i. in animals treated with low-dose ^{213}Bi -DOTATATE; see Fig. 4A. One animal in the low-dose showed a weight loss of $> 15\%$ at day 27 post-treatment. Dramatic weight loss was observed in the

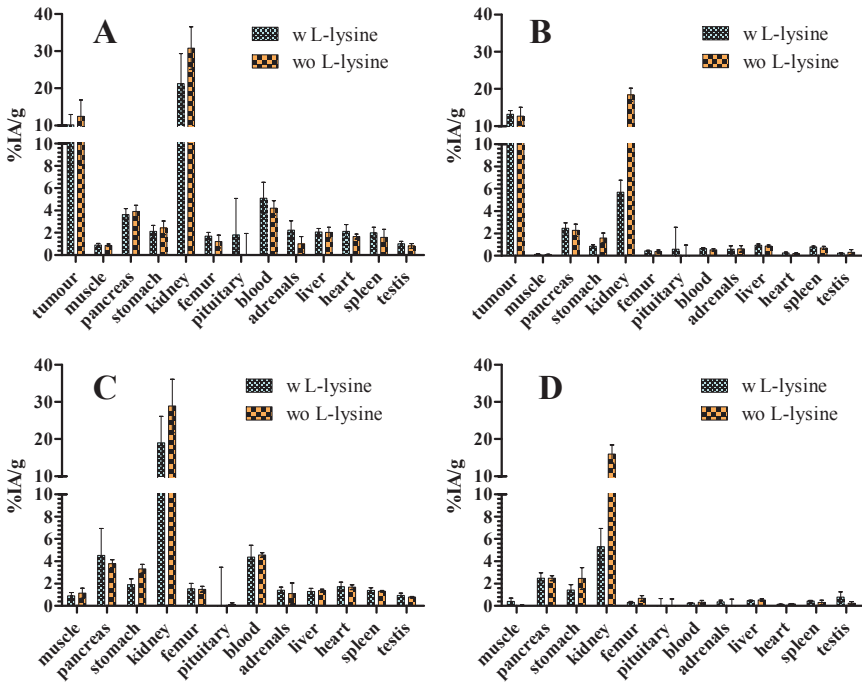


Figure 3, Biodistribution comparison of ²¹³Bi-DOTATATE (0.3 nmol) with (w) or without (wo) L-lysine (35 mg) pre-injection. 3A) AR42J tumour-bearing animals 10 min p.i. 3B) AR42J tumour-bearing animals 60 min p.i. 3C) nontumour-bearing animals 10 min p.i. 3D) nontumour-bearing animals 60 min p.i., n = 5. The uptake was expressed as percentage of injected activity per gram of tissue (%IA/g).

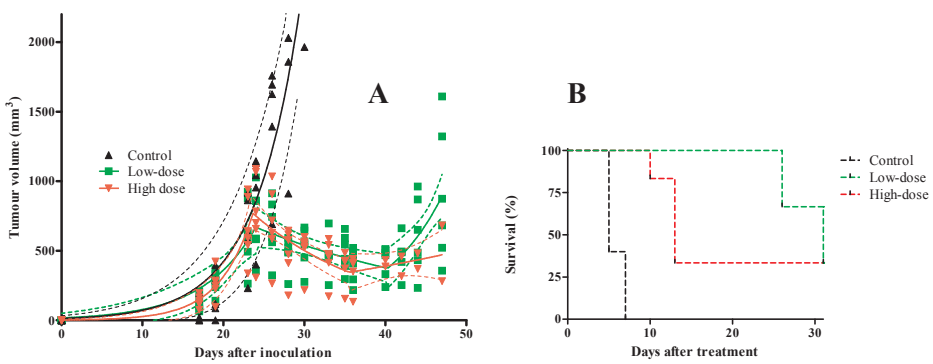


Figure 4A, Tumour growth in mice before and after injection of DOTATATE in control animals (4×0.3 nmol DOTATATE) and ²¹³Bi-DOTATATE at different concentration, in low-dose cohort (16.8 ± 1.3 MBq) and high-dose cohort (33.1 ± 3.7 MBq). Treatment started 23 days after inoculation of AR42J cells. The solid line indicates the extrapolated fit calculated for tumour growth, and dotted lines indicate the 95% confidence interval for the fit. **4B**, Survival of AR42J-bearing animals after ²¹³Bi-DOTATATE therapy. Low-dose animals received 16.8 ± 1.3 MBq ²¹³Bi-DOTATATE, high-dose 33.1 ± 3.7 MBq, and control 4×0.3 nmol DOTATATE on 2 consecutive days.

high-dose cohort within 14 days post-treatment, necessitating euthanasia of 67% of the animals; see Fig. 4B. Therefore, tumour regrowth doubling time in the high-dose cohort was not determined. The tumour doubling time in the control was 4.0 ± 0.2 days and both the initial growth and regrowth patterns in the therapy cohorts proceeded with similar doubling times. A median survival of 5 days was found in the control, > 30 days in the low-dose, and 13 days in the high-dose, see Fig. 4B. The tumour growth in one animal of the control cohort showed an unusual growth pattern; therefore the data of this animal was excluded from the calculation of the tumour doubling time and survival analysis.

Animals in the high-dose cohort showed significantly ($P = < 0.05$) elevated hemoglobin (Hgb) and hematocrit (Hct) values compared to the low-dose (Hgb (g/dL) 51 ± 7 vs. 39 ± 3 ; and Hct (%) 16 ± 2 vs. 12 ± 1).

MTD in nontumour-bearing mice administration w/wo L-lysine

Renal protection using L-lysine prior to ^{213}Bi -DOTATATE administration resulted in prolonged survival for both the medium-dose(+) (21.7 ± 1.9 MBq) and high-dose(+) cohorts (28.3 ± 0.8 MBq), Fig. 5. Medium- and high-dose cohorts without L-lysine showed reduced survival rates compared to medium- and high-dose cohorts pre-treated with L-lysine. No animals in high dose(-) cohort survived beyond 40 days following treatment. No significant difference in survival was observed following low-dose administration of ^{213}Bi -DOTATATE with or without L-lysine ($P = 0.32$) or medium-dose with or without L-lysine ($P = 0.06$). Weight loss was observed in cohorts treated with medium-dose(-), high-dose(-) and high-dose(+) cohorts.

At 90 days post-treatment, all control animals survived. A survival rate of 87.5% was found in the low-dose(-) cohort, 62.5% in the medium-dose(-) and 0% in high-dose(-), Fig. 5A.

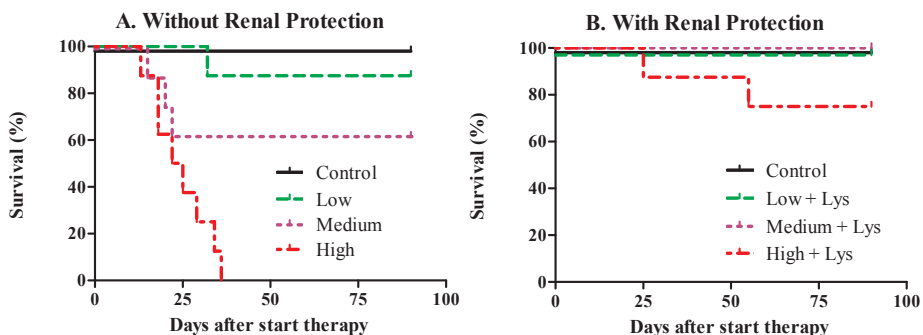


Figure 5A-B, Survival percentage after ^{213}Bi -DOTATATE therapy without (-) or with (+) L-lysine (35 mg) pre-injection in nontumour-bearing mice; cohort low-dose(-) received cumulatively 13.0 ± 1.6 MBq, low-dose(+) 13.2 ± 0.9 MBq, medium-dose(-) 20.7 ± 0.8 MBq, medium-dose(+) 21.7 ± 1.9 MBq, high-dose(-) 28.7 ± 1.2 MBq and high-dose(+) 28.3 ± 0.8 MBq ($n = 8$ /cohort). Control animals received 4×0.3 nmol DOTATATE ($n = 8$).

Cohorts receiving L-lysine pre-treatment, Fig. 5B, a very high survival rate was observed: 100% in the low-dose(+) and 100% in the medium-dose(+). In the high-dose(+) cohort, 75% of the animals survived. A median survival of > 90 days was found in control and all cohorts except the high-dose without L-lysine (median survival of 24 days, $P=0.0012$). By integrating the radioactivity over time in the kidney, data obtained from biodistribution study w/wo pre-treatment of L-lysine, a time-integrated activity coefficient (expressed as min/g tissue) of 6.0 ± 2.4 min/g in mice pre-treated with L-lysine and 12.0 ± 3.7 min/g in mice without pre-treatment of L-lysine was found. Based on logistic regression analysis, a LD_{50} of 20 ± 8 Gy was found; see Fig. 6. The number of mice that were euthanized within 90 days was indicated as a function of renal absorbed dose obtained from both biodistribution studies w/wo L-lysine.

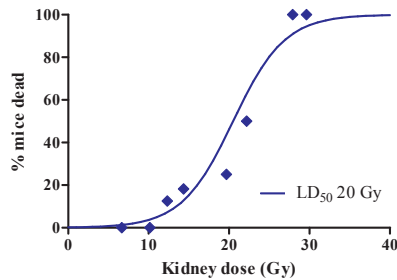


Figure 6, Dose-effect relation between mean renal radiation absorbed dose and the percentage of mice that died before the end of the experiment at 90 days. LD_{50} kidney dose was 20 ± 8 Gy, a threshold $LD_5 = 11 \pm 4$ Gy ($P < 0.001$). All points represent at least three mice.

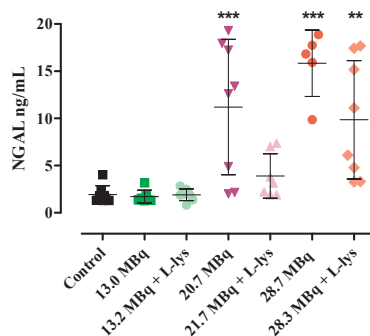


Figure 7, NGAL (ng/mL±SEM) level in control and ^{213}Bi -DOTATATE-treated cohorts with (+) or without (-) pre-treatment of L-lysine (35 mg). Cohort low-dose(-) received cumulatively 13.0 ± 1.6 MBq, low-dose(+) 13.2 ± 0.9 MBq, medium-dose(-) 20.7 ± 0.8 MBq, medium-dose(+) 21.7 ± 1.9 MBq, high-dose(-) 28.7 ± 1.2 MBq and high-dose(+) 28.3 ± 0.8 MBq. Control animals received 4×0.3 nmol DOTATATE. ** P value < 0.01 and *** P value < 0.001 versus control values.

The highest NGAL level was found in the high-dose(-) cohort, 15.8 ± 3.5 ng/mL. Whereas the NGAL level of control, low-dose cohort w/wo L-lysine was the lowest, 1.9 ± 0.9 , 1.9 ± 0.6 and 1.7 ± 0.7 ng/mL, respectively. A significant difference in NGAL level was found in medium-dose(-), high-dose(-), and high-dose(+) vs. control; see Fig. 7.

DISCUSSION

In this preclinical study, TAT with ^{213}Bi -DOTATATE was systematically studied to understand the injected mass of peptide-dependent uptake, radioactivity-related toxicity, and reduction in tumour burden. ^{111}In had already been used as a surrogate for ^{213}Bi earlier in other preclinical studies [20, 21]. We demonstrated ^{111}In is an appropriate surrogate radionuclide for *in vivo* preclinical studies of PK in tumours allowing the results obtained from ^{111}In to be used for ^{213}Bi -dosimetry calculation. Both ^{213}Bi and ^{111}In form highly stable complexes with DOTA-somatostatin analogues, including DOTATATE, and show similar affinities for SSTR₂ in tumour.

For PRRT, it is essential to determine the optimal injected mass of radioligand by defining PK of radiopeptides in animal models, given that the injected mass of radioligand influences tumour uptake, the resultant radiation absorbed dose, and eventually the efficacy of the therapy. Moreover, increasing the injected mass of radioligand can diminish the pharmacological selectivity by binding to other SSTR-positive organs [22], which is not beneficial in the case of TAT and may cause off-target toxicities. The optimal injected mass of ^{111}In -OctreoScan[®] to obtain the best signal to background ratio for tumour versus other organs was reported as 0.07 nmol in mice (3.5 pmol/g mice) [23]. De Jong *et al.* showed a “bell-shape” curve for dependent tumour uptake in AR42J tumour-bearing rats as a function of injected mass of peptide, where 0.4 nmol ^{111}In -DOTATOC (1.8 pmol/g rat) gave the maximum tumour uptake [24].

In this study, the highest absorbed tumour dose (0.66 Gy/MBq) was found at injected mass of peptide of 0.03 nmol (1.07 pmol/g mice). However, lower and more practical specific activity (MBq/nmol) ^{213}Bi -DOTATATE, 0.3 nmol (10.7 pmol/g mice) was chosen for the administration in this study allowing sufficient tumour uptake to realize therapeutic effects. A similar mean radiation absorbed dose of ^{213}Bi -DOTATATE was determined for 0.1 and 0.3 nmol injected mass of peptide, as the tumour uptakes as function of time of both 0.1 and 0.3 nmol peptide were similar.

^{111}In -DOTATATE is not an appropriate surrogate of ^{213}Bi -DOTATATE to determine renal uptake as a significant difference was observed at 60 min p.i. between ^{111}In -DOTATATE and ^{213}Bi -DOTATATE. With an absence of SSTR₂ receptors in the kidney, the high renal uptake is not related to SSTR expression. The renal uptake of the labelled peptide is thought to be influenced by the difference in the electrostatic charge of DOTA-complex with ^{111}In and

^{213}Bi [9, 10, 25], leading to different interactions with megalin or cubilin [26]. Furthermore, $^{213}\text{Bi}^{3+}$ is known to bind strongly to metallothionein in the kidneys [27], which might lead to a high renal uptake. Apart from high renal uptake, a significantly higher uptake was also found in the pituitary and a higher radioactivity level in plasma. The pituitary gland is a very small organ. During organ harvesting, a systematic uncertainty is introduced by the chance to include surrounding tissue in the weight used for the uptake per gram calculation, resulting to an under- or overestimation of pituitary uptake, which might explain our findings. The high renal uptake and slow clearance rate of ^{213}Bi -DOTATATE indicates tubular reabsorption of ^{213}Bi -DOTATATE; this might be the cause of higher radioactivity in plasma as well. ^{111}In -DOTATATE showed a slightly significantly higher uptake than ^{213}Bi -DOTATATE in pancreas tissue, as yet we do not have an explanation for this difference.

In this study, we were not able to examine the differences in PKs of these radiopharmaceuticals in pituitary, plasma and pancreas, due to the small number of animal per group and limited time points.

Despite the differences in PK profiles of ^{111}In -DOTATATE and ^{213}Bi -DOTATATE in some organs and tissues, ^{111}In -DOTATATE still showed to be a proper substitute for tumour uptake, since the PK profile of the tumour uptake was similar to that of ^{213}Bi -DOTATATE. However, the use of a surrogate radionuclide should to be carefully chosen, since each alternate radionuclide has limitations.

Weight loss in animals is often an indicator of toxicity, and the most radiosensitive organs for PRRT are the bone marrow and kidney [8, 28, 29]. In this study, we observed severe weight loss in 67% of animals exposed to high-dose ^{213}Bi -DOTATATE (cumulative 33.1 ± 3.7 MBq), within 2 weeks after treatment, indicating acute toxicity. This might be explained by the high renal uptake resulting in a high renal absorbed dose, which increased the risk of acute nephrotoxicity due to limited sublethal damage tissue repair. To investigate acute renal toxicity, a short-term toxicity study over 90 days was performed instead of a follow-up period over 6–12 months, which is commonly performed to investigate long-term chronic nephrotoxicity. A significant reduction of renal activity (50%) was found in animals pre-treated with L-lysine in this study. Our findings indicate that pre-treatment with L-lysine improved survival of animals receiving medium- and high-dose ^{213}Bi -DOTATATE resulting from the reduction of renal activity. Song *et al.* showed in their study a threefold reduction in renal activity following lysine pre-treatment [13]. This result differs significantly from our findings but might be attributed to their method of lysine application used during the therapy procedures, rather than immediately prior. Kobayashi *et al.* demonstrated that the kidney uptake was influenced by the timing of L-lysine administration [30], such that renal blocking by L-lysine was maximized when i.p. administration of L-lysine was given immediately before administration of the radiolabelled of anti-Tac murine MoAb fragment. In our study, we have chosen to start the therapy 2–10 min after i.p. administration of L-lysine to protect the kidneys, since DOTATATE is a relative small molecule and

rapidly cleared from the blood. Radioactivity in the blood or uptake of the bone marrow is generally used as an indicator for myelotoxicity. Pre-administration of L-lysine did not significantly affect the radioactivity measured in neither whole blood nor femur uptake in tumour-bearing mice. The mean radiation absorbed dose for whole blood and femur (see supplemental data) was 3.3 Gy and 1.3 Gy in mice with pre-treatment of L-lysine in the high-dose cohort, whereas without L-lysine, these values were 2.7 and 1.0 Gy. These absorbed doses were lower than the MTD of 25 MBq ^{213}Bi -DOTA-AMBA in PC3-tumour bearing mice, corresponding to the MTD at a mean absorbed dose of 4 Gy in the blood [31]. Therefore, we concluded the bone marrow is not a limiting organ in our study.

The LD₅₀ found for the renal absorbed dose was 20 Gy in this study. Acute renal toxicity at 100–140 Gy was reported by Behr *et al.*, after administration of ^{90}Y -fab fragments, leading to death of all mice within 2–3 weeks [32]. This corresponds to our observation in cohorts after high-dose ^{213}Bi -DOTATATE administration, with more than 90% of the animals dead at radiation absorbed dose > 28 Gy. Hence, the relative biological effect (RBE) was 4–5 for acute renal toxicity, leading to death within 2–3 weeks, when comparing the absorbed doses in both studies. This estimate for the RBE for ^{213}Bi -DOTATATE appears to be comparable to the RBE value of 4 used for delayed renal toxicity by Song *et al.* [13]. Specific uptake in functional units of the kidney might cause changes in radiation absorbed doses to radiation-sensitive structures like the glomeruli that could result in less damage than predicted from whole-organ radiation dosimetry. Small-scale micro-dosimetry using the sub-organ model of Hobbs *et al.* [33] indicates a possible lowering of the absorbed dose to the glomeruli when ^{213}Bi is taken up in the proximal tubules by 44% in comparison to homogeneous uptake in the mouse cortex assuming equal kinetics. We found no indication for this sparing effect; otherwise, the RBE would be in the order of 6–8. A direct comparative study would be needed to determine both the RBE and the PK of ^{213}Bi - and ^{90}Y or ^{177}Lu labelled peptides inside the kidneys and its functional units.

In this pilot study, NGAL was used as a biomarker to evaluate late-stage renal changes after therapy. NGAL is sensitive to acute kidney injury (AKI) for detection of renal functions in early nephrotoxicity state [16, 34]. No nephrotoxicity was found in the low-dose(-) and low-dose(+) cohorts, corresponding to another study done using similar injected mass of radioactivity (MBq) ^{213}Bi -DOTATATE as TAT in nude mice in two different tumour models wherein nephrotoxicity was investigated by $^{99\text{m}}\text{Tc}$ -DMSA as a kidney marker [35]. Overall, NGAL levels were lower in mice pre-treated with L-lysine than mice without pre-treatment at similar dose of ^{213}Bi -DOTATATE. However, no significant difference was found between those cohorts, which might be explained since NGAL was measured day 90 after TAT, whereby some repair and recovery of the kidney might already occur. Furthermore, the mean renal absorbed dose for the medium-dose(-) and the high-dose(+) cohorts was 23 Gy and 16 Gy, respectively. These absorbed doses were similar to the calculated renal LD₅₀, at which 50% of the treated animals would develop acute nephrotoxicity. The sigmoid

dose-effect curve for renal toxicity (Fig. 6) shows a steep slope, contributing to a great variation in NGAL values observed at absorbed doses just above and below the LD₅₀ value. In this study, NGAL proved to be a valuable tool to examine AKI for TAT using ²¹³Bi as radionuclide supporting its use in future investigations of nephrotoxicity caused by ²¹³Bi. The use of NGAL as a biomarker of nephrotoxicity is feasible and cost effective compared to conventional approaches to determine renal functionality in preclinical studies. Creatinine, the most commonly used parameter to determine kidney injury, lacks the ability to evaluate kidney injury at early stages following PRRT. ^{99m}Tc-MAG3 and ^{99m}Tc-DMSA for preclinical applications are invasive, by the use of high radioactivity for imaging, and require additional data extraction and analysis. In addition to NGAL, kidney injury molecule-1 (KIM-1) and cystatine-C are promising biomarkers for both acute and chronic kidney disease [15]. The ability to study early and late kidney injury is essential in TAT, using a combination of both conventional methods and these commercially available biomarkers could provide more information leading to more understanding of the underlying mechanisms involved in kidney injury after TAT.

CONCLUSION

²¹³Bi-DOTATATE showed therapeutic effects to reduce tumour size and prolong survival. Potential nephrotoxicity caused by ²¹³Bi-DOTATATE was overcome by pre-treatment with L-lysine. ²¹³Bi-DOTATATE with L-lysine pre-treatment shows promise as TAT of SSTR₂-expressing tumours. The biomarker NGAL offers a new approach to study nephrotoxicity following TAT.

SUPPLEMENTAL DATA

Table S1, Biodistribution data in AR42J tumour-bearing nude mice. Uptake at 3, 10, 30 and 60 min p.i. and expressed in percentage injected activity per gram tissue (%IA/g) after ^{111}In -DOTATATE (0.03 nmol, 1.07 pmol/g) administration (n = 4/cohort)

^{111}In-DOTATATE (0.03 nmol) uptake (%IA/g) in organs as function of time post injection				
Organs	3 min	10 min	30 min	60 min
Tumour	6.9 ± 3.6	10.7 ± 2.5	15.1 ± 7.5	12.8 ± 6.7
Muscles	1.2 ± 0.7	0.9 ± 0.3	0.3 ± 0.1	0.07 ± < 0.05
Pancreas	6.0 ± 1.5	1.6 ± 1.4	4.7 ± 2.7	9.2 ± 1.9
Stomach	5.6 ± 0.7	7.9 ± 2.2	8.1 ± 1.3	7.6 ± 1.1
Kidney	19.2 ± 8.4	16.0 ± 4.1	14.0 ± 4.1	12.3 ± 3.7
Pituitary	1.0 ± 1.7	0.2 ± 0.2	0.5 ± 0.8	< 0.05
Red blood cell	3.5 ± 2.5	1.7 ± 0.5	0.6 ± 0.2	0.3 ± 0.08
Plasma	13.3 ± 1.6	8.2 ± 1.6	3.2 ± 1.0	0.8 ± 0.1
Adrenals	2.7 ± 1.6	3.4 ± 2.3	4.7 ± 4.4	4.6 ± 5.6

Table S2, Biodistribution data in AR42J tumour-bearing nude mice. Uptake at 3, 10, 30 and 60 min p.i. and expressed in percentage injected activity per gram tissue (%IA/g) after ^{111}In -DOTATATE (0.1 nmol, 3.6 pmol/g mice) administration (n = 4/cohort)

^{111}In-DOTATATE (0.1 nmol) uptake (%IA/g) in organs as function of time post injection				
Organs	3 min	10 min	30 min	60 min
Tumour	2.8 ± 1.8	11.8 ± 3.6	10.9 ± 3.6	9.9 ± 2.6
Muscles	1.5 ± 0.6	0.7 ± 0.2	0.4 ± 0.4	0.3 ± 0.4
Pancreas	11.9 ± 4.0	9.9 ± 4.2	7.0 ± 1.4	4.7 ± 0.5
Stomach	4.4 ± 1.1	5.2 ± 1.1	6.3 ± 2.0	6.0 ± 1.8
Kidney	21.6 ± 3.9	15.6 ± 3.1	16.1 ± 5.5	16.7 ± 8.6
Pituitary	0.3 ± 0.2	0.2 ± 0.09	0.1 ± 0.2	< 0.05
Red blood cell	5.2 ± 0.7	1.7 ± 0.5	0.8 ± 0.4	0.2 ± 0.1
Plasma	13.2 ± 1.7	8.6 ± 1.4	3.4 ± 1.7	1.0 ± 0.6
Adrenals	2.1 ± 0.6	1.9 ± 0.3	2.1 ± 0.7	1.3 ± 0.2

Table S3, Biodistribution data in AR42J tumour-bearing nude mice. Uptake at 3, 10, 30 and 60 min p.i. and expressed in percentage injected activity per gram tissue (%IA/g) after ^{111}In -DOTATATE (0.3 nmol, 10.7 pmol/g mice) administration (n=4/cohort)

^{111}In-DOTATATE (0.3 nmol) uptake (%IA/g) in organs as function of time post injection				
Organs	3 min	10 min	30 min	60 min
Tumour	4.9 ± 2.2	8.0 ± 1.2	9.9 ± 3.0	9.9 ± 0.7
Muscles	1.1 ± 0.1	0.5 ± 0.1	0.3 ± 0.1	< 0.05
Pancreas	4.9 ± 0.7	3.5 ± 0.3	3.2 ± 0.4	3.0 ± 1.0
Stomach	4.5 ± 0.8	3.9 ± 0.4	3.5 ± 0.2	3.4 ± 0.8
Kidney	17.2 ± 5.4	12.8 ± 2.2	16.9 ± 6.3	13.4 ± 2.8
Pituitary	0.3 ± < 0.05	0.2 ± 0.05	0.1 ± < 0.05	< 0.05
Red blood cell	2.6 ± 0.6	1.3 ± 0.4	0.6 ± 0.1	< 0.05
Plasma	13.4 ± 1.4	7.2 ± 2.0	3.4 ± 0.5	0.7 ± 0.2
Adrenals	2.3 ± 0.6	1.2 ± 0.4	1.0 ± 0.1	0.8 ± 0.3

Table S4, Biodistribution data in AR42J tumour-bearing nude mice. Uptake at 3, 10, 30 and 60 min p.i. and expressed in percentage injected activity per gram tissue (%IA/g) after ^{111}In -DOTATATE (1 nmol, 35.7 pmol/g mice) administration (n=4/cohort)

^{111}In-DOTATATE (1 nmol) uptake (%IA/g) in organs as function of time post injection				
Organs	3 min	10 min	30 min	60 min
Tumour	5.6 ± 2.0	6.7 ± 2.9	2.9 ± 0.6	7.0 ± 1.1
Muscles	1.2 ± 0.4	1.0 ± 0.5	0.2 ± 0.09	< 0.05
Pancreas	3.5 ± 2.4	1.9 ± 1.0	0.7 ± 0.2	1.5 ± 0.3
Stomach	2.4 ± 1.1	1.7 ± 0.6	0.8 ± 0.2	1.8 ± 0.6
Kidney	17.5 ± 9.7	14.2 ± 7.0	6.0 ± 1.8	14.1 ± 3.4
Pituitary	0.1 ± 0.09	0.8 ± 1.4	< 0.05	< 0.05
Red blood cell	2.3 ± 0.4	1.3 ± 0.5	0.3 ± 0.1	0.4 ± 0.1
Plasma	11.3 ± 4.9	7.6 ± 3.1	1.4 ± 0.5	0.6 ± 0.2
Adrenals	1.4 ± 0.7	1.8 ± 1.1	0.5 ± 0.09	0.5 ± 0.05

Table S5, Biodistribution data in AR42J tumour-bearing nude mice. Uptake at 3, 10, 30 and 60 min p.i. and expressed in %IA/g after ^{111}In -DOTATATE (3 nmol, 107 pmol/g mice) administration (n = 4/cohort)

^{111}In-DOTATATE (3 nmol) uptake (%IA/g) in organs as function of time post injection				
Organs	3 min	10 min	30 min	60 min
Tumour	2.9 ± 1.1	3.8 ± 0.3	3.6 ± 0.2	3.3 ± 0.3
Muscles	1.3 ± 0.3	0.8 ± 0.3	0.3 ± 0.1	< 0.05
Pancreas	2.2 ± 0.4	1.6 ± 0.2	1.0 ± 0.2	0.8 ± 1.0
Stomach	3.2 ± 0.5	2.3 ± 0.2	1.5 ± 0.6	1.6 ± 0.7
Kidney	19.1 ± 3.1	14.6 ± 2.9	14.5 ± 1.1	14.7 ± 2.1
Pituitary	0.2 ± 0.06	0.1 ± 0.06	0.08 ± 0.06	< 0.05
Red blood cell	4.3 ± 1.9	2.4 ± 0.3	0.6 ± 0.2	< 0.05
Plasma	13.8 ± 1.7	8.4 ± 0.9	2.8 ± 0.7	0.6 ± 0.2
Adrenals	1.9 ± 0.7	1.1 ± 0.7	0.6 ± 0.2	0.3 ± 0.06

Table S6. Calculated total radiation absorbed dose after ²¹³Bi-DOTATATE (in Gy/MBq) with or without L-lysine (35 mg) in tumour-bearing mice, including the radiation dose caused by ²¹³Bi daughters in different organs, the contribution to the dose by α -particles and by β -particles ($+\gamma$) is indicated separately.

Organs	Radiation absorbed dose per administered activity (Gy/MBq) with or without L-lysine												
	With L-lysine					Without L-lysine							
	²¹³ Bi	²¹³ Po	²⁰⁹ Tl	²⁰⁹ Pb	Total	²¹³ Bi	²¹³ Po	²⁰⁹ Tl	²⁰⁹ Pb	Total			
	α	β	α	$\beta + \gamma$	β	α	β	α	β	α	β		
Tumour	9.20E-03	2.87E-02	6.05E-01	8.60E-04	1.41E-02	6.14E-01	4.40E-02	9.90E-03	3.14E-02	6.51E-01	1.58E-02	6.61E-01	4.80E-02
Pancreas	2.00E-03	4.50E-03	1.34E-01	1.00E-04	8.90E-04	1.36E-01	5.00E-03	2.00E-03	4.50E-03	1.32E-01	1.00E-04	7.00E-04	1.34E-01
Stomach	9.00E-04	2.60E-03	6.00E-02	7.00E-05	2.20E-04	6.10E-02	3.00E-03	1.30E-03	3.90E-03	8.84E-02	1.10E-04	5.90E-04	9.00E-02
Kidney	8.00E-03	2.37E-02	5.25E-01	6.30E-04	1.40E-03	5.33E-01	2.60E-02	1.61E-02	4.71E-02	1.06E+00	1.30E-03	6.20E-03	1.07E+00
Adrenals	8.00E-04	1.80E-03	5.49E-02	4.00E-05	1.30E-04	5.60E-02	2.00E-03	5.00E-04	1.50E-03	3.56E-02	2.00E-05	2.00E-04	3.60E-02
Femur	6.00E-04	1.60E-03	4.13E-02	4.00E-05	1.00E-04	4.20E-02	2.00E-03	5.00E-04	1.30E-03	3.16E-02	3.00E-05	1.00E-04	3.20E-02
Blood	1.60E-03	5.20E-03	1.08E-01	1.40E-04	2.00E-04	1.09E-01	6.00E-03	1.30E-03	4.30E-03	8.80E-02	1.20E-04	1.60E-04	9.00E-02

REFERENCES

1. Jurcic, J.G., *Antibody therapy of acute myelogenous leukemia*. Cancer Biother Radiopharm, 2000. 15(4): p. 319-26.
2. Norenberg, J.P., et al., *²¹³Bi-[DOTA0, Tyr3]octreotide peptide receptor radionuclide therapy of pancreatic tumors in a preclinical animal model*. Clin Cancer Res, 2006. 12(3 Pt 1): p. 897-903.
3. Kratochwil, C., et al., *(²¹³Bi)-DOTATOC receptor-targeted alpha-radionuclide therapy induces remission in neuroendocrine tumours refractory to beta radiation: a first-in-human experience*. Eur J Nucl Med Mol Imaging, 2014. 41(11): p. 2106-19.
4. de Swart, J., et al., *Utilizing high-energy gamma photons for high-resolution ²¹³Bi SPECT in mice*. J Nucl Med, 2015.
5. Morgenstern, A., F. Bruchertseifer, and C. Apostolidis, *Bismuth-213 and actinium-225 — generator performance and evolving therapeutic applications of two generator-derived alpha-emitting radioisotopes*. Curr Radiopharm, 2012. 5(3): p. 221-7.
6. Kletting, P., et al., *Differences in predicted and actually absorbed doses in peptide receptor radionuclide therapy*. Med Phys, 2012. 39(9): p. 5708-17.
7. Bodei, L., et al., *Long-term evaluation of renal toxicity after peptide receptor radionuclide therapy with ⁹⁰Y-DOTATOC and ¹⁷⁷Lu-DOTATATE: the role of associated risk factors*. Eur J Nucl Med Mol Imaging, 2008. 35(10): p. 1847-56.
8. Bergsma, H., et al., *Subacute haematotoxicity after PRRT with (¹⁷⁷Lu)-DOTA-octreotate: prognostic factors, incidence and course*. Eur J Nucl Med Mol Imaging, 2016. 43(3): p. 453-63.
9. Froidevaux, S., et al., *Neuroendocrine tumor targeting: study of novel gallium-labeled somatostatin radiopeptides in a rat pancreatic tumor model*. Int J Cancer, 2002. 98(6): p. 930-7.
10. Lazniczek, M. and A. Laznickova, *Different radioactivity uptake between somatostatin analogues labelled with (¹¹¹In) and (⁹⁰Y) in rat kidney*. Anticancer Res, 2012. 32(3): p. 815-22.
11. Rolleman, E.J., et al., *Molecular imaging of reduced renal uptake of radiolabelled [DOTA0,Tyr3] octreotate by the combination of lysine and Gelifusine in rats*. Nuklearmedizin, 2008. 47(3): p. 110-5.
12. Szymanska, J.A., E.M. Mogilnicka, and B.W. Kaszper, *Binding of bismuth in the kidneys of the rat: the role of metallothionein-like proteins*. Biochem Pharmacol, 1977. 26(3): p. 257-8.
13. Song, E.Y., et al., *Pharmacokinetics and toxicity of (²¹³Bi)-labeled PAI2 in preclinical targeted alpha therapy for cancer*. Cancer Biol Ther, 2007. 6(6): p. 898-904.
14. Behr, T.M., et al., *High-linear energy transfer (LET) alpha versus low-LET beta emitters in radioimmunotherapy of solid tumors: therapeutic efficacy and dose-limiting toxicity of ²¹³Bi- versus ⁹⁰Y-labeled CO17-1A Fab' fragments in a human colonic cancer model*. Cancer Res, 1999. 59(11): p. 2635-43.
15. Wasung, M.E., L.S. Chawla, and M. Madero, *Biomarkers of renal function, which and when?* Clin Chim Acta, 2015. 438: p. 350-7.
16. Bolignano, D., et al., *Neutrophil gelatinase-associated lipocalin (NGAL) as a marker of kidney damage*. Am J Kidney Dis, 2008. 52(3): p. 595-605.
17. Chan, H.S., et al., *Optimizing labelling conditions of ²¹³Bi-DOTATATE for preclinical applications of peptide receptor targeted alpha therapy*. EJNMMI Radiopharmacy and Chemistry 2016. 1(9).
18. de Blois, E., et al., *Characteristics of SnO₂-based ⁶⁸Ge/⁶⁸Ga generator and aspects of radiolabelling DOTA-peptides*. Appl Radiat Isot, 2011. 69(2): p. 308-15.
19. Stabin, M.G. and M.W. Konijnenberg, *Re-evaluation of absorbed fractions for photons and electrons in spheres of various sizes*. J Nucl Med, 2000. 41(1): p. 149-60.

20. Song, H., et al., *Targeting aberrant DNA double-strand break repair in triple-negative breast cancer with alpha-particle emitter radiolabeled anti-EGFR antibody*. *Mol Cancer Ther*, 2013. 12(10): p. 2043-54.
21. Dadachova, E., *Radioimmunotherapy of infection with Bi-labeled antibodies*. *Curr Radiopharm*, 2008. 1(3): p. 234-239.
22. Breeman, W.A., et al., *Effect of dose and specific activity on tissue distribution of indium-111-pentetreotide in rats*. *J Nucl Med*, 1995. 36(4): p. 623-7.
23. Ten Bokum, A.M., et al., *Tissue distribution of octreotide binding receptors in normal mice and strains prone to autoimmunity*. *Nucl Med Commun*, 2002. 23(10): p. 1009-17.
24. de Jong, M., et al., *Tumour uptake of the radiolabelled somatostatin analogue [DOTA0, Tyr3] octreotide is dependent on the peptide amount*. *Eur J Nucl Med*, 1999. 26(7): p. 693-8.
25. Jaggi, J.S., et al., *Renal tubulointerstitial changes after internal irradiation with alpha-particle-emitting actinium daughters*. *J Am Soc Nephrol*, 2005. 16(9): p. 2677-89.
26. Verroust, P.J. and E.I. Christensen, *Megalyn and cubilin—the story of two multipurpose receptors unfolds*. *Nephrol Dial Transplant*, 2002. 17(11): p. 1867-71.
27. Sun, H., et al., *Interactions of bismuth complexes with metallothionein(II)*. *J Biol Chem*, 1999. 274(41): p. 29094-101.
28. Bodei, L., et al., *Peptide receptor radionuclide therapy for advanced neuroendocrine tumors*. *Thorac Surg Clin*, 2014. 24(3): p. 333-49.
29. Kwekkeboom, D.J., et al., *Treatment with the radiolabeled somatostatin analog [177 Lu-DOTA 0, Tyr3]octreotate: toxicity, efficacy, and survival*. *J Clin Oncol*, 2008. 26(13): p. 2124-30.
30. Kobayashi, H., et al., *L-lysine effectively blocks renal uptake of I-125- or Tc-99m-labeled anti-Tac disulfide-stabilized Fv fragment*. *Cancer Res*, 1996. 56(16): p. 3788-3795.
31. Wild, D., et al., *Alpha- versus beta-particle radiopeptide therapy in a human prostate cancer model (213Bi-DOTA-PESIN and 213Bi-AMBA versus 177Lu-DOTA-PESIN)*. *Cancer Res*, 2011. 71(3): p. 1009-18.
32. Behr, T.M., et al., *Overcoming the nephrotoxicity of radiometal-labeled immunoconjugates: improved cancer therapy administered to a nude mouse model in relation to the internal radiation dosimetry*. *Cancer*, 1997. 80(12 Suppl): p. 2591-610.
33. Hobbs, R.F., et al., *A nephron-based model of the kidneys for macro-to-micro alpha-particle dosimetry*. *Phys Med Biol*, 2012. 57(13): p. 4403-24.
34. Devarajan, P., *Neutrophil gelatinase-associated lipocalin—an emerging troponin for kidney injury*. *Nephrol Dial Transplant*, 2008. 23(12): p. 3737-43.
35. Chan, H.S., et al., *Influence of tumour size on the efficacy of targeted alpha therapy with (213) Bi-[DOTA(0), Tyr(3)]-octreotate*. *EJNMMI Res*, 2016. 6(1): p. 6.

4

Chapter 4

Influence of tumour size on the efficacy of targeted alpha therapy with ^{213}Bi -[DOTA⁰,Tyr³]-octreotate

Ho Sze Chan, Mark W. Konijnenberg, Erik de Blois, Stuart Koelewijn, Richard P. Baum, Alfred Morgenstern, Frank Bruchertseifer, Wouter A. Breeman, Marion de Jong

EJNMMI Research. 2016; 6(1):6

ABSTRACT

Background:

Targeted alpha therapy has been postulated to have great potential for the treatment of small cluster of tumour cells as well as small metastases. ^{213}Bi Bismuth, an α -emitter with a half-life of 46 min, has shown to be effective in pre-clinical as well as in clinical applications. In this study we evaluated, whether ^{213}Bi -[DOTA⁰, Tyr³]-octreotate (^{213}Bi -DOTATATE), a ^{213}Bi -labelled somatostatin analogue with high affinity for somatostatin receptor subtype 2 (SSTR₂), is suitable for the treatment of larger neuroendocrine tumours overexpressing SSTR₂ in comparison to its effectiveness for smaller tumours. We performed a preclinical targeted radionuclide therapy study with ^{213}Bi -DOTATATE in animals bearing tumours of different size (50 and 200 mm³) using two tumour models: H69 (human small cell lung carcinoma) and CA20948 (rat pancreatic tumour).

Methods:

Pharmacokinetics was determined for calculation of dosimetry in organs and tumours. H69- or CA20948- xenografted mice with tumour volumes of approximately 120 mm³ were euthanized at 10, 30, 60 and 120 min post injection of a single dose of ^{213}Bi -DOTATATE (1.5–4.8 MBq). To investigate the therapeutic efficacy of ^{213}Bi -DOTATATE, xenografted H69- and CA20948 tumour-bearing mice with tumour sizes of 50 or 200 mm³ were administered daily with a therapeutic dose of ^{213}Bi -DOTATATE (0.3 nmol, 2–4 MBq) for three consecutive days. The animals were followed for 90 days after treatment. At day 90, mice were injected with 25 MBq $^{99\text{m}}\text{Tc}$ -DMSA and imaged by SPECT/CT to investigate possible renal dysfunction due to ^{213}Bi -DOTATATE treatment.

Results:

Higher tumour uptakes were found in CA20948 tumour-bearing animals compared to those in H69 tumour-bearing mice with the highest tumour uptake of $19.6 \pm 6.6\%$ IA/g in CA20948 tumour-bearing animals, while for H69 tumour-bearing mice, the highest tumour uptake was found to be $9.8 \pm 2.4\%$ IA/g. Nevertheless, as the anti-tumour effect was more pronounced in H69 tumour-bearing mice, the survival rate was higher. Furthermore, in the small tumour groups, no regrowth of tumour was found in two H69 tumour-bearing mice and in one of the CA20948 tumour-bearing mice. No renal dysfunction was observed in ^{213}Bi -DOTATATE-treated mice after the doses were applied.

Conclusion:

^{213}Bi -DOTATATE demonstrated a great therapeutic effect in both small and larger tumour lesions. Higher probability for stable disease was found in animals with small tumours. ^{213}Bi -DOTATATE was effective in different neuroendocrine (H69 and CA20948) tumour models with overexpression of SSTR₂ in mice.

BACKGROUND

Peptide receptor radionuclide therapy (PRRT) is an effective treatment option for patients with an inoperable neuroendocrine tumour (NET) or with metastatic disease [1, 2]. Approximately 80% of patients with NET show great anti-tumour response upon PRRT. The most commonly used radiolabelled peptides for treatment in NET are ^{177}Lu -[DOTA⁰, Tyr³]-octreotate (^{177}Lu -DOTATATE) and ^{90}Y -[DOTA⁰, Tyr³]-octreotide (^{90}Y -DOTATOC). ^{90}Y and ^{177}Lu are β -particles emitting radionuclides, with a maximum tissue penetration of 12 mm and 2 mm, respectively. For treatment of small tumour clusters and metastases, β -emitters may lack efficacy due to the relatively large tissue penetration and low linear energy transfer (LET). Targeted alpha therapy (TAT) with α -emitters has been described to be more suitable for these purposes, since the path length in tissue of α -particles is relatively short (in tissue 50–100 μm) compared to that of β -particles. Moreover, α -particles have a much higher LET (~ 100 keV/ μm) and are therefore more powerful than β -particles (0.2 keV/ μm) for therapeutic applications [3]. Bismuth-213 (^{213}Bi), an α -emitter with a $T_{1/2}$ of 45.6 min, has already been proven to be effective in TAT [4–7]. Recently, a clinical trial showed a promising anti-tumour effect in patients with progressive advanced neuroendocrine liver metastasis refractory to ^{90}Y -DOTATOC or ^{177}Lu -DOTATOC treatment after treatment with ^{213}Bi -DOTATOC [8]. TAT with ^{213}Bi -DOTATOC was able to overcome the resistance against β -radiation in patients with different neuroendocrine tumours, in metastasis and in primary tumours, resulting in a high number of long-lasting anti-tumour responses.

The objective of this study was to investigate the therapeutic efficacy of ^{213}Bi -DOTATATE in tumours of different sizes in mice (small vs large). Two different tumour models with somatostatin receptor subtype 2 (SSTR₂) expression were used: CA20948 (rat pancreatic tumour) and H69 (human small cell lung carcinoma). Both tumours have relatively high SSTR₂ expression and both have often been applied as a model in preclinical studies of PRRT in NET [9–11]. The radiation sensitivity of CA20948 for low-LET radiation has been determined yielding $\alpha/\beta = 8.3$ Gy [12]. The H69 cell line shows a higher radiation sensitivity $\alpha/\beta = 2.3$ Gy [13]. Radiation damage by the high-LET α radiation from ^{213}Bi is expected to follow a linear (-exponential) curve which was comparable for both cell lines. For PRRT the dose-limiting organs are bone marrow and kidneys. ^{213}Bi -DOTATATE shows accumulation in the kidneys, resulting in high radiation doses to the kidneys; in this study, we therefore determined the safe dose of radioactivity administered for TAT in this mouse model. Renal function was evaluated after TAT by SPECT/CT at different time points post treatment using $^{99\text{m}}\text{Tc}$ -DMSA (dimercaposuccinic acid), a renal marker for tubular damage.

METHODS

²¹³Bi-eluate

A ²¹³Bi/²²⁵Ac generator (222 MBq) was provided by the Institute for Transuranium Elements (Karlsruhe, Germany). Prior to elution, the generator was rinsed using 0.01 M HCl (3 mL) and eluted using 0.1 M/0.1 M HCl/NaI (0.6 mL). After elution, the generator was rinsed with 0.01 M HCl and stored in 0.01 M HCl [4]. The activity of ²¹³Bi was determined using a Germanium detector (MetorX, Genie 2000 software, Canberra) [14].

²¹³Bi-DOTATATE labelling

Eluate containing ²¹³Bi (0.1M/0.1M in HCl/NaI) was added to a solution containing 7.0 nmol DOTATATE, 0.15 M TRIS buffer and 2.6 mM ascorbic acid in a total reaction volume of 800 µL. The reaction mixture was incubated for 5 min at 95°C followed by 5 min at room temperature. To chelate any unbound/free ²¹³Bi, 50 nmol DTPA (Sigma Aldrich, Zwijndrecht, the Netherlands) was added (manuscript submitted). Analysis by instant thin-layer chromatography (ITLC, Varian) and reverse-phase high-performance liquid chromatography (HPLC, 2695 separation module, Alliance, Waters, Etten-Leur, The Netherlands) of the labelled peptide was performed to determine the incorporation yield (%) and radiochemical purity (RCP) expressed as percentage of labelled peptide of interest compared to other detectable compounds [15]. The whole labelling procedure took on average 20 minutes to produce a ready-to-inject vial.

^{99m}Tc-DMSA labelling

The ^{99m}Tc-DMSA kit was purchased from Mallinckrodt (Petten, the Netherlands) and labelled according to the indicated procedure.

Cell culture

The rat pancreatic tumour cell line CA20948 (derived from a rat pancreas tumour at our institute) with high SSTR₂ expression, was cultured in DMEM (Gibco, Life technologies) supplemented with 10% heat-inactivated fetal bovine serum. H69 tumour cells, human small cell lung carcinoma cells with SSTR₂ expression (American Tissue Culture Collection, Wesel, Germany), were cultured in RPMI 1640 (Gibco, Life technologies) supplemented with 10% heat-inactivated fetal bovine serum and 50 IU/ml penicillin/streptomycin. All cells were cultured at 37 °C in a 5% CO₂/humidified air atmosphere.

Animal models

All animal studies were in agreement with the Animal Welfare Committee requirements of Erasmus MC and conducted in accordance to accepted guidelines. Male 6–8-weeks-old BALB/c (nu/nu) nude mice were obtained from Charles River (Kiblegg, Germany). Sub-

cutaneous tumours were established in mice by inoculation of approximately 5×10^6 cells (CA20948 or H69), suspended in 200 μL sterile culture medium Hanks' balanced salt solution (HBSS) in the case of CA20948 cells. Three days after inoculation of CA20948 cells, a tumour with a tumour size $\sim 50 \text{ mm}^3$ (used for the "smaller" tumour size group) was reached, and 2 weeks after inoculation, a tumour size $\sim 200 \text{ mm}^3$ (used for the "larger" tumour size group) was reached. For H69 cells, 200 μL , containing 1/3 Matrigel and 2/3 HBSS medium (Gibco, Life technologies), was used. The cells were injected subcutaneously (s.c.) into the right flank of the mice. One week after inoculation of tumour cells, tumours with a volume of $\sim 50 \text{ mm}^3$ (used for the "smaller" tumour size group) could be detected and after 3 weeks tumour volumes reached $\sim 200 \text{ mm}^3$ (used for the "larger" tumour size group). Tumour volumes were estimated using a calliper.

Pharmacokinetics of ^{213}Bi -DOTATATE as function of time in different tumour models

When tumour volumes reached $\sim 120 \text{ mm}^3$, animals were divided into five groups with seven animals in each group for both H69 and CA20948 tumour-bearing animals. Four groups of mice received a single intravenously (i.v.) injection of ^{213}Bi -DOTATATE (200 μL) via the tail vein, $3.8 \pm 0.6 \text{ MBq}/0.3 \text{ nmol}/200 \mu\text{L}$ for H69 tumour-bearing animals and $2.1 \pm 0.2 \text{ MBq}/0.3 \text{ nmol}/200 \mu\text{L}$ for CA20948 tumour-bearing animals. At 10, 30, 60 and 120 min post injection (p.i.), animals in the four groups were euthanized and tissues and organs of interest (including tumour, kidney, pancreas, spleen, liver, muscles, blood, femur, femur marrow and adrenals) were collected and counted using a gamma counter (Wallac Wizard 3, PerkinElmer, USA). Control animals received a single injection of ^{213}Bi -DOTA-TATE plus an excess of DOTATATE (10^{-6} M) i.v. via the tail vein (blocking dose) to determine the non-receptor-specific binding of ^{213}Bi -DOTATATE. The animals of the control group were euthanized 60 min p.i.; tissues and organs of interest were harvested and counted using a gamma counter. Data was expressed in mean percentage of total injected radioactivity per gram tissue ($\% \text{IA}/\text{g}$) \pm SD.

Targeted Alpha Therapy

Tumour cells were inoculated into the right flank of the mice, and the tumours were allowed to grow until tumour volumes of approximately 50 mm^3 and 200 mm^3 were reached, respectively. On the day of treatment ($T=0$ days), the animals (H69-bearing animals: small tumour $n=10$, large tumour $n=7$; CA20948-bearing animals: small tumour $n=8$, large tumour $n=5$) were injected i.v. via the tail vein with ^{213}Bi -DOTATATE ($2\text{--}4 \text{ MBq}/0.3 \text{ nmol}/200 \mu\text{L}$) for three consecutive days. The control group (H69-bearing animals: small tumour $n=10$, large tumour $n=9$; CA20948-bearing animals; small tumour $n=5$, large tumour $n=5$) received i.v. via the tail vein three times $0.3 \text{ nmol}/200 \mu\text{L}$ of unlabelled DOTATATE for three consecutive days.

All animals were followed for 90 days after treatment. The behavior and the health status of the animals were observed daily, and the weight of the animals and the tumour volumes were monitored twice a week.

Determination of renal function by ^{99m}Tc -DMSA imaging

Renal function imaging was performed by a four-headed multi-pinhole SPECT/CT camera (Bioscan Inc., Washington D.C., USA). For ^{99m}Tc imaging, an energy peak at 140 keV was selected with an energy window width $\pm 10\%$. A nine-pinhole aperture (diameter of each pinhole 1.4 mm) was used on each camera head. For the CT topogram, an axial length of 27 mm was used to cover the renal region. Animals were imaged under anesthesia by isoflurane and O_2 . The body temperature of the animals was maintained using a heated bed. Renal imaging of H69 (control $n=4$, ^{213}Bi -DOTATATE treated $n=8$) and CA20948 tumour-bearing animals (control $n=2$, ^{213}Bi -DOTATATE treated $n=4$) was performed 2 h after i.p. administration of ^{99m}Tc -DMSA (25 MBq). ^{99m}Tc -DMSA images were acquired for 12 min (20 projections, 60 s/projection) [16].

Absorbed dose in organs

The absorbed radiation dose (defined as the mean absorbed dose in Gy) in organs and tumours was estimated from the results obtained in the biodistribution studies as described by Konijnenberg et al. [17] in a spherical geometry using Monte Carlo code MCNP5 (Version 1.4) for the electrons and γ -rays [18] and MCNPX (version 2.5) [19] for the α -particles, all energy emission spectra were taken from ICRP database [20], and particle histories of 1×10^7 was used for simulation to reduce the variation ($< 5\%$) in the data. The mean absorbed energies for 10 MBq ^{213}Bi -DOTATATE injection were calculated for spheres of 1, 10, 100, 200, 300 and 500 mg containing tissue with a mass density of 1g/mL to determine the spherical node S -values. A homogeneous activity distribution over the sphere was assumed. The absorbed dose D_i was calculated for each volume i according to the MIRD-schema:

$$D_i = \tilde{A}_i \times S(i \leftarrow i)$$

with \tilde{A}_i the time-integrated activity (TIA) in organ i and $S(i \leftarrow i)$ the absorbed dose rate per unit activity (S -value). Only the self-dose S -values were considered and were obtained by interpolation between the sphere S -values for the measured organs or tumour mass. For small tumours, a minimum tumour mass of 50 mg was used for the absorbed dose calculation. The \tilde{A}_i in each organ was determined for ^{213}Bi and its daughters taking the biodistribution into account according to the methods shown in Additional file 1. The absorbed dose to the kidneys was calculated both with the spherical S -values, as with the nephron model by Hobbs et al. [21]. Three hypothetical activity distributions were considered for this heterogeneous model: (1) homogeneous in the cortex, (2) proximal tubular cell uptake and (3) glomerular cell uptake.

Statistics

Statistical analysis was performed using *t*-test and using the nonparametric Mann-Whitney test. *P*-values < 0.05 were considered statistically significant. For statistical significances in tumour growth patterns, one-way ANOVA was used. Values are presented as the mean and the standard deviation (SD).

RESULTS

Labelling

An incorporation yield of $\geq 99\%$ and a RCP $\geq 85\%$ were found for the radiopeptide, as determined by ITLC and HPLC, respectively.

Pharmacokinetic studies

Biodistribution studies using ^{213}Bi -DOTATATE in H69 tumour-bearing mice revealed relatively high tumour uptake. The highest tumour uptake was reached at 30 min p.i., $9.8 \pm 2.4\% \text{IA/g}$. Tumour uptake $T_{1/2}$ was 7 ± 2 min, and tumour clearance $T_{1/2}$ was 2.3 ± 1.1 h. An even higher renal activity compared to tumour uptake was found at all time points, the highest renal activity being found at 10 min p.i.: $44 \pm 10\% \text{IA/g}$. At 120 min p.i. the renal activity still was $25 \pm 3\% \text{IA/g}$. Blood clearance in H69 tumour-bearing animals was fast, and clearance $T_{1/2}$ was 11 ± 2 min, see Fig. 1A-C. All other organs had relative low uptake at 120 min p.i., $< 2\% \text{IA/g}$, see Table 1.

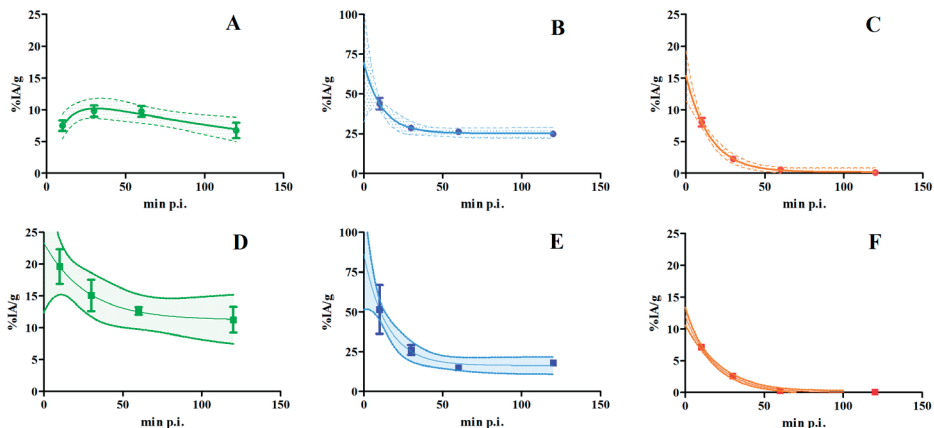


Figure 1A-F, Selected pharmacokinetics of ^{213}Bi -DOTATATE from Tables 1 and 2. ^{213}Bi -DOTATATE pharmacokinetics in H69 tumour-bearing mice, uptake in tumours (A) and kidney (B), and radioactivity in blood (C) are shown over time in H69 tumour-bearing animals. Same data are shown for CA20948 tumour-bearing animals: uptake in tumours (D), and kidneys (E) and radioactivity in blood (F). Solid curves show the mean uptake value expressed in $\% \text{IA/g} \pm \text{SD}$. The dotted curves indicate the 95% confidential interval.

Table 1, Pharmacokinetics of ^{213}Bi -DOTATATE at 10, 30, 60 and 120 min post injection (p.i.) in H69 tumour-bearing animals, expressed in mean %IA/g \pm SD, n = 7

Uptake (%IA/g)	10 min p.i.	30 min p.i.	60 min p.i.	120 min p.i.
Tumour	7.5 \pm 2.2	9.8 \pm 2.4	9.8 \pm 2.3	6.8 \pm 3.2
Muscle	2.1 \pm 0.8	1.1 \pm 0.2	1.0 \pm 1.4	0.5 \pm 0.4
Kidney	44.0 \pm 9.6	28.5 \pm 3.7	26.2 \pm 2.6	25.0 \pm 3.8
Pancreas	3.2 \pm 0.3	2.8 \pm 0.3	1.8 \pm 0.2	1.4 \pm 0.2
Liver	2.1 \pm 0.8	0.9 \pm 0.09	0.4 \pm 0.06	0.3 \pm 0.05
Blood	8.1 \pm 1.8	2.3 \pm 1.1	0.6 \pm 0.2	0.1 \pm 0.06
Spleen	2.3 \pm 0.6	1.0 \pm 0.09	0.4 \pm 0.07	0.2 \pm 0.07
Adrenal	3.6 \pm 1.2	2.0 \pm 0.6	0.9 \pm 0.4	0.7 \pm 0.4
Femur	2.8 \pm 0.4	1.5 \pm 0.4	1.0 \pm 0.5	0.4 \pm 0.4

%IA/g = mean percentage of total injected radioactivity per gram tissue.

Tumour uptake of ^{213}Bi -DOTATATE in CA20948 tumour-bearing mice was already highest at 10 min p.i., 19.6 \pm 6.6%IA/g, and the tumour uptake $T_{1/2}$ was therefore unable to estimate. A clearance $T_{1/2}$ of 2.2 \pm 0.9 h was found for CA20948 tumours. Similar renal activity was found in CA20948 tumour-bearing animals. Renal activity was highest at 10 min p.i., 52 \pm 17%IA/g. Renal clearance $T_{1/2}$ was 10 \pm 3 min, whereas blood clearance $T_{1/2}$ was 14 \pm 1 min, see Fig. 1D-F. At 120 min p.i., uptakes in other organs remained low, < 2%IA/g, see Table 2.

Table 2, Pharmacokinetics of ^{213}Bi -DOTATATE at 10, 30, 60 and 120 min post injection (p.i.) in CA20948 tumour-bearing animals, expressed in mean %IA/g \pm SD, n = 7

Uptake (%IA/g)	10 min p.i.	30 min p.i.	60 min p.i.	120 min p.i.
Tumour	19.6 \pm 6.6	15.1 \pm 6.6	12.7 \pm 1.6	11.2 \pm 5.4
Muscle	3.1 \pm 0.8	1.5 \pm 0.8	1.4 \pm 1.9	0.2 \pm 0.2
Kidney	51.5 \pm 16.6	26.0 \pm 3.3	15.0 \pm 1.5	18.0 \pm 1.9
Pancreas	3.6 \pm 0.2	3.1 \pm 0.4	1.5 \pm 0.3	1.2 \pm 0.2
Liver	2.0 \pm 0.2	1.0 \pm 0.1	0.2 \pm 0.04	0.2 \pm 0.03
Blood	7.1 \pm 1.0	2.6 \pm 0.4	0.3 \pm 0.2	0.07 \pm 0.04
Spleen	2.0 \pm 0.2	1.1 \pm 0.4	0.2 \pm 0.05	0.2 \pm 0.04
Adrenal	3.4 \pm 0.7	2.2 \pm 0.8	0.6 \pm 0.1	0.4 \pm 0.1
Femur	2.4 \pm 0.2	1.4 \pm 0.2	0.6 \pm 0.1	0.2 \pm 0.04

%IA/g = mean percentage of total injected radioactivity per gram tissue.

Dosimetry

Dosimetry calculations in both tumour models were based on the data obtained from the biodistribution studies at 10, 30, 60 and 120 min p.i. In H69 tumour-bearing mice, a relatively high tumour absorbed radiation dose was estimated: 0.45 Gy/MBq injected ^{213}Bi -DOTATATE calculated for 100 mg tumour. The renal-absorbed dose was four times as high as the tumour-absorbed radiation dose: 2 Gy/MBq injected ^{213}Bi -DOTATATE. The absorbed radiation dose of ^{213}Bi -DOTATATE in pancreas, spleen and liver was low compared to those in the tumour and kidney, 0.15, 0.06 and 0.06 Gy/MBq, respectively. Similar results were observed in CA20948 tumour-bearing animals. A lower tumour-absorbed radiation dose was found than that in kidneys: 0.78 Gy/MBq in tumour vs 1.6 Gy/MBq. Absorbed radiation doses in pancreas, spleen and liver were 0.13, 0.05 and 0.06 Gy/MBq, respectively. For both tumour-bearing animal models, an absorbed dose of < 0.02 Gy/MBq was found in bone marrow.

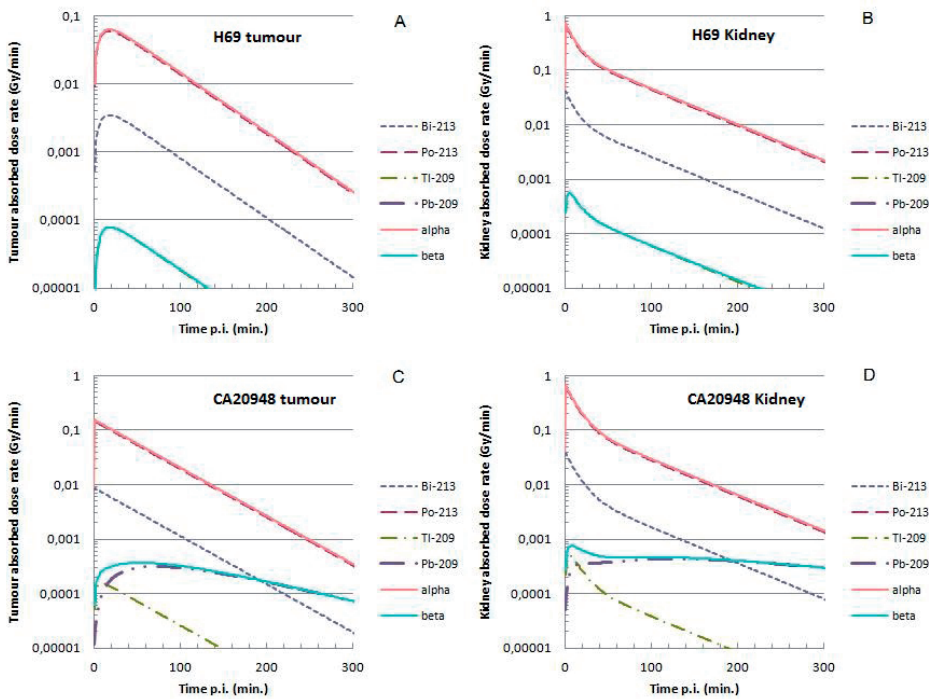


Figure 2, Calculated absorbed radiation dose rates in the tumour and kidney after 10 MBq ^{213}Bi -DOTA-TATE, based on the data obtained in the biodistribution study. Absorbed dose rate as function of time in H69 tumour-bearing animals; tumour (A) and kidney (B). Same data are shown of tumour (C) and kidney (D) for CA20948 tumour-bearing animals. Red lines indicate the absorbed dose rate contributed by all alpha particles and blue lines by all beta particles. The dotted lines indicate the individual absorbed dose rate of ^{213}Bi , ^{213}Po , ^{209}Tl and ^{209}Pb .

Tumour- and kidney-absorbed radiation doses in H69 or CA20948 tumour-bearing animals were mainly caused by the α -particles emitted. The absorbed dose rate was higher in CA20948 than in H69 tumours, and the kidney-absorbed radiation dose was similar; see Fig. 2A-D. For an instantaneous uptake in the H69 tumour, its absorbed dose would rise by 12% to 0.50 Gy/MBq, whereas the absorbed dose to the CA20948 tumour is less dependent on the uptake kinetics: the dose is lowered by 2% to 0.77 Gy/MBq when the same uptake kinetics as for the H69 tumour is assumed.

Targeted Alpha Therapy

Therapeutic anti-tumour effects were observed in all animals treated with ^{213}Bi -DOTATATE, see Fig. 3. The tumour volume doubling time was 16 ± 6 days for the H69 and 10 ± 5 days for the CA20948 tumours, without any difference between the growth rate of small tumours and large tumours. The mean times to reach the end volume of 2000 mm^3 of control and treated animals of both tumour models are indicated in Table 3. For small tumours, tumour sizes $< 50 \text{ mm}^3$ could not be measured accurately; therefore, 50 mm^3 was used as the minimum tumour sizes in our calculation and this was in three cases of H69 tumour-bearing animals with a small tumour and in all cases of CA20948 tumour-bearing animals with a small tumour. Overall calculated cumulative tumour-absorbed dose in small tumours was higher than large tumours. In CA20948 tumours, the cumulative tumour-absorbed dose was higher than in H69 tumours.

Shrinkage of tumours was observed in H69 tumour-bearing animals with large tumours and a delay of tumour growth around 70 days after ^{213}Bi -DOTATATE (cumulative injected activity of $9.4 \pm 0.7 \text{ MBq}$) treatment. In CA20948 tumour-bearing animals with large

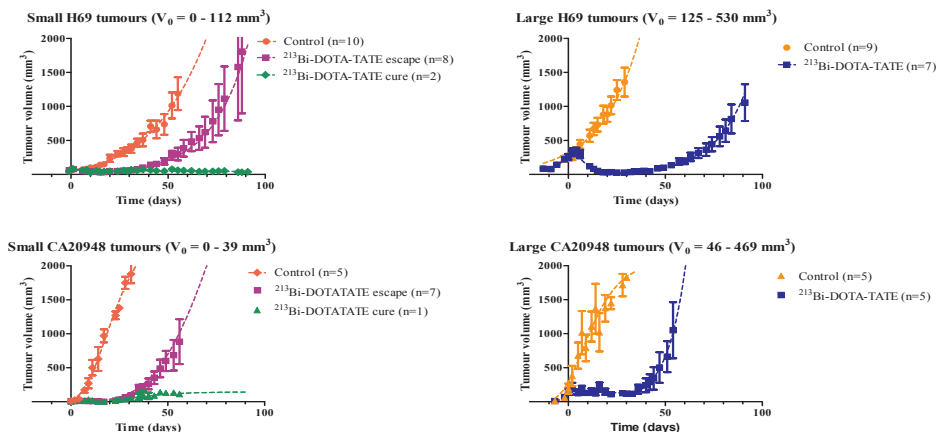


Figure 3, Overview of mean tumour volumes \pm standard deviation (SD) in mm^3 per group after treatment of ^{213}Bi -DOTATATE (2–4 MBq per injection) or unlabelled DOTATATE (control) in H69 and CA20948 tumour-bearing mice for three consecutive days. V_0 is the starting tumour volume. The dotted curves show the extrapolated growth curves of the tumours assuming 100% survival of animals.

Table 3, An overview of mean time (days = d) to reach a tumour volume of 2000 mm³ after ²¹³Bi-DOTATATE therapy

	H69 small	H69 large	CA20948 small	CA20948 large
Control	73 ± 19 d	38 ± 11 d	43 ± 20 d	27 ± 14 d
Therapy	102 ± 19 d	110 ± 19 d	76 ± 15 d	77 ± 25 d
Tumour dose (Gy)	5 ± 1 Gy	2.0 ± 0.6 Gy	17 ± 1 Gy	10 ± 5 Gy
Growth delay (control vs therapy)	28 ± 9 d***	73 ± 24 d*	33 ± 17 d NS	50 ± 13 d**

NS = not significant

* = *P* value ≤ 0.05, ** = *P* value ≤ 0.01 and *** = *P* value ≤ 0.001.

The tumour dose (Gy) ± SD was estimated based on the tumour size at *T*=0 of therapy and the injected activity (MBq). Growth delay (days) was the Δ*T* for tumour to reach 2000 mm³ of therapy group vs control group.

tumours, the inhibition of tumour growth was initiated around 30 days after therapy (cumulative injected activity 10.2 ± 0.4 MBq ²¹³Bi-DOTATATE), leading to a tumour growth delay time of 50 days. Similar results were found in CA20948 tumour-bearing animals with small tumours after therapy (cumulative injected activity 7.7 ± 0.4 MBq); a delay in tumour growth of around 30 days was observed, and in one of the animals no tumour regrowth was observed. The delay time was estimated excluding animal with cure or stable disease. In H69 tumour-bearing animals with small tumours, a delay of tumour growth was found for around 30 days after therapy (cumulative injected activity 7.4 ± 0.5 MBq), and in two animals, no tumour regrowth was observed until the end of the study at day 90. Here, the two animals with cure/stable disease were excluded from the estimated delay time.

Survival

All animals treated with ²¹³Bi-DOTATATE showed a higher survival rate than control animals, see Fig. 4. In the control, non-TAT H69 tumour-bearing animals, a median survival of 34 days was found for animals bearing large tumours and 81 days for animals bearing small tumours. H69 tumour-bearing animals with small tumours had a median survival of > 90 days after ²¹³Bi-

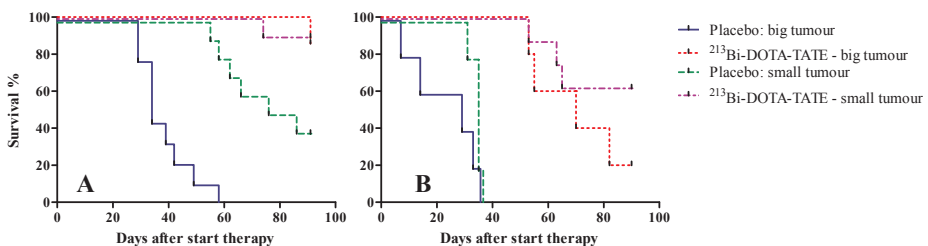


Figure 4, Survival (percentage) after ²¹³Bi-DOTATATE or DOTATATE treatment in A) H69 tumour-bearing and B) CA20948 tumour-bearing mice.

DOTATATE therapy (control vs treated, P -value = < 0.0001). Similar results were obtained in H69 tumour-bearing animals with large tumours after TAT; a median survival > 90 days was found (control vs treated, P -value=0.0195). In the CA20948 tumour-bearing animals without TAT, a median survival of 29 days was found for animals bearing large tumours, whereas for animals bearing small tumours, this was 35 days. After ^{213}Bi -DOTATATE, a median survival of 70 days was found in the large-tumour-animal group (control vs treated, P -value = not significant) and > 90 days in the small-tumour-animal group (control vs treated, P -value=0.005).

$^{99\text{m}}\text{Tc}$ -DMSA uptake in kidney

Renal function was investigated in H69 and CA20948 tumour-bearing animals at day 90 after ^{213}Bi -DOTATATE therapy or unlabelled DOTATATE treatment. Renal function was determined by renal uptake of $^{99\text{m}}\text{Tc}$ -DMSA (25MBq). No significant differences in $^{99\text{m}}\text{Tc}$ -DMSA uptake

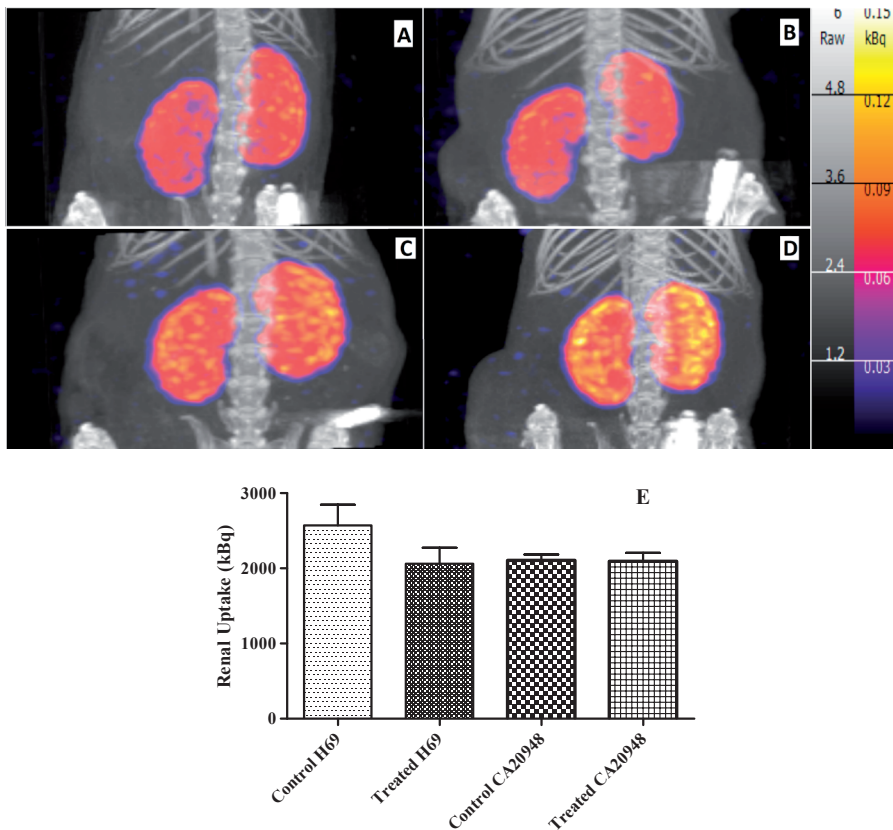


Figure 5A-D, $^{99\text{m}}\text{Tc}$ -DMSA renal SPECT images in H69 control (A), ^{213}Bi -DOTATATE-treated H69 mice (B), CA20948 control (C) and ^{213}Bi -DOTATATE-treated CA20948 mice (D). **5E**, Renal uptake (in kBq) of $^{99\text{m}}\text{Tc}$ -DMSA (25 MBq) in H69 and CA20948 tumour-bearing mice after therapy with ^{213}Bi -DOTATATE or DOTATATE.

in the kidneys were observed in ^{213}Bi -DOTATATE-treated mice and control animals for both tumour models. In H69 tumour-bearing mice, a mean renal uptake of 2.6 ± 0.8 MBq (mean concentration of 2.9 ± 0.6 kBq/mm³) in the control group ($n=4$) versus 2.1 ± 0.9 MBq (mean concentration of 2.9 ± 0.8 kBq/mm³) in ^{213}Bi -DOTATATE-treated animals ($n=8$) was found. Similar results were obtained in CA20948 tumour-bearing animals: mean uptake of 2.1 ± 0.2 MBq (mean concentration of 3.1 ± 0.4 kBq/mm³) in ^{213}Bi -DOTATATE treated animals ($n=4$) and 2.1 ± 0.3 MBq (mean concentration 3.2 ± 0.3 kBq/mm³) in control ($n=2$) were found. Figure 5A-E shows $^{99\text{m}}\text{Tc}$ -DMSA uptake in kidneys of both tumour models.

DISCUSSION

In this study, we compared the efficacy of ^{213}Bi -DOTATATE TAT in tumours of different sizes in two different tumour models, both with expression of SSTR₂. ^{213}Bi -DOTATATE showed a very good therapeutic effect in both small and large tumours in the two different tumour models. Tumour-absorbed doses (Gy) in CA20948 tumour-bearing animals were higher compared to those in H69 tumour-bearing mice. Despite these findings, ^{213}Bi -DOTATATE showed greater therapeutic effects in H69 tumour-bearing animals than in CA20948 tumour-bearing animals; a higher survival rate was observed in H69 tumour-bearing animals at the end of the study. However, no significant difference in tumour (re)growth inhibition time between the two tumour models was found, even though the absorbed dose in tumour was higher in CA20948 tumour-bearing animals. *In vitro*, CA20948 cells appeared also more radioresistant than H69 cells; at external beam irradiation with 2 Gy, a survival fraction of H69 was 37% [13] and for CA20498, 52% was found [12].

In this study, we observed a higher anti-tumour effect in small tumours. In H69 tumour-bearing mice with small tumours, two animals showed stable disease and in eight animals, a partial response was found after treatment. In the case of CA20948 tumour-bearing animals with small tumours, one animal showed stable disease till the end of the study and partial response was found in eight of the animals after ^{213}Bi -DOTATATE therapy. In H69 and CA20948 tumour-bearing animals with large tumours, a partial response was found. A longer tumour growth delay was found in animals with large tumours of both tumour models compared to small tumours. The time a tumour takes to reach 2000 mm³ in small tumours is longer than in large tumours; therefore, Δ delay time for tumour growth was used. Nevertheless, in animals showing regrowth, the small tumours were less responsive than the large tumours in both models.

The reason for partial remission can be explained as the distribution of the radiation-absorbed dose depends on the tumour size, the physical properties of the radionuclide and its possible inhomogeneous intratumoural distribution. In those cases where the tumour dimensions are smaller than the range of the ionizing particles, a large proportion of the absorbed

energy can “escape”, resulting in an suboptimal effect of ^{213}Bi -DOTATATE TAT [22]. In larger tumours, also pronounced therapeutic effects were observed after ^{213}Bi -DOTATATE therapies in both tumour models. However, no complete remissions were observed in these animals. Besides tumour perfusion [23] and inhomogeneous distribution of SSTR_2 , tumour size [17, 22], vessel density, permeability and tumour growth doubling time can play a critical role for the success of PRRT; this is especially true for α -emitters, where the penetration depth in tissue is relatively short (50–100 μm). In large tumours, often heterogeneity of receptor distribution [24] is observed, resulting in insufficient efficacy of the treatment and leading to probability survival of tumour cells. Therefore multiple fractions of therapy might improve the effect in larger tumours [25], especially in the case of TAT.

For somatostatin receptor-targeted PRRT, nephrotoxicity is often the dose-limiting factor, since reabsorption of radiolabelled somatostatin analogues by cells in the proximal tubule of the nephron occurs [26].

In this study the calculated renal absorbed dose using our simplified model was compared to the model described by Hobbs et al. [21]. We assumed all renal uptakes to be localized in the proximal tubular cells and took the glomerular cells as target. The absorbed dose in the glomeruli was 57% lower than for the mean absorbed kidney dose. On the other hand, the dose to the glomeruli is almost a factor 20 higher when all activity was concentrated in the glomerular cells. The homogeneous mean absorbed dose we calculated with the sphere model was 24% higher than when calculated with the cortex model from Hobbs et al. [21]. $^{99\text{m}}\text{Tc}$ -DSMA can provide information on renal function after renal tubular damage and has been used as renal marker in PRRT [27]. In this study, we did not find any changes in renal function in animals after TAT (highest cumulative activity used was 11.5 MBq ^{213}Bi -DOTATATE). Kidney histology was performed in CA20948-bearing animals (data not shown), and no significant differences were observed in control vs treated animals. However, ^{213}Bi -DOTATATE is known to accumulate in the kidney, leading to a high renal-absorbed dose. In patients, the maximum tolerated dose in kidney is postulated to be 23–28 Gy [28–30]. Kidney protectants during TAT are therefore advised [9, 31, 32], especially when higher treatment activities are used. In another study, we found a maximum tolerated activity of 21.2 ± 1.7 MBq in presence of i.p. L-lysine as kidney protectant prior to the ^{213}Bi -DOTATATE treatment; in absence of L-lysine, the maximum tolerated activity was $< 13.1 \pm 1.2$ MBq (manuscript in preparation).

Even though we have not been able to achieve complete remission of all tumours, this study demonstrated that TAT can be effective for the treatment of both large and small tumours. These findings are in line with those of Kratochwil et al. [8] who demonstrated the effectiveness of TAT in eight patients refractory to PRRT with ^{177}Lu and ^{90}Y . We therefore believe that TAT is most promising for the treatment of NET. In combination with PRRT using ^{90}Y - and ^{177}Lu -peptides [33, 34], even greater therapeutic efficacy might be achieved, especially for in the treatment of patients with larger NET.

CONCLUSION

TAT with ^{213}Bi -DOTATATE shows very good therapeutic efficacy for the treatment of both large and small tumours in these mouse models. In small tumours, ^{213}Bi -DOTATATE demonstrated greater anti-tumour effect by its higher probability for inducing stable disease. Furthermore, TAT using ^{213}Bi -DOTATATE demonstrated to be safe in our experimental setting, with kidneys as dose-limiting organs. ^{213}Bi -DOTA-TATE therefore held great promise for targeted therapy for neuroendocrine tumours that express SSTR₂.

ADDITIONAL FILE 1

1. Single compartment clearance model for ^{213}Bi conjugates activity in organs or tumours.

The ^{213}Bi activity in the volume is cleared with a biologic clearance constant λ_b ($= \ln(2)/T_b$, with T_b the clearance half-life) and the kinetics follows an exponential decay function:

$$A_{Bi}(t) = A_{Bi}(0)e^{-(\lambda_{Bi}+\lambda_b)t}$$

The activity integration from time 0 to T of the ^{213}Bi activity and time integrated activity \tilde{A}_{Bi} is then:

$$\tilde{A}_{Bi}(T) = \int_0^T A_{Bi}(t) dt = \frac{A_{Bi}(0)}{\lambda_{Bi}+\lambda_b}(1 - e^{-(\lambda_{Bi}+\lambda_b)T}) \Rightarrow \lim_{T \rightarrow \infty} \tilde{A}_{Bi}(T) = \tilde{A}_{Bi} = \frac{A_{Bi}(0)}{\lambda_{Bi}+\lambda_b}$$

^{213}Bi decays with a branching ratio BR ($= 0.9791$) to ^{213}Po and the ^{213}Po kinetics follows:

$$A_{Po}(t) = \frac{BR \lambda_{Po}}{\lambda_{Po}-\lambda_{Bi}} \times A_{Bi}(0)(e^{-(\lambda_{Bi}+\lambda_b)t} - e^{-(\lambda_{Po}+\lambda_b)t})$$

The activity integration over time of the ^{213}Po activity and time integrated activity \tilde{A}_{Po} is then:

$$\begin{aligned} \tilde{A}_{Po}(T) &= \frac{BR \lambda_{Po}}{\lambda_{Po}-\lambda_{Bi}} A_{Bi}(0) \left(\frac{1-e^{-(\lambda_{Bi}+\lambda_b)T}}{\lambda_{Bi}+\lambda_b} - \frac{1-e^{-(\lambda_{Po}+\lambda_b)T}}{\lambda_{Po}+\lambda_b} \right) \\ \Rightarrow \tilde{A}_{Po} &= \frac{BR \lambda_{Po}}{\lambda_{Po}-\lambda_{Bi}} A_{Bi}(0) \left(\frac{1}{\lambda_{Bi}+\lambda_b} - \frac{1}{\lambda_{Po}+\lambda_b} \right) \\ \Rightarrow \tilde{A}_{Po} &\approx BR A_{Bi}(0) \frac{1}{\lambda_{Bi}+\lambda_b} \end{aligned}$$

The decay and biodistribution of the other daughters ^{209}Tl and ^{209}Pb are described quite similarly:

$$A_{Tl}(t) = \frac{(1-BR) \lambda_{Tl}}{\lambda_{Tl}-\lambda_{Bi}} \times A_{Bi}(0)(e^{-(\lambda_{Bi}+\lambda_b)t} - e^{-(\lambda_{Tl}+\lambda_b)t})$$

$$\text{with: } \tilde{A}_{Tl}(T) = \frac{(1-BR) \lambda_{Tl}}{\lambda_{Tl}-\lambda_{Bi}} A_{Bi}(0) \left(\frac{1-e^{-(\lambda_{Bi}+\lambda_b)T}}{\lambda_{Bi}+\lambda_b} - \frac{1-e^{-(\lambda_{Tl}+\lambda_b)T}}{\lambda_{Tl}+\lambda_b} \right)$$

$$\Rightarrow \tilde{A}_{Tl} = \frac{(1-BR) \lambda_{Tl}}{\lambda_{Tl}-\lambda_{Bi}} A_{Bi}(0) \left(\frac{1}{\lambda_{Bi}+\lambda_b} - \frac{1}{\lambda_{Tl}+\lambda_b} \right)$$

$$A_{Pb}(t) = \frac{BR \lambda_{Po} \lambda_{Pb}}{\lambda_{Po}-\lambda_{Bi}} \times A_{Bi}(0) \left(\frac{e^{-(\lambda_{Bi}+\lambda_b)t} - e^{-(\lambda_{Pb}+\lambda_b)t}}{\lambda_{Pb} - \lambda_{Bi}} - \frac{e^{-(\lambda_{Po}+\lambda_b)t} - e^{-(\lambda_{Pb}+\lambda_b)t}}{\lambda_{Pb} - \lambda_{Po}} \right) +$$

$$\begin{aligned}
 & \frac{(1 - BR) \lambda_{Tl} \lambda_{Pb}}{\lambda_{Tl} - \lambda_{Bi}} \times A_{Bi}(0) \left(\frac{e^{-(\lambda_{Bi} + \lambda_b)t} - e^{-(\lambda_{Pb} + \lambda_b)t}}{\lambda_{Pb} - \lambda_{Bi}} - \frac{e^{-(\lambda_{Tl} + \lambda_b)t} - e^{-(\lambda_{Pb} + \lambda_b)t}}{\lambda_{Pb} - \lambda_{Tl}} \right) \\
 \Rightarrow \tilde{A}_{Pb}(T) &= \frac{BR \lambda_{Po} \lambda_{Pb}}{\lambda_{Po} - \lambda_{Bi}} \times A_{Bi}(0) \left(\frac{\frac{1 - e^{-(\lambda_{Bi} + \lambda_b)T}}{\lambda_{Bi} + \lambda_b} - \frac{1 - e^{-(\lambda_{Pb} + \lambda_b)T}}{\lambda_{Pb} + \lambda_b}}{\lambda_{Pb} - \lambda_{Bi}} - \frac{\frac{1 - e^{-(\lambda_{Po} + \lambda_b)T}}{\lambda_{Po} + \lambda_b} - \frac{1 - e^{-(\lambda_{Pb} + \lambda_b)T}}{\lambda_{Pb} + \lambda_b}}{\lambda_{Pb} - \lambda_{Po}} \right) + \\
 & \frac{(1 - BR) \lambda_{Tl} \lambda_{Pb}}{\lambda_{Tl} - \lambda_{Bi}} \times A_{Bi}(0) \left(\frac{\frac{1 - e^{-(\lambda_{Bi} + \lambda_b)T}}{\lambda_{Bi} + \lambda_b} - \frac{1 - e^{-(\lambda_{Pb} + \lambda_b)T}}{\lambda_{Pb} + \lambda_b}}{\lambda_{Pb} - \lambda_{Bi}} - \frac{\frac{1 - e^{-(\lambda_{Tl} + \lambda_b)T}}{\lambda_{Tl} + \lambda_b} - \frac{1 - e^{-(\lambda_{Pb} + \lambda_b)T}}{\lambda_{Pb} + \lambda_b}}{\lambda_{Pb} - \lambda_{Tl}} \right) \\
 \Rightarrow \tilde{A}_{Pb} &= \frac{BR \lambda_{Po} \lambda_{Pb}}{\lambda_{Po} - \lambda_{Bi}} \times A_{Bi}(0) \left(\frac{\frac{1}{\lambda_{Bi} + \lambda_b} - \frac{1}{\lambda_{Pb} + \lambda_b}}{\lambda_{Pb} - \lambda_{Bi}} - \frac{\frac{1}{\lambda_{Po} + \lambda_b} - \frac{1}{\lambda_{Pb} + \lambda_b}}{\lambda_{Pb} - \lambda_{Po}} \right) + \\
 & \frac{(1 - BR) \lambda_{Tl} \lambda_{Pb}}{\lambda_{Tl} - \lambda_{Bi}} \times A_{Bi}(0) \left(\frac{\frac{1}{\lambda_{Bi} + \lambda_b} - \frac{1}{\lambda_{Pb} + \lambda_b}}{\lambda_{Pb} - \lambda_{Bi}} - \frac{\frac{1}{\lambda_{Tl} + \lambda_b} - \frac{1}{\lambda_{Pb} + \lambda_b}}{\lambda_{Pb} - \lambda_{Tl}} \right)
 \end{aligned}$$

2. Single compartment uptake and clearance model for ^{213}Bi conjugates activity.

Uptake kinetics in organ or tumour with rate constant λ_u ($= \ln(2)/T_u$, with T_u the uptake half-life) and clearance back to plasma with rate constant λ_b

^{213}Bi kinetics:

$$\begin{aligned}
 A_{Bi}(t) &= \frac{\lambda_u}{\lambda_u - \lambda_b} A_{Bi}(0) e^{-\lambda_{Bi}t} (e^{-\lambda_b t} - e^{-\lambda_u t}) \quad \Rightarrow \\
 \tilde{A}_{Bi}(T) &= \frac{\lambda_u}{\lambda_u - \lambda_b} A_{Bi}(0) \left(\frac{1 - e^{-(\lambda_{Bi} + \lambda_b)T}}{\lambda_{Bi} + \lambda_b} - \frac{1 - e^{-(\lambda_{Bi} + \lambda_u)T}}{\lambda_{Bi} + \lambda_u} \right) \\
 \Rightarrow \tilde{A}_{Bi} &= \frac{A_{Bi}(0) \lambda_u}{(\lambda_{Bi} + \lambda_b)(\lambda_{Bi} + \lambda_u)}
 \end{aligned}$$

^{213}Po kinetics:

$$\begin{aligned}
 A_{Po}(t) &= \frac{\lambda_{Po} \lambda_u BR}{(\lambda_u - \lambda_b)(\lambda_{Po} - \lambda_{Bi})} A_{Bi}(0) (e^{-(\lambda_{Bi} + \lambda_b)t} - e^{-(\lambda_{Bi} + \lambda_u)t} - e^{-(\lambda_{Po} + \lambda_b)t} + e^{-(\lambda_{Po} + \lambda_u)t}) \quad \Rightarrow \\
 \tilde{A}_{Po}(T) &= \frac{\lambda_{Po} \lambda_u BR}{\lambda_{Po} - \lambda_{Bi}} A_{Bi}(0) \left(\frac{1 - e^{-(\lambda_{Bi} + \lambda_b)T}}{\lambda_{Bi} + \lambda_b} - \frac{1 - e^{-(\lambda_{Bi} + \lambda_u)T}}{\lambda_{Bi} + \lambda_u} - \frac{1 - e^{-(\lambda_{Po} + \lambda_b)T}}{\lambda_{Po} + \lambda_b} + \frac{1 - e^{-(\lambda_{Po} + \lambda_u)T}}{\lambda_{Po} + \lambda_u} \right) \\
 \Rightarrow \tilde{A}_{Po} &= \frac{\lambda_{Po} \lambda_u}{\lambda_{Po} - \lambda_{Bi}} BR A_{Bi}(0) \left(\frac{1}{(\lambda_{Bi} + \lambda_b)(\lambda_{Bi} + \lambda_u)} - \frac{1}{(\lambda_{Po} + \lambda_b)(\lambda_{Po} + \lambda_u)} \right)
 \end{aligned}$$

²⁰⁹Tl kinetics:

$$A_{Tl}(t) = \frac{\lambda_{Tl}\lambda_u(1-BR)}{(\lambda_u-\lambda_b)(\lambda_{Tl}-\lambda_{Bi})} A_{Bi}(0) \left(e^{-(\lambda_{Bi}+\lambda_b)t} - e^{-(\lambda_{Bi}+\lambda_u)t} - e^{-(\lambda_{Tl}+\lambda_b)t} + e^{-(\lambda_{Tl}+\lambda_u)t} \right) \Rightarrow$$

$$\tilde{A}_{Tl}(T) = \frac{\lambda_{Tl}\lambda_u(1-BR)}{\lambda_{Tl}-\lambda_{Bi}} A_{Bi}(0) \left(\frac{1-e^{-(\lambda_{Bi}+\lambda_b)T}}{\lambda_{Bi}+\lambda_b} - \frac{1-e^{-(\lambda_{Bi}+\lambda_u)T}}{\lambda_{Bi}+\lambda_u} - \frac{1-e^{-(\lambda_{Tl}+\lambda_b)T}}{\lambda_{Tl}+\lambda_b} + \frac{1-e^{-(\lambda_{Tl}+\lambda_u)T}}{\lambda_{Tl}+\lambda_u} \right)$$

$$\Rightarrow \tilde{A}_{Tl} = \frac{\lambda_{Tl}\lambda_u(1-BR)}{\lambda_{Tl}-\lambda_{Bi}} A_{Bi}(0) \left(\frac{1}{(\lambda_{Bi}+\lambda_b)(\lambda_{Bi}+\lambda_u)} - \frac{1}{(\lambda_{Tl}+\lambda_b)(\lambda_{Tl}+\lambda_u)} \right)$$

²⁰⁹Pb kinetics:

$$\begin{aligned} A_{Pb}(t) = & \lambda_{Pb} A_{Bi}(0) \frac{\lambda_u}{\lambda_u + \lambda_b} \\ & \times \left\{ \frac{\lambda_{Po} BR}{(\lambda_{Po} - \lambda_{Bi})} \left(\frac{e^{-(\lambda_{Pb}+\lambda_b)t} - e^{-(\lambda_{Pb}+\lambda_u)t} - e^{-(\lambda_{Bi}+\lambda_b)t} + e^{-(\lambda_{Bi}+\lambda_u)t}}{\lambda_{Bi} - \lambda_{Pb}} \right. \right. \\ & \left. \left. + \frac{e^{-(\lambda_{Po}+\lambda_b)t} - e^{-(\lambda_{Po}+\lambda_u)t} - e^{-(\lambda_{Pb}+\lambda_b)t} + e^{-(\lambda_{Pb}+\lambda_u)t}}{\lambda_{Po} - \lambda_{Pb}} \right) \right. \\ & \left. + \frac{\lambda_{Tl}(1-BR)}{(\lambda_{Tl} - \lambda_{Bi})} \left(\frac{e^{-(\lambda_{Pb}+\lambda_b)t} - e^{-(\lambda_{Pb}+\lambda_u)t} - e^{-(\lambda_{Bi}+\lambda_b)t} + e^{-(\lambda_{Bi}+\lambda_u)t}}{\lambda_{Bi} - \lambda_{Pb}} \right. \right. \\ & \left. \left. + \frac{e^{-(\lambda_{Tl}+\lambda_b)t} - e^{-(\lambda_{Tl}+\lambda_u)t} - e^{-(\lambda_{Pb}+\lambda_b)t} + e^{-(\lambda_{Pb}+\lambda_u)t}}{\lambda_{Tl} - \lambda_{Pb}} \right) \right\} \end{aligned}$$

$$\Rightarrow \tilde{A}_{Pb} = \lambda_{Pb} A_{Bi}(0) \lambda_u \times \left\{ \frac{\lambda_{Po} BR \lambda_{Po}}{(\lambda_{Po} - \lambda_{Bi})} \left(\frac{1}{(\lambda_{Bi} - \lambda_{Pb})(\lambda_{Pb} + \lambda_b)(\lambda_{Pb} + \lambda_u)} - \frac{1}{(\lambda_{Bi} - \lambda_{Pb})(\lambda_{Bi} + \lambda_b)(\lambda_{Bi} + \lambda_u)} \right) \right. \\ \left. + \frac{\lambda_{Tl} BR \lambda_{Tl}}{(\lambda_{Tl} - \lambda_{Bi})} \left(\frac{1}{(\lambda_{Po} - \lambda_{Pb})(\lambda_{Po} + \lambda_b)(\lambda_{Po} + \lambda_u)} - \frac{1}{(\lambda_{Po} - \lambda_{Pb})(\lambda_{Pb} + \lambda_b)(\lambda_{Pb} + \lambda_u)} \right) \right. \\ \left. + \frac{\lambda_{Tl} BR \lambda_{Tl}}{(\lambda_{Tl} - \lambda_{Bi})} \left(\frac{1}{(\lambda_{Bi} - \lambda_{Pb})(\lambda_{Pb} + \lambda_b)(\lambda_{Pb} + \lambda_u)} - \frac{1}{(\lambda_{Bi} - \lambda_{Pb})(\lambda_{Bi} + \lambda_b)(\lambda_{Bi} + \lambda_u)} \right) \right. \\ \left. + \frac{\lambda_{Tl} BR \lambda_{Tl}}{(\lambda_{Tl} - \lambda_{Bi})} \left(\frac{1}{(\lambda_{Tl} - \lambda_{Pb})(\lambda_{Tl} + \lambda_b)(\lambda_{Tl} + \lambda_u)} - \frac{1}{(\lambda_{Tl} - \lambda_{Pb})(\lambda_{Pb} + \lambda_b)(\lambda_{Pb} + \lambda_u)} \right) \right\}$$

REFERENCES

1. Bodei, L., et al., *PRRT: Defining the paradigm shift to achieve standardization and individualization*. J Nucl Med, 2014. 55(11): p. 1753-6.
2. van der Zwan, W.A., et al., *GEPNETs UPDATE: Radionuclide therapy in neuroendocrine tumors*. Eur J Endocrinol, 2015. 172(1): p. R1-R8.
3. Mulford, D.A., D.A. Scheinberg, and J.G. Jurcic, *The promise of targeted {alpha}-particle therapy*. J Nucl Med, 2005. 46 Suppl 1: p. 199S-204S.
4. Morgenstern, A., F. Bruchertseifer, and C. Apostolidis, *Targeted alpha therapy with 213Bi*. Curr Radiopharm, 2011. 4(4): p. 295-305.
5. Jurcic, J.G., et al., *Radiolabeled anti-CD33 monoclonal antibody M195 for myeloid leukemias*. Cancer Res, 1995. 55(23 Suppl): p. 5908s-5910s.
6. Norenberg, J.P., et al., *213Bi-[DOTA0, Tyr3]octreotide peptide receptor radionuclide therapy of pancreatic tumors in a preclinical animal model*. Clin Cancer Res, 2006. 12(3 Pt 1): p. 897-903.
7. Wild, D., et al., *Alpha- versus beta-particle radiopeptide therapy in a human prostate cancer model (213Bi-DOTA-PESIN and 213Bi-AMBA versus 177Lu-DOTA-PESIN)*. Cancer Res, 2011. 71(3): p. 1009-18.
8. Kratochwil, C., et al., *(2)(1)(3)Bi-DOTATOC receptor-targeted alpha-radionuclide therapy induces remission in neuroendocrine tumours refractory to beta radiation: a first-in-human experience*. Eur J Nucl Med Mol Imaging, 2014. 41(11): p. 2106-19.
9. Melis, M., et al., *Dose-response effect of Gelofusine on renal uptake and retention of radiolabelled octreotate in rats with CA20948 tumours*. Eur J Nucl Med Mol Imaging, 2009. 36(12): p. 1968-76.
10. de Jong, M., et al., *Tumor response after [(90)Y-DOTA(0),Tyr(3)]octreotide radionuclide therapy in a transplantable rat tumor model is dependent on tumor size*. J Nucl Med, 2001. 42(12): p. 1841-6.
11. Bison, S.M., et al., *Peptide receptor radionuclide therapy (PRRT) with [(177)Lu-DOTA(0),Tyr(3)] octreotate in combination with RAD001 treatment: further investigations on tumor metastasis and response in the rat pancreatic CA20948 tumor model*. EJNMMI Res, 2014. 4: p. 21.
12. Verwijnen, S., et al., *Low-dose-rate irradiation by 131I versus high-dose-rate external-beam irradiation in the rat pancreatic tumor cell line CA20948*. Cancer Biother Radiopharm, 2004. 19(3): p. 285-92.
13. Bjork-Eriksson, T., et al., *Discrimination of human tumor radioresponsiveness using low-dose rate irradiation*. Int J Radiat Oncol Biol Phys, 1998. 42(5): p. 1147-53.
14. McDevitt, M.R., et al., *An 225Ac/213Bi generator system for therapeutic clinical applications: construction and operation*. Appl Radiat Isot, 1999. 50(5): p. 895-904.
15. de Blois, E., et al., *Characteristics of SnO2-based 68Ge/68Ga generator and aspects of radiolabeling DOTA-peptides*. Appl Radiat Isot, 2011. 69(2): p. 308-15.
16. Forrer, F., et al., *From outside to inside? Dose-dependent renal tubular damage after high-dose peptide receptor radionuclide therapy in rats measured with in vivo (99m)Tc-DMSA-SPECT and molecular imaging*. Cancer Biother Radiopharm, 2007. 22(1): p. 40-9.
17. Konijnenberg, M.W., *Therapeutic application of CCK2R-targeting PP-F11: influence of particle range, activity and peptide amount*. European Journal of Nuclear Medicine & Molecular Imaging Research, 2014. 4: p. 15.
18. Team, X.-M., *MCNP- a general Monte Carlo N-particle transport code, version 5 vol. 1: Overview and theory*, 2003, Los Alamos National Lab Report.
19. Hendricks, J.S., *MCNPX Extensions Version 2.5.0*. MCNPX. Vol. LA-UR-05-2675. 2005.

20. Eckerman K., E.A., *MIRD: Radionuclide Data and Decay Schemes. 2nd edition.* 2008, Reston (US): Society of Nuclear Medicine and Molecular Imaging.
21. Hobbs, R.F., et al., *A nephron-based model of the kidneys for macro-to-micro alpha-particle dosimetry.* Phys Med Biol, 2012. 57(13): p. 4403-24.
22. O'Donoghue, J.A., M. Bardies, and T.E. Wheldon, *Relationships between tumor size and curability for uniformly targeted therapy with beta-emitting radionuclides.* J Nucl Med, 1995. 36(10): p. 1902-9.
23. Gillies, R.J., et al., *Causes and effects of heterogeneous perfusion in tumors.* Neoplasia, 1999. 1(3): p. 197-207.
24. Bol, K., et al., *Can DCE-MRI explain the heterogeneity in radiopeptide uptake imaged by SPECT in a pancreatic neuroendocrine tumor model?* PLoS One, 2013. 8(10): p. e77076.
25. Pach, D., et al., *Repeated cycles of peptide receptor radionuclide therapy (PRRT)—results and side-effects of the radioisotope 90Y-DOTA TATE, 177Lu-DOTA TATE or 90Y/177Lu-DOTA TATE therapy in patients with disseminated NET.* Radiother Oncol, 2012. 102(1): p. 45-50.
26. Valkema, R., et al., *Long-term follow-up of renal function after peptide receptor radiation therapy with (90)Y-DOTA(0), Tyr(3)-octreotide and (177)Lu-DOTA(0), Tyr(3)-octreotate.* J Nucl Med, 2005. 46 Suppl 1: p. 83S-91S.
27. Weyer, K., et al., *Renal uptake of 99mTc-dimercaptosuccinic acid is dependent on normal proximal tubule receptor-mediated endocytosis.* J Nucl Med, 2013. 54(1): p. 159-65.
28. Dawson, L.A., et al., *Radiation-associated kidney injury.* Int J Radiat Oncol Biol Phys, 2010. 76(3 Suppl): p. S108-15.
29. Bodei, L., et al., *Long-term evaluation of renal toxicity after peptide receptor radionuclide therapy with 90Y-DOTATOC and 177Lu-DOTATATE: the role of associated risk factors.* Eur J Nucl Med Mol Imaging, 2008. 35(10): p. 1847-56.
30. Guerriero, F., et al., *Kidney dosimetry in (1)(7)(7)Lu and (9)(0)Y peptide receptor radionuclide therapy: influence of image timing, time-activity integration method, and risk factors.* Biomed Res Int, 2013. 2013: p. 935351.
31. Bernard, B.F., et al., *D-lysine reduction of indium-111 octreotide and yttrium-90 octreotide renal uptake.* J Nucl Med, 1997. 38(12): p. 1929-33.
32. Kobayashi, H., et al., *L-lysine effectively blocks renal uptake of I-125- or Tc-99m-labeled anti-Tac disulfide-stabilized Fv fragment.* Cancer Res, 1996. 56(16): p. 3788-3795.
33. de Jong, M., et al., *Combination radionuclide therapy using 177Lu- and 90Y-labeled somatostatin analogs.* J Nucl Med, 2005. 46 Suppl 1: p. 13S-7S.
34. Walrand, S., et al., *Tumour control probability derived from dose distribution in homogeneous and heterogeneous models: assuming similar pharmacokinetics, (125)Sn-(177)Lu is superior to (90)Y-(177)Lu in peptide receptor radiotherapy.* Phys Med Biol, 2012. 57(13): p. 4263-75.



Chapter 5

***In vitro* comparison of ^{213}Bi - and ^{177}Lu -radiation for peptide receptor radionuclide therapy**

Ho Sze Chan, Erik de Blois, Alfred Morgenstern, Frank Bruchertseifer, Marion de Jong, Wouter Breeman, Mark Konijnenberg

PLoS One. 2017 Jul 21;12(7)

ABSTRACT

Absorbed doses for α -emitters are different from those for β -emitters, as the high linear energy transfer (LET) nature of α -particles results in a very dense energy deposition over a relatively short path length near the point of emission. This highly localized and therefore high energy deposition can lead to enhanced cell-killing effects at absorbed doses that are non-lethal in low-LET type of exposure. Affinities of DOTA-DPhe¹-Tyr³-octreotate (DOTA-TATE), ¹¹⁵In-DOTATATE, ¹⁷⁵Lu-DOTATATE and ²⁰⁹Bi-DOTATATE were determined in the K562-SST₂ cell line. Two other cell lines were used for radiation response assessment; BON and CA20948, with a low and high expression of somatostatin receptors, respectively. Cellular uptake kinetics of ¹¹¹In-DOTATATE were determined in CA20948 cells. CA20948 and BON were irradiated with ¹³⁷Cs, ¹⁷⁷Lu-DTPA, ¹⁷⁷Lu-DOTATATE, ²¹³Bi-DTPA and ²¹³Bi-DOTATATE. Absorbed doses were calculated using the MIRDCell dosimetry method for the specific binding and a Monte Carlo model of a cylindrical 6-well plate geometry for the exposure by the radioactive incubation medium. Absorbed doses were compared to conventional irradiation of cells with ¹³⁷Cs and the relative biological effect (RBE) at 10% survival was calculated.

Results:

IC₅₀ of (labelled) DOTATATE was in the nM range. Absorbed doses up to 7 Gy were obtained by 5.2 MBq ²¹³Bi-DOTATATE, in majority the dose was caused by α -particle radiation. Cellular internalization determined with ¹¹¹In-DOTATATE showed a linear relation with incubation time. Cell survival after exposure of ²¹³Bi-DTPA and ²¹³Bi-DOTATATE to BON or CA20948 cells showed a linear-exponential relation with the absorbed dose, confirming the high LET character of ²¹³Bi. The survival of CA20948 after exposure to ¹⁷⁷Lu-DOTATATE and the reference ¹³⁷Cs irradiation showed the typical curvature of the linear-quadratic model. 10% Cell survival of CA20948 was reached at 3 Gy with ²¹³Bi-DOTATATE, a factor 6 lower than the 18 Gy found for ¹⁷⁷Lu-DOTATATE and also below the 5 Gy after ¹³⁷Cs external exposure.

Conclusion:

²¹³Bi-DTPA and ²¹³Bi-DOTATATE lead to a factor 6 advantage in cell killing compared to ¹⁷⁷Lu-DOTATATE. The RBE at 10% survival by ²¹³Bi-ligand compared to ¹³⁷Cs was 2.0 whereas the RBE for ¹⁷⁷Lu-DOTATATE was 0.3 in the CA20948 *in vitro* model.

INTRODUCTION

The receptor-mediated endocytosis pathway is one of the main pathways to deliver biomolecules in cells. Peptide receptor radionuclide therapy (PRRT) uses this process to deliver cytotoxic dose by the emission of β -particles to neuroendocrine tumours (NET). Somatostatin peptide analogues, such as DOTA-DPhe¹-Tyr³-octreotide (DOTATOC) and DOTA-DPhe¹-Tyr³-octreotate (DOTATATE), are the most common delivery systems for treatment of NET. By radiolabelling these analogues with β -emitting radionuclide such as ^{90}Y ($T_{1/2}=64.1$ h) or ^{177}Lu ($T_{1/2}=6.6$ d), high radiation doses can be delivered to tumour cells, causing mostly single-strand breaks (SSB) in the DNA of the tumour cells. Dependent on the number of SSB, cells can undergo cell arrest, with either activation of the cellular repair mechanism for repair or apoptosis as a consequence [1]. Combination of several repairable SSB lesions may lead to additional cell kill.

α -Emitters (e.g. ^{213}Bi , $T_{1/2}=46$ min; ^{225}Ac , $T_{1/2}=9.9$ d; ^{211}At , $T_{1/2}=7.2$ h) are increasingly used for targeted alpha therapy (TAT) because of their emission of high linear energy transfer (LET) particles with a relative short path length. Labelled ^{213}Bi -peptides have already been proven to be promising in PRRT with NETs in preclinical as well in clinical studies [2–5]. α -Emitters emit high LET particles, causing double-strand breaks (DSB) in DNA when targeted to the tumour cells [6]. Therefore, the cytotoxic property in cells is found to be greater for α -emitters than for β -emitters [6, 7].

The cytotoxic response of the cells is related to the absorbed dose delivered to the cells. Several studies have been investigating the absorbed dose caused in cells by α -emitters [8–10]. Those studies showed the challenge involved in describing dose-related survival in cells with α -particles radiation. Huang and co-workers distinguished three clear differences in cell dosimetry calculations for α -emitters compared to β -emitters or to external beam therapy; 1) short path length, 2) small target volume and 3) non-uniform distribution of radionuclides [11]. For β -emitters and external γ -beams, hundreds to thousands of ionizations are required for a cell-killing effect, whereas using α -emitters, this can be reached with 4–10 ionizations. Due to the low number of ionizations, leading to large variations in the number of α -particle tracks traversing the cells, the validity of the mean absorbed dose which assumes Poisson statistics, was not always given for α -emitters [12]. Moreover, variability in experiments strongly influenced the calculated absorbed dose, for example the models in which the absorbed dose was calculated; single cells, clusters of cells or whole organs. Furthermore, inhomogeneous uptake can also influence the calculated absorbed dose. The dose limits for α -emitters showed a high model dependence for selected survival endpoints, and therefore, the relative biological effect (RBE) should be considered within the same model and using the same endpoint. As mentioned, the calculation of the absorbed dose *in vitro* for α -emitters can be quite complicated. Many studies only mention the radioactivity administered to the cells instead of using absorbed dose. Therefore, the

effective cytotoxic properties of α -emitters as published cannot easily be compared to each other on an absorbed dose level.

In this study we calculated the average absorbed dose delivered to single cells using non-specific and receptor-specific binding absorbed dose calculation methods. The non-specific binding method describes the homogeneous irradiation from medium without specific binding of labelled peptide to the receptors on the cell, whereas the specific binding method describes the specific binding of the labelled peptide to the receptor on the cell and the addition of homogeneous irradiation from medium to the cells. Affinity studies in K562-SSTR₂ (transgenic human erythroleukemic cells transfected with somatostatin receptor subtype 2 (SSTR₂)) cells were performed to determine the IC₅₀ of DOTATATE, ¹¹⁵In-DOTATATE, ¹⁷⁵Lu-DOTATATE, and ²⁰⁹Bi-DOTATATE. An internalization assay with CA20948 (rat pancreatic tumour) cell using ¹¹¹In-DOTATATE was performed to obtain information of the kinetics of cell uptake. Based on results obtained from cell uptake, small-scale dosimetry calculations were performed to provide the additional absorbed dose caused by specific binding to the cells to obtain the correlation between absorbed dose and cell survival. We evaluated the RBE at the absorbed dose of 10% survival (D_{10}) of ²¹³Bi-DTPA, ²¹³Bi-DOTATATE, ¹⁷⁷Lu-DTPA, ¹⁷⁷Lu-DOTATATE and external radiation using ¹³⁷Cs using two different cell lines; CA20948 [13] with high and BON (human carcinoid) with low SSTR₂ expression [14]. The aim of the study was to compare the effective cytotoxic properties of different irradiation methods i.e. external photon irradiation and targeted radionuclide therapy in the same study.

MATERIALS AND METHODS

All chemicals were purchased from Sigma Aldrich, culture media for cell culture and *in vitro* assays were purchased from Gibco, Life Technologies, unless otherwise indicated.

Cell culture

K562-SSTR₂ is a human erythroleukemic transgenic cell line with an overexpression of SSTR₂ [15] and was a gift of prof. L. Hofland and prof. P.M. van Hagen (Erasmus MC, Rotterdam, the Netherlands). Cells were cultured in RPMI 1640 supplemented with 10% of fetal calf serum (Gibco, Life Technologies). CA20948 tumour cells [16] were cultured in DMEM supplemented with 10% fetal calf serum. Human carcinoid BON cells (American Tissue Culture Collection, Wesel, Germany) were cultured in F12-DMEM. The medium was supplemented with 10% fetal calf serum. All cells were cultured in T175 tissue culture flasks at 37°C in a humidified atmosphere of 5% CO₂.

Radiolabelling and radioiodination of peptides

^{111}In -DOTATATE with a molar activity (MA) of 15 MBq/nmol was prepared by incubation of 15 MBq $^{111}\text{InCl}_3$ ($T_{1/2} = 2.8$ d, γ of 171 and 245 keV, Covidien), DOTATATE (Mw 1436 g/mol, Biosynthema, St. Louis, MO, USA), sodium acetate 2.5 M, ethanol and a mixture of gentisic acid/ascorbic acid 50 mM in a volume of 140 μL at 80°C for 20 min. After incubation, 5 μL 10 mM DTPA (diethylenetriaminepentaacetic acid) was added to stop the reaction and to chelate any “unbound” or “free” ^{111}In . MA is expressed in MBq per nmol peptide.

^{177}Lu -DOTATATE (at MA 53 MBq/nmol) was prepared under the same labelling conditions as ^{111}In -DOTATATE described above. $^{177}\text{LuCl}_3$ was purchased from IDB Holland B.V (Baarle Nassau, the Netherlands).

For the labelling of ^{213}Bi , an $^{225}\text{Ac}/^{213}\text{Bi}$ generator (≤ 222 MBq) was eluted with a fixed elution volume of 600 μL 0.1M/0.1M NaI/HCl [17]. The ^{213}Bi containing elution was added to a mixture of 7 nmol DOTATATE, 60 μL TRIS 2M, 1.85 μL ascorbic acid 20% and MQ (final volume 800 μL). The reaction was performed at 95°C for 5 min and cooled on ice for 2 min afterwards. 5 μL of DTPA 10 mM was added to stop the labelling and chelate “unbound”/“free” ^{213}Bi [18].

To determine the incorporation of the radioactivity, ITLC (Instant Thin-Layer Chromatography) was performed after each labelling. HPLC (High Performance Liquid Chromatography) was performed to determine the radiochemical purity (RCP) of the radiopeptides as described by the Blois et al. [19]. RCP of the labelled peptide was expressed as percentage of intact labelled peptide of interest versus of all other radioactive detectable compounds. Tyr³-octreotide (Mw = 1034 g/mol, Biosynthema, St. Louis, MO, USA) was used to prepare ^{125}I -Tyr³-octreotide using chloramine-T as described elsewhere [20]. Analysis and purification of the radioiodinated peptide were performed using HPLC as described by de Blois et al [19].

Labelling of non-radio-peptide

The labelling of ^{115}In -DOTATATE was performed by addition of $^{115}\text{InHNO}_3$ (ICP standard, 1 g/L) to DOTATATE at a molar ratio of 5:1. The pH was adjusted to a pH of 4 by adding sodium acetate (2.5 M) and the labelling mixture was heated for 30 min at 80°C . Quality control was performed using HPLC as described previously [19]. UV-detection was performed at 278 nm. Under these conditions, DOTATATE was fully incorporated with ^{115}In . After quality control the labelled peptide was purified and collected using the same HPLC method. The concentration of the labelled peptide was determined by UV spectrophotometer at 278 nm. This procedure was also performed for the labelling of ^{175}Lu -DOTATATE and ^{209}Bi -DOTATATE.

IC₅₀

IC₅₀ values of DOTATATE, ¹¹⁵In-DOTATATE, ¹⁷⁵Lu-DOTATATE or ²⁰⁹Bi-DOTATATE were determined using K562-SST₂ membranes [21]. In short, cell membranes were isolated as described by Reubi [22]. Freshly dispersed membrane preparations (corresponding to 25 µg protein) were incubated at room temperature for 60 min with ¹²⁵I-Tyr³-octreotide (40k cpm) with or without increasing concentrations of DOTATATE, ¹¹⁵In-DOTATATE, ¹⁷⁵Lu-DOTATATE, or ²⁰⁹Bi-DOTATATE in HEPES buffer (10 mM HEPES, 5mM MgCl₂ and 0.02 g/L bacitracin, pH 7.6) containing 0.2% BSA. After incubation for 1 h, 1 mL HEPES (4°C) was added to stop the reaction. Non-bound radioligand was separated from the membrane-bound radioligand by centrifugation for 2 min at 10000 g. The remaining pellet was washed twice with ice-cold HEPES buffer and counted in a γ-counter (Wallac Wizard 3, Perkin Elmer, Groningen, the Netherlands) [21]. One-way ANOVA was used to calculate significant differences of IC₅₀ values of DOTATATE, ¹¹⁵In-DOTATATE, ¹⁷⁵Lu-DOTATATE, and ²⁰⁹Bi-DOTATATE.

Internalisation as function of peptide amount in SSTR₂ positive CA20948 cell line

0.5x10⁶ CA20948 cells were incubated with ¹¹¹In-DOTATATE, ranging from 1 nM to 390 nM, for 1 h at 37°C. After incubation, ¹¹¹In-DOTATATE was removed from the cells by washing the cells twice with 1 mL ice-cold PBS. Ice-cold strip medium (1 mL, HBSS containing 20 mM sodium acetate, pH 5) was added to the cells and incubated for 10 min to remove membrane-bound (f_{mem}) ¹¹¹In-DOTATATE from the receptor. The strip medium was collected and 1 mL of ice-cold strip medium was added to the cells for 10 min incubation and collected again. Sodium hydroxide (1 mL, 1M) was added to the cells to detach the cells from the well and to determine the radioactivity inside the cells, this is the internalized fraction (f_{int}). The f_{int} was collected separately from the f_{mem} . The collected fractions were measured by the γ-counter. The results were plotted as % activity (%A) compared to total applied activity. To determine the non-specific binding, an excess of DOTATATE (1x10⁻⁶M) was added to ¹¹¹In-DOTATATE and incubated for 1 h. The f_{mem} and f_{int} fractions were measured on the γ-counter. No internalization assays were performed with BON cell line due to the low expression of SSTR₂ receptors. The specific binding of f_{mem} and f_{int} is the binding in 0.5x10⁶ CA20948 cells minus the non-specific binding. The specific binding for 0.5x10⁶ CA20948 cells were extrapolated to an uptake in 500 cells, these extrapolated uptakes were used to calculate the binding of 500 cells used for clonogenic assay. ¹¹¹In-DOTATATE was only used to investigate the cell uptake kinetics, in this study potential cytotoxic effects caused by absorbed dose were neglected.

Clonogenic assay

Survival curves of BON and CA20948 cells were determined by clonogenic assay after irradiation with ^{137}Cs , ^{177}Lu -DTPA, ^{177}Lu -DOTATATE, ^{213}Bi -DTPA or ^{213}Bi -DOTATATE. Before irradiation of the cells, 500 cells were seeded in 6-well plates (pre-coated with poly-L-lysine) 24 h before the experiment. The cells were treated with increasing doses of radioligand, diluted in internalization medium (30 mM HEPES and 0.25% BSA), and incubated for 1 h at 37°C in a humidified atmosphere of 5% CO_2 . After irradiation, internalization medium containing radioligand was removed. Cells were washed twice with PBS and incubated with medium containing 10% FBS for 12 d. Every 2 or 3 d, medium was replaced by fresh culture medium. In order to be able to compare the cytotoxic effect of ^{213}Bi -DOTATATE vs ^{177}Lu -DOTATATE, the starting amount of labelled peptide was kept constant, therefore excess peptide was added to the ^{177}Lu -DOTATATE to a start concentration of 390 nM. Similarly, clonogenic assay was performed with different doses of external irradiation with ^{137}Cs (dose-rate of 0.6 Gy/min): 0.5, 1, 2, 4, 5, 6, 8 and 10 Gy.

After incubation over a period of 12 days at 37°C in a humidified atmosphere of 5% CO_2 , cells were washed twice with PBS, fixed with 1 mL 100% ethanol and stained with 1 mL hematoxylin. The 6-well plates containing colonies were scanned with a HP-scanner at 200 dpi. The colonies in each well were counted by a clonocounter [23]. The survival was plotted as a function of absorbed dose and fitted to linear-quadratic (LQ) or linear-exponential curves.

Non-specific binding absorbed dose

The cell absorbed dose during the incubation period was calculated with a dosimetry model of the 6-well plate, as described by Verwijnen et al. [24]. The 3.5 cm diameter well cavity was modeled in the Monte Carlo radiation transport code Monte Carlo N-Particle eXtended MCNPX (version 2.5.0, Los Alamos National Laboratory, USA) with homogeneously distributed radioactivity over the 2 mL volume aqueous liquid within the cavity. Dose scoring regions of 25 μm were used to calculate the absorbed fractions of energy as a function of depth in the bottom 200 μm of the well, see Fig. 1. The division the layers of the well were as followed; 18 layers of 100 μm and 8 layers of 25 μm at the bottom of the well.

Radiation energy spectra for ^{177}Lu , ^{213}Bi and its daughters were derived from the MIRD radionuclide data handbook [25]. For each emission (α -, β - particles, low energy Auger- and internal conversion electrons and γ -rays) 10 million particle histories were used for particle transport calculations in MCNPX. Absorbed energy was calculated in the dose scoring regions within the cavity filled with radioactivity and the cross dose to the other 5 well cavities. Absorbed dose rates per unit activity (or S-values) for each radionuclide and dose scoring region were calculated following the MIRD schema [26].

The cells in the clonogenic assay were assumed to lie on the bottom surface of the 6-well plate cavities and therefore the macroscopic mean absorbed dose \bar{D} to the cells during the

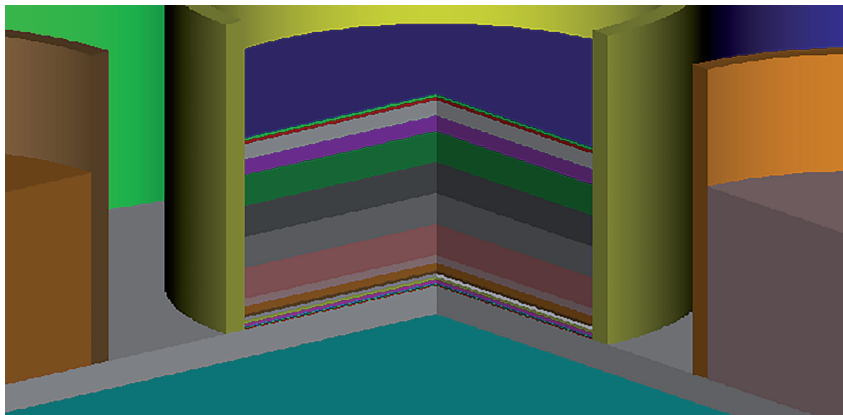


Figure 1, Illustration of layers (25 µm) divided over a total volume of 2 mL for the calculation of the absorbed dose in a 6-well plate. The lowest layer of 25 µm was used for the calculation of absorbed dose at the bottom of the well containing 500 cells.

1 h incubation was calculated from the S-value in the bottom 25 µm layer and the time-integrated activity \tilde{A} by:

$$\bar{D}(25\mu\text{m}\leftarrow\text{fluid}) = \tilde{A}_{\text{fluid}}(1) \times S(25\mu\text{m}\leftarrow\text{fluid}) = \int_{T_0}^T A_{\text{fluid}} e^{-\lambda t} dt \times S(25\mu\text{m}\leftarrow\text{fluid})$$

The integration was performed for the activity in the fluid from $T_0 = 0$ to $T = 1$ h, also taking into account the progeny activity from ^{213}Bi together with their specific S-values. The contributions to the absorbed dose by α -particles were considered separately from the dose by β -particles, low energy electrons and γ -rays.

Specific binding absorbed dose

For cell dosimetry calculation, the total uptake (f_{mem} and f_{int}) of 0.5×10^6 cells (CA20948) was extrapolated to the uptake of 500 cells. The percentage of uptake was then used for cell dosimetry with the assumption that the radioactivity was bound to the cell membrane ($f_{int} = 0$ and $f_{mem} = 1$) over a period of 12 d without dissociation of the radioactivity.

The dosimetry for the specific uptake of radioactivity in the cells was calculated with the multicellular dosimetry code MIRD cell [27]. For the calculation of dosimetry in CA20948, a cell radius of 6 µm was taken, as the uptake in the cells was not further differentiated, only uptake on the cell surface and homogeneous cell uptake were considered. Initially 500 cells were plated over the 9.62 cm² surface of the well. For evenly distributed cells over the surface the mean inter-cell distance would be 770 µm. In reality the cells were more clustered to the center of the well. Furthermore, the inter-cell distance was larger than the range of the α -particles and hence the cross-dose contribution from radioactivity taken up in neighboring cells was assumed to be minimal.

Table 1, S-values (mGy/MBq.s) of ²¹³Bi, ²¹³Po, ²⁰⁹Tl, ²⁰⁹Pb and ¹⁷⁷Lu for a cell with a radius of 6 μm according to MIRDcell code

	Self-dose		Cross-dose S(C←C')	
	S(C ← C)	S (C ← CS)	Cell distance 50 μm	Cell distance 100 μm
²¹³ Bi	1.71	1.14	7.02 ⁻³	3.03 ⁻⁴
²¹³ Po	49.2	33.0	0.40	OOOR
²⁰⁹ Tl	0.73	0.44	1.31 ⁻³	3.15 ⁻⁴
²⁰⁹ Pb	0.34	0.22	1.61 ⁻³	3.46 ⁻⁴
²¹³ Bi + progeny	50.2	33.6	0.52	3.48 ⁻²
¹⁷⁷ Lu	0.67	0.42	2.00 ⁻³	4.18 ⁻⁴

OOOR= out of range C = cell, C' = other cell, CS = cell surface

The number of disintegrations within each cell (or Time-Integrated Activity per cell \tilde{a}) was calculated by integration of the decay function of ¹⁷⁷Lu and ²¹³Bi and its progeny over the 12 d irradiation time multiplied by the f_{int} and f_{mem} per cell. This assumes that f_{mem} will remain bound to the cells and f_{int} remains trapped in the cell over a period of 12 d. The cellular S values were obtained from the MIRD cell code for a cell with a radius of 6 μm and indicated in Table 1. The absorbed doses to the cell are indicated per decay of ²¹³Bi and its daughters ²¹³Po, ²⁰⁹Tl, ²⁰⁹Pb and for ¹⁷⁷Lu in the cell or on the surface of a spherical cell with a radius of 6 μm. Also the cross-dose S-values for cells with radioactivity at 50 μm and at 100 μm are indicated.

The mean self-absorbed dose to the cells was calculated by the product of \tilde{A}_{cell} the mean cumulated activity per cell with the cellular S-values specific for the binding site:

$$\overline{D}_{cell} = \tilde{A}_{cell} [f_{int} S(C \leftarrow C) + f_{mem} (C \leftarrow CS)], \text{ with}$$

$$\tilde{A}_{cell}(\text{Bi-213}) = \int_{T_0}^T \tilde{A}_{cell}^{Bi} e^{-\lambda_{Bi}t} dt$$

$$\tilde{A}_{cell}(\text{Po-213}) = \int_{T_0}^T \tilde{A}_{cell}^{Bi} \frac{BR_{Po} \lambda_{Po}}{\lambda_{Bi} - \lambda_{Po}} (e^{-\lambda_{Po}t} - e^{-\lambda_{Bi}t}) dt$$

$$\tilde{A}_{cell}(\text{Tl-209}) = \int_{T_0}^T \tilde{A}_{cell}^{Bi} \frac{BR_{Tl} \lambda_{Tl}}{\lambda_{Bi} - \lambda_{Tl}} (e^{-\lambda_{Tl}t} - e^{-\lambda_{Bi}t}) dt$$

$$\tilde{A}_{cell}(\text{Pb-209}) = \int_{T_0}^T \tilde{A}_{cell}^{Bi} \left\{ \frac{BR_{Po} \lambda_{Po} \lambda_{Pb}}{\lambda_{Bi} - \lambda_{Pb}} \left(\frac{e^{-\lambda_{Pb}t} - e^{-\lambda_{Bi}t}}{\lambda_{Bi} - \lambda_{Pb}} + \frac{e^{-\lambda_{Po}t} - e^{-\lambda_{Pb}t}}{\lambda_{Po} - \lambda_{Pb}} \right) - \frac{BR_{Tl} \lambda_{Tl} \lambda_{Pb}}{\lambda_{Bi} - \lambda_{Tl}} \left(\frac{e^{-\lambda_{Pb}t} - e^{-\lambda_{Tl}t}}{\lambda_{Tl} - \lambda_{Pb}} + \frac{e^{-\lambda_{Pb}t} - e^{-\lambda_{Bi}t}}{\lambda_{Bi} - \lambda_{Pb}} \right) \right\} dt$$

The integration over time was performed between $T_0 = 1$ h and $T = 12$ d. It was assumed that no radioligand cleared from the cells once it was bound. The absorbed dose originating from the cellular uptake during the 1 h incubation period was neglected.

RESULTS

Labelling

The incorporation for all used radiolabelled peptide was > 99% and the RCP of ^{111}In -DOTATATE, ^{177}Lu -DOTATATE and ^{213}Bi -DOTATATE were > 95%, > 95%, and > 85%, respectively. The RCP of ^{125}I -Tyr³-octreotide was > 99%. The chemical yield of ^{115}In -DOTATATE, ^{175}Lu -DOTATATE and ^{209}Bi -DOTATATE were > 99%.

Affinity study and internalization

Under the conditions applied, DOTATATE, ^{111}In -DOTATATE, ^{175}Lu -DOTATATE and ^{209}Bi -DOTATATE showed similar affinities to SSTR₂ on the membranes of K562-SSTR₂ cells. IC₅₀ values of 3.0 ± 0.9 nM, 2.5 ± 0.4 nM, 2.7 ± 0.4 nM and 5.2 ± 1.0 nM were found, respectively. No significant differences were found between the IC₅₀ values.

Internalization in SSTR₂ positive CA20948 cell line

Internalization was performed to determine the amount of radioligand bound to the receptors, at the cell membrane and internalized into the cell. Optimized concentration of ^{111}In -DOTATATE for internalization on CA20948 was 1 nM. At this concentration, the f_{int} increased linearly as a function of incubation time. However, the f_{mem} remained constant at a level of 0.008 %A as a function of incubation time, see Fig. 2.

Binding assays with ^{213}Bi -DOTATATE involved high concentrations of unlabelled peptide due to the low molar activity of labelled peptide. At the highest peptide amount used for the experiment (390 nM), an equilibrium of association and dissociation was found within 30 min for f_{mem} and 10 min for f_{int} . Here we mimicked the internalization of ^{213}Bi -DOTATATE and ^{177}Lu -DOTATATE by using ^{111}In -DOTATATE as a surrogate to study the uptake kinetics with the concentration used in the clonogenic assay. Cells were incubated

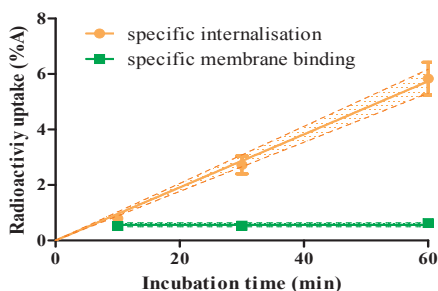


Figure 2, Specific membrane binding and specific internalization of 1 nM ^{111}In -DOTATATE on 0.5×10^6 cells of CA20948 as function of incubation time, $n = 3$. The lines indicate the fitted curves with the 95% confidence intervals, internalization data linear curve ($R^2 = 0.97$) with slope: 0.096 ± 0.003 %IA/min and for the f_{mem} the mean value of 0.56 ± 0.06 %IA.

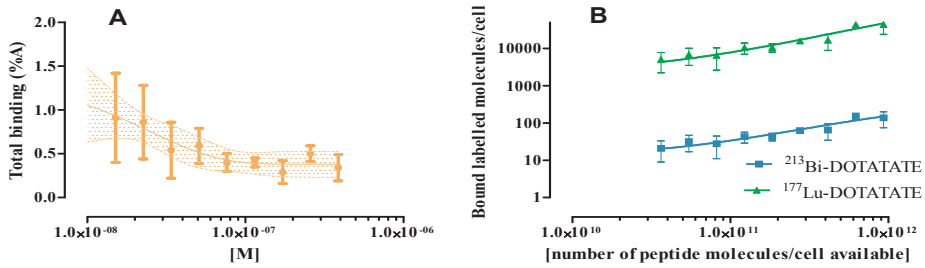


Figure 3A-3B, A) Total binding of 1.5×10^{-8} to 3.9×10^{-7} M ^{111}In -DOTATATE with 0.5 million CA20948 cells after 60 min incubation ($n=3$) and B) the number of labelled ^{213}Bi -DOTATATE or ^{177}Lu -DOTATATE molecules bound per cell (y-axis) versus the total number of peptide present per cell (x-axis) during clonogenic assay. The line and shaded area in Fig. 3A indicate the fit ($R^2=0.4$) and its 95% confidence interval of a single exponential curve $Ae^{-k[M]} + B$ with $A=1.0 \pm 0.5\%A$, $k=39 \pm 24 \mu\text{mol}^{-1}$ and $B=0.38 \pm 0.07\%A$.

with decreasing concentrations of peptide (ranging 390 to 15 nM) for 1 h. The uptake was found to be relatively low, the f_{mem} and f_{int} were difficult to distinguish from each other, and therefore the sum of f_{mem} and f_{int} was used for further cell dosimetry calculations, see Fig. 3A. The uptake was used to calculate the number labelled peptide, ^{213}Bi -DOTATATE or ^{177}Lu -DOTATATE, bound per cells during clonogenic assay with ^{213}Bi -DOTATATE and ^{177}Lu -DOTATATE in CA20948, see Fig. 3B.

Clonogenic assay of BON and CA20948 cells using external irradiation

The survival of BON and CA20948 cells after exposure to escalating absorbed doses with a ^{137}Cs source is showed in Fig. 4. Up to absorbed doses of 4 Gy similar survival curves were found for both cell lines. At absorbed doses above 4 Gy, CA20948 showed to be more

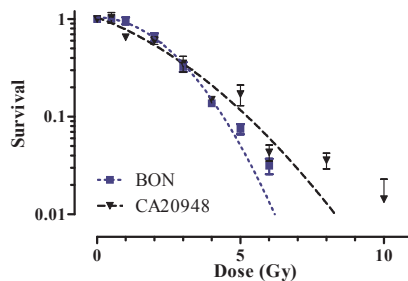


Figure 4, Survival curves of BON and CA20948 cells obtained after exposure at different doses of ^{137}Cs γ -radiation, $n=3$.

The x-axis is expressed in dose (Gy) and the y-axis in survival fraction. Each data point is plotted as the mean survival \pm SD. The curves through the data lead to the following LQ model parameters; BON: $\alpha < 0.11 \text{ Gy}^{-1}$, $\beta=0.12 \pm 0.02 \text{ Gy}^{-2}$ and CA20948: $\alpha=0.21 \pm 0.07 \text{ Gy}^{-1}$, $\beta=0.05 \pm 0.02 \text{ Gy}^{-2}$.

radio-resistant than BON, see Table 2. Curves according to the LQ model were fitted with high correlation coefficients ($R^2 = 0.98$ and 0.93 , respectively), indicating that the curvature of the BON cells was more profound than for CA20948.

Table 2, Survival fraction of BON and CA20948 cells after exposure of ^{137}Cs at 2, 4, 6 and 8 Gy

Cell line	SF2	SF4	SF6	SF8
BON	0.65 ± 0.10	0.14 ± 0.016	0.031 ± 0.010	0.07 ± 0.002
CA20948	0.60 ± 0.09	0.15 ± 0.013	0.043 ± 0.014	0.036 ± 0.014

DOSIMETRY

The time-integrated activity coefficient in the well cavity during the 1 h incubation period was 2361 MBq.s per MBq ^{213}Bi , leading to an absorbed dose of 1.60 Gy/MBq in the 2 mL fluid and 1.12 Gy/MBq in the bottom 25 μm layer. The absorbed dose was delivered 96.2 % by the α -particles, see Table 3.

Table 3, Absorbed fraction of energy ϕ and absorbed dose rate per MBq radioactivity ^{213}Bi and its daughters calculated in the bottom 25 μm of the 2 mL fluid, which contributed to the calculated absorbed dose

	^{213}Bi ϕ S (25 μm ←well) (%)	^{213}Po ϕ S (25 μm ←well) (mGy/MBq.s)	^{213}Po ϕ S (25 μm ←well) (%)	^{213}Po ϕ S (25 μm ←well) (mGy/MBq.s)	^{209}Tl ϕ S (25 μm ←well) (%)	^{209}Tl ϕ S (25 μm ←well) (mGy/MBq.s)	^{209}Pb ϕ S (25 μm ←well) (%)	^{209}Pb ϕ S (25 μm ←well) (mGy/MBq.s)
α	1.00	0.0082	0.82	0.4570				
β	0.56	0.0159			0.50	0.0218	0.64	0.0084
Auger/IC	0.61	0.0008			0.72	0.0015		
γ	0.03	0.0001			0.01	0.0010		
Total		0.0249		0.4570		0.0243		0.0084

Clonogenic assay of BON and CA20948 cells using radiolabelled ligand

BON and CA20948 cells were treated with increasing amounts of radioactivity coupled to the radioligand; ^{213}Bi -DTPA, ^{213}Bi -DOTATATE, ^{177}Lu -DTPA and ^{177}Lu -DOTATATE. The BON cells showed increased cytotoxic effect at increasing radioactivity of ^{213}Bi -DTPA and ^{213}Bi -DOTATATE. In BON cells, similar survival curves were found after irradiation with ^{213}Bi -DOTATATE or ^{213}Bi -DTPA. No significant differences were observed in the slopes of the survival curves (Fig. 5A). The α/β ratio obtained from the linear-quadratic model describing irradiation by ^{137}Cs was found to be < 0.01 Gy for BON and 4.5 ± 3.6 Gy for CA20948. The survival curves of BON and CA20948 treated with non-specific binding of ^{213}Bi -ligand fitted with a one-phase decay model. In CA20948 cells, a decreased survival at increased radioactivity of ^{213}Bi -radioligand was observed. No significant differences in survival were observed between ^{213}Bi -DOTATATE and ^{213}Bi -DTPA, see Fig. 5B.

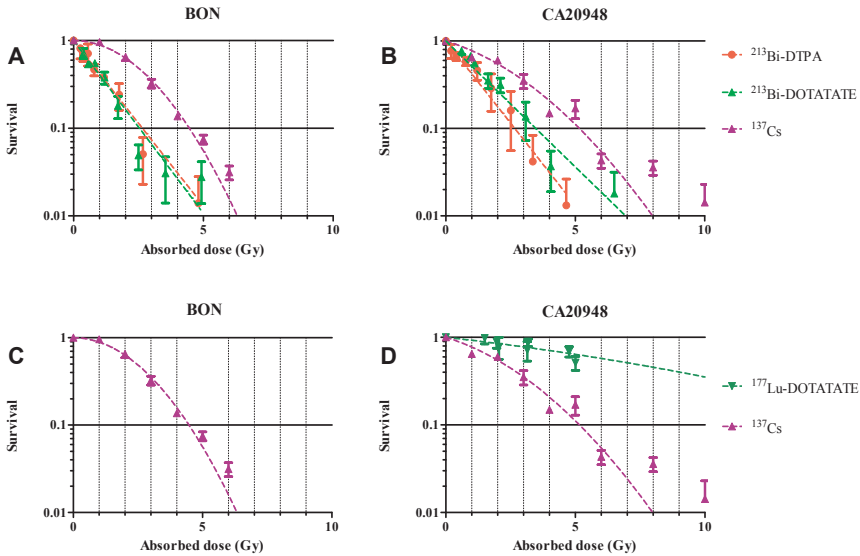


Figure 5A-5D, Survival curves of BON and CA20948 after exposure of ¹³⁷Cs γ -radiation, ¹⁷⁷Lu-DOTATATE, ²¹³Bi-DTPA, and ²¹³Bi-DOTATATE, n = 3. The x-axis is expressed in absorbed dose to the cells (Gy) and the y-axis in percentage survival. Each data point is plotted as the mean survival \pm SEM. Cells were incubated with ¹⁷⁷Lu-DOTATATE, ²¹³Bi-DOTATATE and ²¹³Bi-DTPA for 1h. Cells were fixed and colonies were measured 12 d after treatment.

No reduction of BON cell survival was found after treatment with ¹⁷⁷Lu-DOTATATE for 1 h. A very low binding was present, resulting in low calculated dose, < 1Gy (Fig. 5C). As for irradiation of CA20948 cells with ¹⁷⁷Lu-DTPA, cell survival was found to be around 100% after irradiation with > 6 MBq ¹⁷⁷Lu-DTPA for 1 h (data not plotted). In case of ¹⁷⁷Lu-DOTATATE, a reduction of cell survival was found with increased radioactivity, see Fig. 5D. The LQ model parameters α , β and α/β calculated after ¹³⁷Cs, ²¹³Bi-DTPA, ²¹³Bi-DOTATATE, ¹⁷⁷Lu-DOTATATE irradiation for BON and CA20948 are shown in Table 4.

Table 4, The LQ model parameters α , β and α/β calculated for BON and CA20948

	BON			CA20948		
	α /(Gy)	β /(Gy ²)	α/β (Gy)	α /(Gy)	β /(Gy ²)	α/β (Gy)
¹³⁷ Cs	< 0.11	0.12 \pm 0.02	0	0.21 \pm 0.07	0.05 \pm 0.02	4.5 \pm 3.6
²¹³ Bi-DTPA	0.87 \pm 0.1	-	-	0.74 \pm 0.08	-	-
²¹³ Bi-DOTATATE	0.91 \pm 0.05	-	-	0.56 \pm 0.03	-	-
¹⁷⁷ Lu-DOTATATE	-	-	-	0.08 \pm 0.03	0.003 \pm 0.004	25.2 \pm 37.8

DISCUSSION

In this study we selected DOTATATE as a targeting ligand. To investigate the distribution, time-dependent and peptide amount-dependent uptake, DOTATATE was labelled with the γ -emitting radionuclide ^{111}In . The results obtained were used for further cell averaged dosimetry. The effect on cell survival caused by radiation was compared using β -emitting ^{177}Lu -DOTATATE and α -emitting ^{213}Bi -DOTATATE. Cellular uptake is an important and critical parameter for the success of peptide receptor radionuclide therapy due to receptor-mediated process, therefore a high and a low SSTR₂ expression cell line were chosen here, to compare the receptor-dependent-survival. Cell averaged dosimetry was performed. The activity uptake in the cells was analyzed for 500 cells and the high LET character of the individual α -particle tracks were averaged out for dosimetry calculation.

^{111}In -DOTATATE, ^{177}Lu -DOTATATE, ^{213}Bi -DOTATATE and DOTATATE were shown to have similar affinity for SSTR₂. IC₅₀ values were similar of labelled peptides i.e. in the nM range. Cellular uptake of 1nM ^{111}In -DOTATATE demonstrated an increase of internalization in cells with increase of incubation time, compared to the time-independent specific membrane bound fraction f_{mem} in CA20948. In this study the specific binding and internalization of 390 nM peptide as function of incubation time was also investigated. Since the MA of ^{213}Bi -DOTATATE obtained after labelling with a $^{213}\text{Bi}/^{225}\text{Ac}$ generator of 222 MBq was low [18], a concentration of 390 nM labelled peptide was required for the sufficiently high radioactivities (approximately 4 MBq) in the clonogenic assays. To mimic the peptide concentrations used for further clonogenic assays, peptide-amount dependent uptakes resulting from incubation with 15 to 390 nM ^{111}In -DOTATATE were investigated. Very low f_{mem} and f_{int} were found in this range of concentrations, see Fig. 3A. Based on the activity measured of ^{177}Lu -DOTATATE or ^{213}Bi -DOTATATE, the data obtained from peptide-amount dependent uptake with ^{111}In -DOTATATE, extrapolated to 500 cells and taking the radionuclides' MA into account, about 150 ± 30 ^{213}Bi -DOTATATE molecules were bound per cell with the highest radioactivity amount used for clonogenic assay. This is low in comparison to the 44000 ± 8000 ^{177}Lu -DOTATATE molecules at the same peptide amount, but still high enough to warrant average cellular dosimetry.

In this study we found that the highest cytotoxic effect was caused by ^{213}Bi -ligands. The theoretical advantage of using α -emitters as therapeutic agents is the independence of dose rate, oxygenation and cell proliferation [28, 29]. Cytotoxic effects caused by ^{213}Bi -DOTATATE demonstrated no discrimination between cell types and level of SSTR₂ expression. We observed a similar cytotoxic effect with ^{213}Bi -DTPA and ^{213}Bi -DOTATATE in CA20948, indicating a cytotoxic dose can be delivered to the cells *in vitro* without specific binding and peptide receptor-mediated endocytosis. The low MA of the labelled peptide led to rapid saturation of the receptors by unlabelled peptides thereby causing a higher concentration of labelled peptide in the incubation medium. The effect and absorbed dose by the specific

binding was therefore reduced in comparison to the contribution by the medium. The absorbed dose during incubation of the cells, which is independent of specific uptake, forms the main contribution to the total dose, 53–76% depending on the amount of activity. The absorbed dose by the specific binding fraction can be increased to levels similar to the dose contribution from the medium exposure by using activities > 10 MBq. This would correspond to a minimal requirement of a ^{225}Ac generator twice the activity used in the current experiments (222 MBq). Furthermore, the irradiation time can then be reduced to 30 min.

In our study the D_{10} in BON was 4.5 Gy for ^{137}Cs , 2.5 Gy with ^{213}Bi -DTPA and 2.6 Gy with ^{213}Bi -DOTATATE. In CA20948, D_{10} values observed with ^{137}Cs , ^{213}Bi -DOTATATE and ^{213}Bi -DTPA in CA20948 were 5.1, 3.3 and 2.6 Gy, respectively. Due to the low uptake at low dose of ^{213}Bi -DOTATATE, heterogeneous distribution of ^{213}Bi -DOTATATE, MA (Bq/nmol) on the cell played a significant role here, the number of DNA hits appeared to be insufficient to influence cell survival. Heterogeneous distribution can influence the amount of ionizations traversing to the DNA of the cell causing irreparable DBS, as described by Pasternak et al [9]. The advantage of increasing the MA of labelled antibodies by an antibody cocktail caused a more homogenous binding to the cells and increased the cell-killing ability of α -emitters [9].

In the case of ^{177}Lu -ligand, peptide receptor-mediated endocytosis is essential to cause cytotoxic effect in the cells. Due to the low LET of β -emitters, at least 1000–4000 β -particles are required to lead to non-dividing cells and cell death. BON cells, with low SSTR₂ expression, showed no reduction in cell survival after irradiation with ^{177}Lu -DOTATATE. In CA20948 cells survival showed a correlation with absorbed dose using ^{177}Lu -DOTATATE, a D_{10} of 17.8 Gy was found after extrapolation of the LQ model fit to D_{10} . For both cell lines, ^{177}Lu -DTPA showed no effect on cell survival. We found that the absorbed dose was low for ^{177}Lu -DTPA in both cell lines and for ^{177}Lu -DOTATATE in BON, < 0.2 Gy. Therefore, D_{10} cannot be determined. Specific binding of ^{177}Lu -DOTATATE (0.33 MBq, lowest radioactivity used to treat cells) to CA20948 resulted in an absorbed dose at least 7 times higher than without specific binding (^{177}Lu -DTPA).

In our study, only 500 cells were plated in the well for the clonogenic assay and were assumed to be spherical in shape with a diameter of 12 μm and homogeneously distributed on the bottom of the well. The average distance between homogeneously distributed cells was approximately 1500 μm . The maximum path length in tissue for α -particle is 50–100 μm and for β -particle is 1–10 mm. Absorbed dose by cross-fire contributed from ^{177}Lu after incubation with ^{177}Lu -DOTATATE can be neglected, since the maximum path length of ^{177}Lu in tissue is approximately 2000 μm [30], the dose caused from cross-fire effect of ^{177}Lu was less than 1×10^{-12} Gy with a distance of the 1500 μm [31]. As for ^{213}Bi -DOTATATE, the maximum path length of ^{213}Bi is 80 μm and the distance between the cells was > 1500 μm , an additional dose to the calculated absorbed dose caused by cross-fire effect was not

taken into account. Despite this we assumed that the cells were homogeneous distributed, as clustering of cells can still occur, leading to an increase of the absorbed dose caused by cross-fire effect of neighboring cells. This was often observed in studies using low energy β -particles such as ^{177}Lu [31]. Therefore, this might have resulted in an underestimation of the absorbed dose caused by ^{177}Lu in our calculations. The bound activity was assumed to remain on the cells during the 12 d irradiation, as externalization was excluded. This assumption will have no effect on the absorbed dose by ^{213}Bi -DOTATATE, since the half-life of ^{213}Bi is short, 90% of the dose was delivered to the cells within 3.5 h. For ^{177}Lu -DOTATATE, the calculated absorbed dose will consequently be an overestimation the actual absorbed dose.

The calculated RBE at D_{10} with ^{213}Bi -DTPA compared to ^{137}Cs irradiation was 2.0 in CA20948 and 1.8 in BON. As for ^{213}Bi -DOTATATE compared to ^{137}Cs in CA20948 and BON, the RBE was found to be 1.5 and 1.7, respectively. At D_{20} , Nayak and co-workers found ^{213}Bi -DOTATOC to be 3.4 times more cytotoxic than ^{177}Lu -DOTATOC in terms of RBE in CAPAN-2 cell line (human pancreatic adenocarcinoma) [7]. In our study we also found that ^{213}Bi -DOTATATE was more potent for cell killing than ^{177}Lu -DOTATATE. The amount of ^{213}Bi -DOTATATE molecules bound per cell was a factor of approximately 300 less than ^{177}Lu -DOTATATE molecules bound per cell. RBE's of 5.4 at D_{10} and 5.7 at D_{20} were found for ^{213}Bi -DOTATATE in comparison to ^{177}Lu -DOTATATE. The RBE was higher compared to that found in the study of Nayak et al., this was probably caused by the high dose contributed from the internalization medium in our study. Graf et al. demonstrated the high cytotoxic effect caused by α -emitters using ^{225}Ac -DOTATOC in rat pancreatic carcinoma cell line, AR42J [6]. An ED_{50} of 14 kBq/mL was found for ^{225}Ac -DOTATOC and 10 MBq/mL for ^{177}Lu -DOTATOC. Higher amounts of γH2AX (biomarker of DSB) were observed in cells treated with ^{225}Ac -DOTATOC. They found a comparative cytotoxicity assessment by a factor approximately of 700 between ^{177}Lu and ^{225}Ac at ED_{50} . In our study, we found a factor of approximately 5.7 between ^{213}Bi -DOTATATE (0.33 MBq/mL) and ^{177}Lu -DOTATATE at ED_{50} (1.88 MBq/mL). The large difference was caused by the 4 α -particles release of ^{225}Ac compared to one α -particles release of ^{213}Bi and the exposure time; 48 h versus 1 h.

Radionuclide therapy with ^{213}Bi -DOTATATE showed to be capable of treating both small metastasis and observable large tumours [5]. Cell uptake for targeted radionuclide therapy is an essential factor for the calculation of absorbed dose in TAT, as well as selected endpoints and experimental design. Absorbed dose calculation methods used in this study described the average absorbed dose caused by TAT with ^{213}Bi , enabling comparisons between different cell irradiation experiments on basis of average absorbed doses at D_{10} .

CONCLUSION

^{213}Bi -DTPA and ^{213}Bi -DOTATATE showed higher cytotoxic effects than ^{177}Lu -DTPA and ^{177}Lu -DOTATATE in highly SSTR₂ expressing cells. RBE's at 10% cell survival ranging from 1.5–2.0 were found for ^{213}Bi -DTPA and ^{213}Bi -DOTATATE in both low and high SSTR₂ expressing cell lines under the conditions applied. Cellular dosimetry calculations allow comparisons to be made between α -, β -emitters and external γ -radiation sources. Per Gy delivered ^{213}Bi -DOTATATE was at least 5 times more effective in cell killing in comparison to ^{177}Lu -DOTATATE.

REFERENCES:

1. Eriksson, D. and T. Stigbrand, *Radiation-induced cell death mechanisms*. *Tumour Biol*, 2010. 31(4): p. 363-72.
2. Kratochwil, C., et al., *(2)(1)(3)Bi-DOTATOC receptor-targeted alpha-radionuclide therapy induces remission in neuroendocrine tumours refractory to beta radiation: a first-in-human experience*. *Eur J Nucl Med Mol Imaging*, 2014. 41(11): p. 2106-19.
3. Norenberg, J.P., et al., *²¹³Bi-[DOTA0, Tyr3]octreotide peptide receptor radionuclide therapy of pancreatic tumors in a preclinical animal model*. *Clin Cancer Res*, 2006. 12(3 Pt 1): p. 897-903.
4. Chan, H.S., et al., *Improved safety and efficacy of ²¹³Bi-DOTATATE-targeted alpha therapy of somatostatin receptor-expressing neuroendocrine tumors in mice pre-treated with L-lysine*. *EJNMMI Res*, 2016. 6(1): p. 83.
5. Chan, H.S., et al., *Influence of tumour size on the efficacy of targeted alpha therapy with (²¹³Bi-[DOTA(0),Tyr(3)]-octreotate*. *EJNMMI Res*, 2016. 6(1): p. 6.
6. Graf, F., et al., *DNA double strand breaks as predictor of efficacy of the alpha-particle emitter Ac-225 and the electron emitter Lu-177 for somatostatin receptor targeted radiotherapy*. *PLoS One*, 2014. 9(2): p. e88239.
7. Nayak, T.K., et al., *Somatostatin-receptor-targeted alpha-emitting ²¹³Bi is therapeutically more effective than beta(-)-emitting ¹⁷⁷Lu in human pancreatic adenocarcinoma cells*. *Nucl Med Biol*, 2007. 34(2): p. 185-93.
8. Hobbs, R.F., et al., *Redefining relative biological effectiveness in the context of the EQDX formalism: implications for alpha-particle emitter therapy*. *Radiat Res*, 2014. 181(1): p. 90-8.
9. Pasternack, J.B., et al., *The advantage of antibody cocktails for targeted alpha therapy depends on specific activity*. *J Nucl Med*, 2014. 55(12): p. 2012-9.
10. Song, H., et al., *Targeting aberrant DNA double-strand break repair in triple-negative breast cancer with alpha-particle emitter radiolabeled anti-EGFR antibody*. *Mol Cancer Ther*, 2013. 12(10): p. 2043-54.
11. Huang, C.Y., et al., *Microdosimetry for targeted alpha therapy of cancer*. *Comput Math Methods Med*, 2012. 2012: p. 153212.
12. Roeske, J.C. and T.G. Stinchcomb, *Dosimetric framework for therapeutic alpha-particle emitters*. *J Nucl Med*, 1997. 38(12): p. 1923-9.
13. Lewis, J.S., et al., *Radiotherapy and dosimetry of ⁶⁴Cu-TETA-Tyr3-octreotate in a somatostatin receptor-positive, tumor-bearing rat model*. *Clin Cancer Res*, 1999. 5(11): p. 3608-16.
14. Jonas, S., et al., *Somatostatin receptor subtypes in neuroendocrine tumor cell lines and tumor tissues*. *Langenbecks Arch Chir*, 1995. 380(2): p. 90-5.
15. Kascakova, S., et al., *Somatostatin analogues for receptor targeted photodynamic therapy*. *PLoS One*, 2014. 9(8): p. e104448.
16. Bernard, B., et al., *Radiolabeled RGD-DTPA-Tyr3-octreotate for receptor-targeted radionuclide therapy*. *Cancer Biother Radiopharm*, 2004. 19(2): p. 173-80.
17. Morgenstern, A., F. Bruchertseifer, and C. Apostolidis, *Bismuth-213 and actinium-225 — generator performance and evolving therapeutic applications of two generator-derived alpha-emitting radioisotopes*. *Curr Radiopharm*, 2012. 5(3): p. 221-7.
18. Chan, H.S., et al., *Optimizing labelling conditions of ²¹³Bi-DOTATATE for preclinical applications of peptide receptor targeted alpha therapy*. *EJNMMI Radiopharmacy and Chemistry* 2016. 1(9).

19. de Blois, E., et al., *Characteristics of SnO₂-based $^{68}\text{Ge}/^{68}\text{Ga}$ generator and aspects of radiolabeling DOTA-peptides*. Appl Radiat Isot, 2011. 69(2): p. 308-15.
20. de Blois, E., H.S. Chan, and W.A. Breeman, *Iodination and stability of somatostatin analogues: comparison of iodination techniques. A practical overview*. Curr Top Med Chem, 2012. 12(23): p. 2668-76.
21. Ferone, D., et al., *In vitro characterization of somatostatin receptors in the human thymus and effects of somatostatin and octreotide on cultured thymic epithelial cells*. Endocrinology, 1999. 140(1): p. 373-80.
22. Reubi, J.C., *New specific radioligand for one subpopulation of brain somatostatin receptors*. Life Sci, 1985. 36(19): p. 1829-36.
23. Niyazi, M., I. Niyazi, and C. Belka, *Counting colonies of clonogenic assays by using densitometric software*. Radiat Oncol, 2007. 2: p. 4.
24. Verwijnen, S., et al., *Low-dose-rate irradiation by ^{131}I versus high-dose-rate external-beam irradiation in the rat pancreatic tumor cell line CA20948*. Cancer Biother Radiopharm, 2004. 19(3): p. 285-92.
25. Eckerman K., E.A., *MIRD: Radionuclide Data and Decay Schemes. 2nd edition*. 2008, Reston (US): Society of Nuclear Medicine and Molecular Imaging.
26. Bolch, W.E., et al., *MIRD pamphlet No. 21: a generalized schema for radiopharmaceutical dosimetry—standardization of nomenclature*. J Nucl Med, 2009. 50(3): p. 477-84.
27. Vaziri, B., et al., *MIRD pamphlet No. 25: MIRDCell V2.0 software tool for dosimetric analysis of biological response of multicellular populations*. J Nucl Med, 2014. 55(9): p. 1557-64.
28. Elgqvist, J., et al., *The potential and hurdles of targeted alpha therapy - clinical trials and beyond*. Front Oncol, 2014. 3: p. 324.
29. Sgouros, G., et al., *MIRD Pamphlet No. 22 (abridged): radiobiology and dosimetry of alpha-particle emitters for targeted radionuclide therapy*. J Nucl Med, 2010. 51(2): p. 311-28.
30. Cremonesi, M., et al., *Dosimetry in Peptide radionuclide receptor therapy: a review*. J Nucl Med, 2006. 47(9): p. 1467-75.
31. Enger, S.A., et al., *Cross-fire doses from beta-emitting radionuclides in targeted radiotherapy. A theoretical study based on experimentally measured tumor characteristics*. Phys Med Biol, 2008. 53(7): p. 1909-20.



Chapter 6

Utilizing high-energy gamma photons for high-resolution ^{213}Bi SPECT in mice

Jan de Swart, Ho Sze Chan, Marlies C. Goorden, Alfred Morgenstern,
Frank Bruchertseifer, Freek J Beekman, Marion de Jong, Mark W. Konijnenberg

JNM. 2016; 57, 3, 486-492

ABSTRACT

The combined alpha, gamma, and X-ray emitter ^{213}Bi (half-life 46 min) is very promising for radionuclide therapy. SPECT imaging of ^{213}Bi is challenging, since the majority of emitted photons has a much higher energy (440 keV) than common in SPECT. We assessed ^{213}Bi imaging capabilities of the Versatile Emission Computed Tomograph (VECTor) dedicated to (simultaneous) preclinical imaging of both SPECT and PET isotopes over a wide photon energy range of 25–600 keV.

Methods

VECTor was equipped with a dedicated clustered pinhole collimator. Both the 79 keV X-rays and 440 keV gamma-rays emitted by ^{213}Bi could be imaged. Phantom experiments were performed to determine the maximum resolution, contrast-to-noise ratio and activity recovery coefficient for different energy window settings. Additionally, imaging of [^{213}Bi -DOTA,Tyr³]-octreotate and ^{213}Bi -DTPA in mouse models was performed.

Results

Using 440 keV gamma-rays instead of 79 keV X-rays in image reconstruction strongly improved the resolution (0.75 mm) and contrast-to-noise characteristics. Results obtained with a single 440 keV energy window setting were close to those with a combined 79 keV/440 keV window. We found a reliable activity recovery coefficient down to 0.240 MBq/mL with 30 minutes imaging time. In a tumor-bearing mouse injected with 3 MBq [^{213}Bi -DOTA,Tyr³]-octreotate, tumor uptake could be visualized with a one hour post-mortem scan. Imaging a non-tumor mouse at 5 minute frames after injecting 7.4 MBq ^{213}Bi -DTPA showed renal uptake and urinary clearance, visualizing the renal excretion pathway from cortex to ureter. Quantification of the uptake data allowed kinetic modeling and estimation of the absorbed dose to the kidneys.

Conclusion

It is feasible to image ^{213}Bi down to 0.75 mm resolution by using a SPECT system equipped with a dedicated collimator.

INTRODUCTION

New opportunities for high linear energy transfer (LET) radionuclide therapy with the alpha particle emitters ^{225}Ac and ^{213}Bi are increasingly being investigated [1–3]. The research for peptide receptor radionuclide therapy with alpha particles is mostly focused on labeling peptides with ^{213}Bi . Not only is its short half-life of 46 minutes in good accordance with the rapid targeting to receptor-positive tumors as well as the rapid clearance of peptides, it also raises less concern for detrimental effects because of the absence of non-specific uptake by daughters detached from its peptide or linker due to alpha decay recoil [4].

^{213}Bi offers the best imaging opportunities through its 440 keV gamma-ray and is therefore important for biodistribution and dosimetry studies [5]. All other gamma-rays and X-rays emitted by ^{213}Bi and its daughters are either too low in abundance or in energy to be suitable for imaging, possibly with the exception of the X-rays from ^{213}Bi at 77 and 79 keV if appropriate correction methods for down-scatter of the 440 keV gamma-rays are applied (see table 1 supplemental data [6]). Patient imaging of the uptake pattern of ^{213}Bi labeled antibody HuM195, targeted to CD33 leukemia, and ^{213}Bi -DOTATOC targeting neuroendocrine tumors has been performed by imaging the 440 keV gamma-ray with high-energy collimators [7–9]. Pre-clinical biodistribution studies with ^{213}Bi are challenging due to its short half-life. Typically ^{213}Bi labeled peptide biodistributions have been determined at 1h and 3h in rats and mice, thereby missing essential information on the kinetics in the uptake phase [2]. Dynamic imaging of this uptake phase will show the kinetic pattern, but usually lacks good quantification. Imaging of the high-energy (440 keV) photons is severely compromised for most small animal SPECT systems, due to penetration of pinhole edges and the collimator wall. Recently, however, a new dedicated small animal SPECT system based on use of many clustered pinholes has been developed that enables imaging over an energy range from 25 to 600 keV [10]. This system has shown to be able to e.g. image SPECT and PET tracers simultaneously at 0.5 mm and 0.75 mm resolution, respectively [10, 11].

The aim of the study was to investigate the capability to (dynamically) image ^{213}Bi in small animals, e.g. using ^{213}Bi labeled peptides. Resolution, contrast-to-noise ratio and activity recovery coefficient for different energy window settings and combinations thereof were optimized in phantom studies. Subsequently imaging of ^{213}Bi -DTPA and [^{213}Bi -DOTA,Tyr³]-octreotate in mice was performed.

MATERIALS AND METHODS

Radiochemistry

^{213}Bi was eluted from a standard $^{225}\text{Ac}/^{213}\text{Bi}$ generator (European Commission, Institute for Transuranium Elements (ITU)). For phantom experiments the elution was not chemi-

cally altered. ^{213}Bi was labeled with diethylene triamine pentaacetic acid (DTPA) for renal function imaging. ^{213}Bi eluate was added directly into a ready-for-use solution containing, 0.15M TRIS and $64\mu\text{M}$ DTPA, at total volume $800\ \mu\text{L}$ and pH 8.5.

For tumor imaging, ^{213}Bi was labeled to [DOTA,Tyr³]octreotate according to the labeling procedure described earlier [12], the incorporation of the radioactivity was > 99%, radiochemical purity was > 85%. Specific activity was $14.8\ \text{MBq/nmol}$.

Small Animal Imaging System

The VECTor (MILabs B.V.) uses three gamma cameras in a triangular set up. It enables high-energy gamma photon imaging including single 511 keV photons by using a tungsten collimator with clustered pinholes with relatively small opening angles. This reduces the image-degrading effects of pinhole edge penetration by these high-energy photons. The collimator contains 162 pinholes with a diameter of 0.7 mm grouped in clusters of 4. All clustered pinholes together observe a field-of-view which has the shape of an hourglass with a diameter of 44 mm and an average longitudinal length of 33 mm [10]. Total body images are obtained by moving the animal through the scanner along a spiral trajectory [13]. Data is collected in list mode.

Image Reconstruction

SPECT images were reconstructed by using projections from all bed positions simultaneously [14] using Pixel-based OSEM [15]. Three photo peak energy window settings were tested: a window set at the 440 keV photo peak, a window set at 79 keV, or both energy windows simultaneously. Scatter and background were corrected for with the triple-energy window method [16]. The 440 and 79 keV photo peak windows had two adjacent background windows each (Fig. S1 in supplemental data). For reconstruction the standard SPECT system matrix was used [17] for the 79 keV energy window, and a 511 keV system matrix for reconstructions using the 440 keV or the combined energy windows.

Phantom Experiments

A 5 mL syringe (internal diameter: 12.06 mm) was filled with $86.2\ \text{MBq}$ ^{213}Bi in a volume of 2.0 mL (fill height: 17.7 mm) for determining the ability to recover different amounts of activity. A volume of interest (VOI) was drawn around the activity in the reconstructed image. On a dynamic scan (20 frames of 30 minutes) the activity concentration at the start of the acquisition was $36.2\ \text{MBq/mL}$ ^{213}Bi , at the start of the last frame $0.0062\ \text{MBq/mL}$.

A second dynamic scan (90 frames of 5 minutes) of a ^{213}Bi filled syringe was performed. The initial activity concentration in 2.0 mL within the 5 mL syringe was $25.1\ \text{MBq/mL}$ ^{213}Bi and $0.0352\ \text{MBq/mL}$ at the start of the last frame.

Reconstructions of both experiments were done with 4 subsets and 30 iterations, voxel size was 0.8 mm. A post-reconstruction filter (3D Gaussian) with 0.4 mm Full Width at Half

Maximum (FWHM) was applied. All data were corrected for decay. System performance was characterized with the recovery coefficient (RC), defined as the measured apparent radioactivity concentration divided by the true radioactivity concentration. For large objects and sufficient imaging times RC should equal 1.

Spatial resolution was determined by using a Jaszczak resolution phantom (HR-micro phantom, Vanderwilt Techniques) with hollow channels of 0.7, 0.8, 0.9, 1.0, 1.2 and 1.5 mm diameter. It was filled with 119 MBq ²¹³Bi (activity concentration 198 MBq/mL) and scanned for 45 minutes. Images were reconstructed using 32 subsets, 60 iterations and a voxel size of 0.4 mm. No post-reconstruction filters were used. Profiles were determined from five single slices through the measured signal over a 0.4 mm cross-hair line drawn over the rods. Gaussian curves were fitted to these profiles and averaged, and their FWHM values were reported. To assess the impact of lower numbers of counts on resolution, we also reconstructed this dataset using only 20%, 5% and 1% of the counts from the list-mode data. This emulates scans with shorter scan times or lower activities. We reconstructed the lowest activity scan with 4 subsets and 30 iterations on 0.4 mm voxels which are the same reconstruction settings as used for the mouse scans. For the higher activities more iterations were needed to recover finer details and thus we chose the same reconstruction settings as for the high-count reconstructions. Images were post-filtered with a 3D Gaussian with a 0.6, 0.9 and 1.0 mm FWHM for scans with 20%, 5% and 1% of the counts respectively.

An analysis of contrast-noise characteristics was performed similar to [18]. Resolution phantom images were resampled to a fine 0.05 mm grid, and ROIs with a diameter 90% of the rod diameter were placed on top and in between the rods (Fig. S2c in supplemental data). This was repeated over 20 slices. The mean activity inside the ROIs placed over the rods (h_d) and in between the rods (b_d) was determined. The contrast C_d for rod size d is then defined to be

$$C_d = \frac{\overline{h_d} - \overline{b_d}}{\overline{h_d}} \tag{Eq.1}$$

The variability between the ROI mean values was characterized by the noise parameter N_d :

$$N_d = \frac{\sqrt{\sigma_{h_d}^2 + \sigma_{b_d}^2}}{\overline{ROI}_d} \tag{Eq.2}$$

The standard deviation σ of h_d and b_d were calculated over all ROIs in 1/3 of the 20 slices to reduce inter-ROI covariance. The denominator \overline{ROI}_d indicates the mean value taken over all ROIs. The contrast-to-noise ratio was defined as C_d/N_d .

Quantification calibration procedure and determination of the calibration factors are described in the supplemental data and based on the method in [19].

Ex-vivo Experiment

A nu/nu mouse bearing a CA20948 tumor xenograft was injected intravenously (iv) in a tail vein with 3.0 MBq [^{213}Bi -DOTA,Tyr 3]-octreotate. The mouse was euthanized 38 minutes after injection and immediately imaged for 1 hour. A CT scan was made following SPECT with the integrated CT scanner (acquisition parameters 55 kV and 615 μA and reconstructed with filtered Back Projection), which was used only as an anatomical reference. SPECT reconstruction parameters comprised 4 subsets, 30 iterations and a voxel size of 0.4 mm. A post-reconstruction filter (3D Gaussian) of 1.5 mm FWHM was applied. Tumor volume was determined by drawing VOIs in the CT-images. The radioactivity uptake was based on the VOIs drawn in the SPECT images. Organs and tumor tissue were counted for 60 s in a Wallac Wizard gamma counter (PerkinElmer). Counting started 2.3 hours after injection.

In vivo experiment

In an *in vivo* experiment, a balb/c mouse was injected iv in a tail vein with 7.4 MBq ^{213}Bi -DTPA under isoflurane anaesthesia. Dynamic acquisition of the abdominal region was started 3 minutes after injection over a total of nine 5-minute frames. Equal reconstruction parameters were used as for the *ex-vivo* experiment. SPECT-based VOIs were drawn over the urinary bladder and over both kidneys to determine their kinetics. The absorbed dose to the kidneys was determined by using the sphere model within the Olinda/EXM code [19] and calculated for an average single kidney mass of 0.286 mg, determined from the mouse of the *ex-vivo* experiment. All animal studies were conducted in accordance with the guidelines and after approval of the Animal Welfare Committee of the Erasmus MC.

Statistics

Statistical analysis of the syringe experiments was performed with the Graphpad Prism software (GraphPad Software, Inc.). Average values of the RC from ^{213}Bi -filled syringes, normalized to the initial value, were determined for each frame. Deviations from the horizontal line were analyzed according to the D'Agostini & Pearson normality test. Additionally the Runs test was performed to decide whether the residuals followed a random pattern. The cut-off value for the linearity of RC was determined by the 3σ outlier criterion on the moving average.

RESULTS

Quantitative Properties

On the 30-minute dynamic series, the RC was averaged over the linear range (Fig. 1). Cut-off values or lower limits for linearity found are indicated in Table 1. The RC was comparable for all energy window settings. The single 440 keV window setting showed the largest linearity range (lower limit: 0.24 MBq/mL).

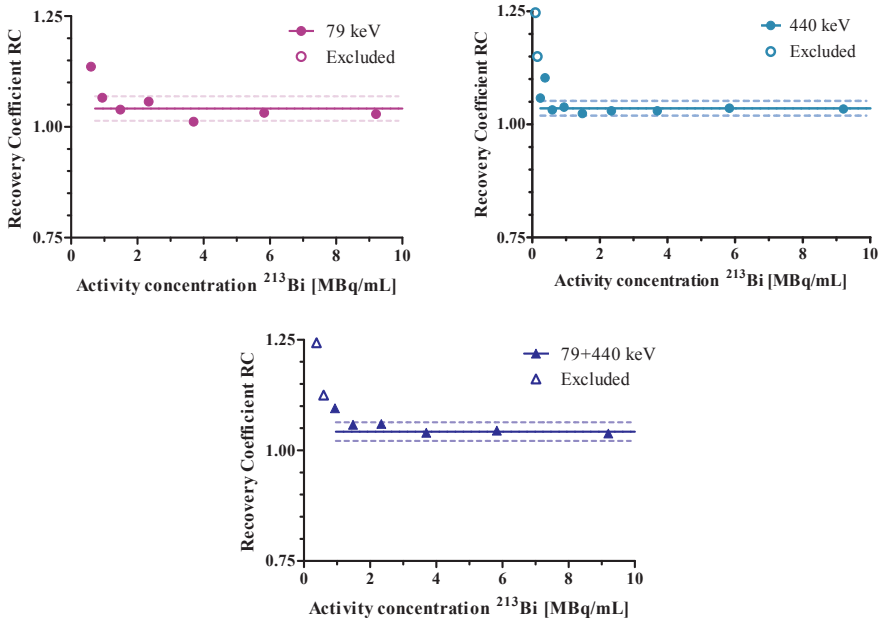


Figure 1, Recovery coefficients for a syringe initially filled with 86.2 MBq ²¹³Bi (in 2.0 mL) scanned in 15 frames of 30 minutes. Results were fitted with a horizontal line when both residuals were normally distributed (D’Agostini-Pearson test) and showed no significant systematic deviation (Runs test). The open markers indicate the excluded RC values. Some data points at low activity concentrations did not fall within the Y-axis boundaries.

Table 1. Results from the measurements of the ²¹³Bi filled phantoms

Energy window	79 keV	440 keV	79 + 440 keV
RC 30 min frames (mean±SE)	1.03 ± 0.007	1.04 ± 0.007	1.04 ± 0.009
Lower limit linearity 30 min (MBq/mL)	0.94	0.24	0.94
RC 5 min frames (mean±SE)	0.93 ± 0.007	1.00 ± 0.003	1.01 ± 0.003
Lower limit linearity 5 min (MBq/mL)	2.33	0.90	0.32
FWHM 0.7 mm rods (mm)	1.1 ± 0.3	1.4 ± 0.3	1.4 ± 0.3
FWHM 0.8 mm rods (mm)	1.6 ± 0.5	1.4 ± 0.2	1.4 ± 0.2
FWHM 0.9 mm rods (mm)	1.4 ± 0.6	1.33 ± 0.14	1.29 ± 0.09
FWHM 1.0 mm rods (mm)	1.4 ± 0.5	1.34 ± 0.29	1.29 ± 0.12
FWHM 1.2 mm rods (mm)	1.6 ± 0.6	1.30 ± 0.14	1.25 ± 0.08
FWHM 1.5 mm rods (mm)	2.0 ± 0.4	1.58 ± 0.14	1.61 ± 0.12

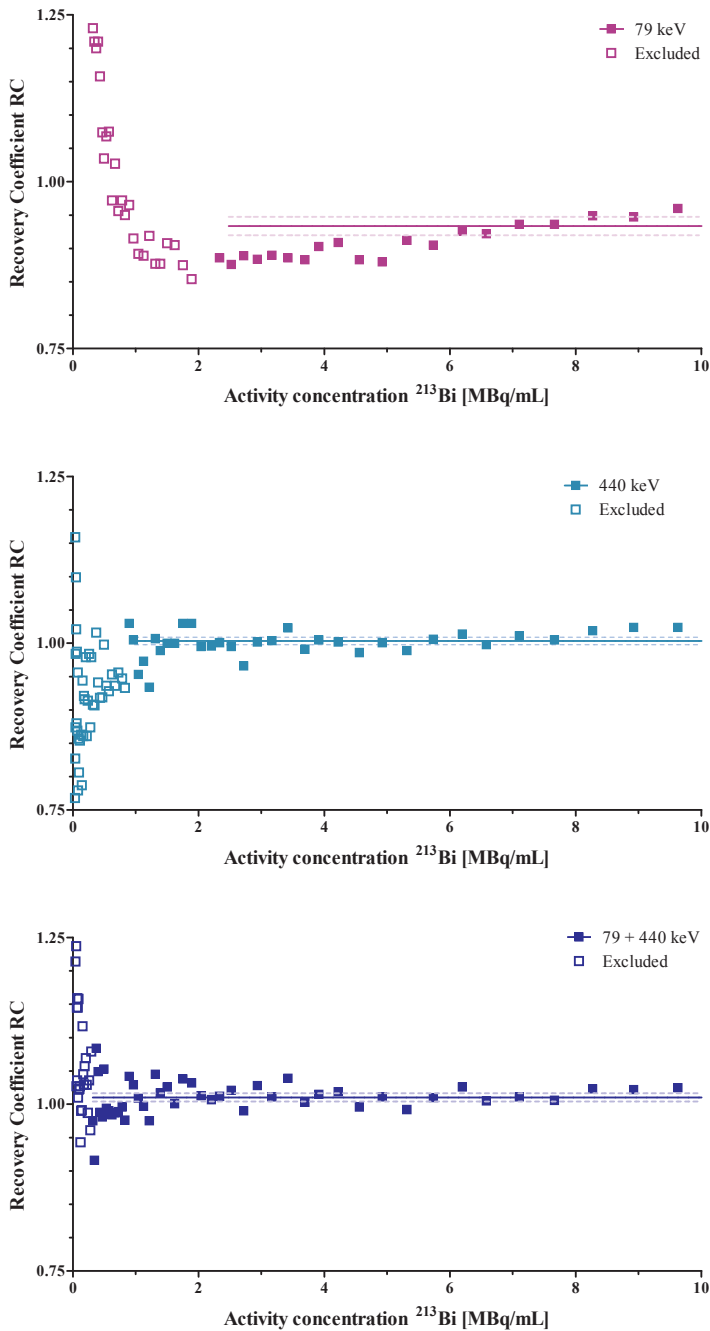


Figure 2, Recovery coefficient for a syringe initially filled with 67.69 MBq ^{213}Bi (in 2.0 mL) scanned in 45 frames of 5 minutes. Fitting was performed with the same statistical rules as in figure 2. Data for the first 13 frames were omitted from the graph, but were included in the averaging.

For the 5-minute dynamic scans, the RC for the 79 keV/440 keV combined energy peaks showed the best results as it remained constant down to 0.32 MBq/mL (Fig. 2). Below 2 MBq/mL a more scattered pattern of the data points was visible, but this was not a statistical deviation due to the equal variations in the signal above and under the average RC line. The RC for the 79 keV photo peak on the 5-minute dynamic scans did not meet all statistical tests. Therefore the RC line in this graph can only serve as an indication.

In general the quantitative properties for activity recovery for images using the 440 keV peak and the combined peaks are comparable. Especially in the 5-minute scans these two settings have better quantitative properties than the single 79 keV peak setting. There was no difference in results when a 0.4 mm or a 0.8 mm voxel size was applied in the reconstruction settings (data not shown).

Spatial Resolution

Resolution phantom images are shown in Fig. 3. Visually, images using the single 440 keV or the combined 79 keV/440 keV energy window setting appear to be much less noisy and have better resolution than the images using the single 79 keV energy window; on the reconstructions 0.7 mm rods could be distinguished for the combined 79 keV/440 keV setting and for the single 440 keV window. Profiles are shown in Fig. 4 and the mean FWHMs for the three energy windows are indicated in Table 1. These values showed a significant difference for the combined 79 keV/440 keV setting compared to the single 79 keV setting. Differences between the 440 keV and the combined 79 keV/440 keV setting were small, but the combined setting resulted in a slightly lower variation, indicating the most stable settings. Contrast and contrast-to-noise curves for all 3 energy window settings are shown in Fig. 5 and are in agreement with the visual assessment; both contrast and contrast-to-noise are much better for the 440 keV or the 79 keV/ 440 keV window settings compared to the single 79 keV energy window. All though 0.7 mm rods could be distinguished in reconstructions, profiles reveal that these are really at the resolution limit. The contrast for

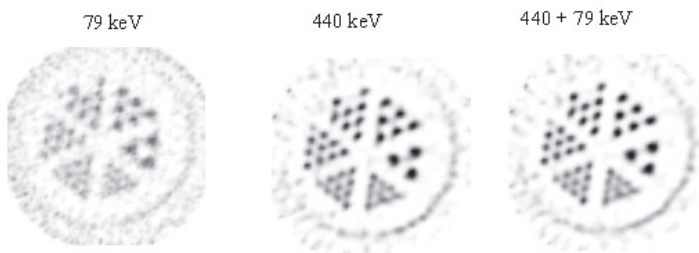


Figure 3, Resolution phantom images of ²¹³Bi SPECT. The phantom has 6 segments containing capillary diameters of 1.5, 1.2, 1.0, 0.9, 0.8 and 0.7 mm. The images show reconstructions for different energy window settings summed over 5 slices (2 mm in total).

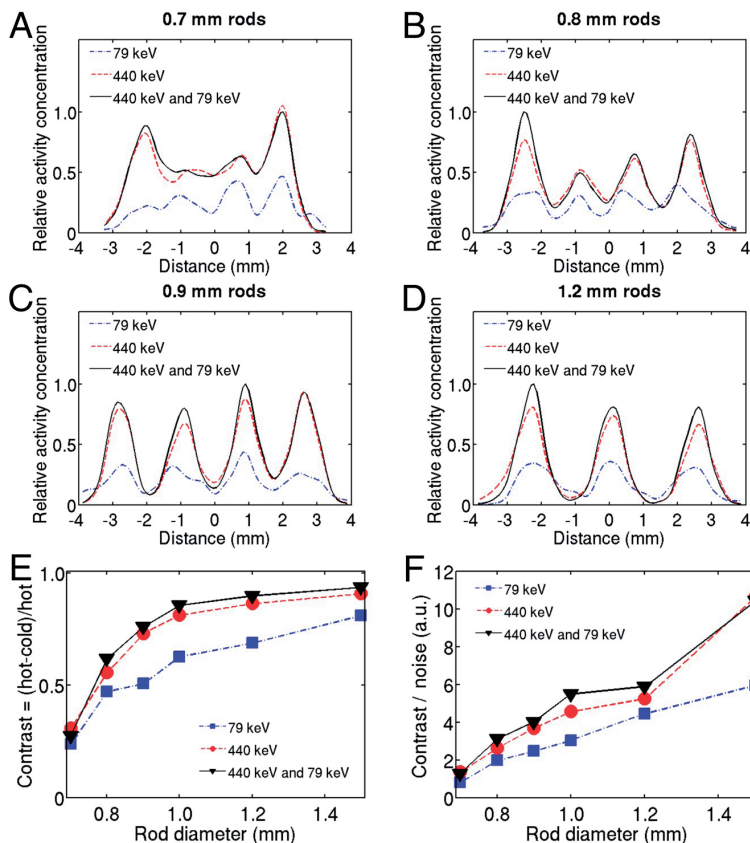


Figure 4, Profiles through 0.7, 0.8, 0.9 and 1.2 mm rods for the single 79 and 440 keV and the combined 79 keV/440 keV energy windows (graphs A, B, C and D). Contrast and contrast-to-noise curves for the different rod sizes are shown in graphs E and F.

these rods was found to be $C_{0.7}=0.34$ for the 79 keV/440 keV combined window setting. To emulate lower activities, we also reconstructed resolution phantom images with only part of the listmode data used (Fig. S3, supplemental data). When only 20%, 5% or 1% of the counts were used respectively, rods that could still be distinguished were 0.8 mm, 0.9 mm and 1.2 mm.

Ex-vivo Experiment

Tumor uptake by [$^{213}\text{Bi-DOTA,Tyr}^3$]-octreotate in the euthanized mouse was clearly visualized with the 440 keV and the combined 79 keV/440 keV energy window setting, but not with the 79 keV setting (Fig. 5), ^{213}Bi uptake in the kidneys was not visible though. The uptake in the xenograft amounted to 38 kBq, corresponding to a concentration of 0.42 MBq/mL for the 90 mm³ volume tumor. The activity in the abdomen below the tumor

corresponded to 0.16 MBq/mL. A region within the mouse on the contralateral side of the tumor, not clearly linked to physiological uptake, showed an uptake of 0.12 MBq/mL. The biodistribution assay of this mouse showed a tumor uptake of 5.3% of the injected activity (%IA) and with activity concentration of 0.36 MBq/g. The uptake in the left kidney was 1.9%IA (0.48 MBq/g).

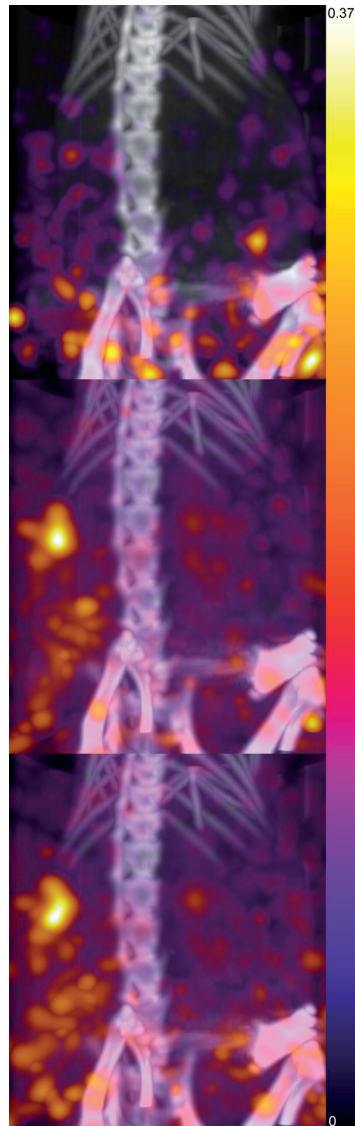


Figure 5, Ex-vivo image of 3.0 MBq [²¹³Bi-DOTA,Tyr³]-octreotate injected in a nude mouse. From top to bottom: mip images reconstructed at 79 keV, 440 keV and at both energy windows. The numbers in the color table indicate the radioactivity concentration in MBq/mL.

In vivo Experiment

In vivo mouse maximum intensity projection (mip) images are shown in Fig. 6 for the combined energy window as this setting was generally found to be optimal. The first frame in Fig. 6 shows activity in both kidneys and bladder after injection with 7.4 MBq ^{213}Bi -DTPA.

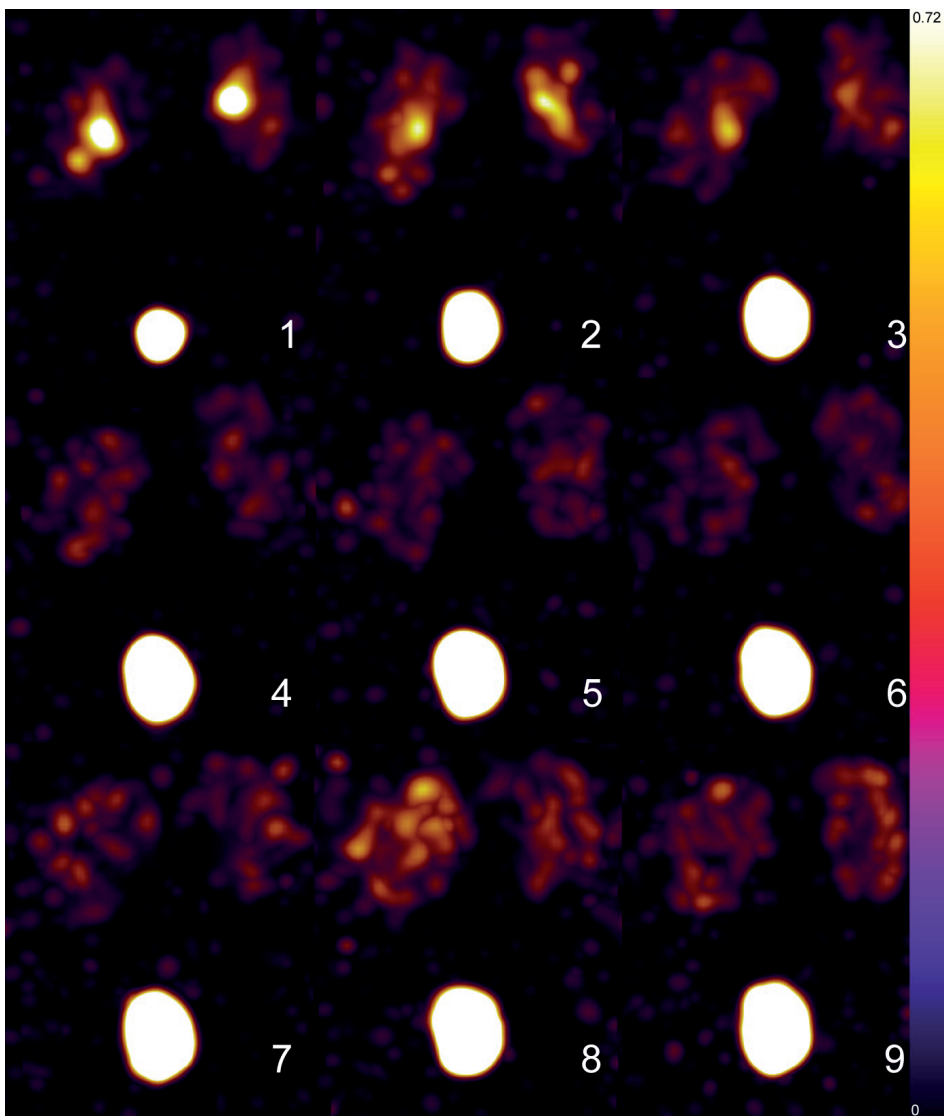


Figure 6, *In vivo* mouse mip images with 7.4 MBq ^{213}Bi -DTPA. Images were reconstructed using the combined 79 keV/440 keV photo peak setting. In the 9 consecutive 5-minute frames kidneys show up in each frame, initially showing the ureters at the top of the image with gradually a distribution to the renal cortices and filling of the bladder. The numbers in the color table indicate the radioactivity concentration in MBq/mL.

The filling of the urinary bladder was also visible by its enlargement over time and in the first frame already exceeded the maximum displayed intensity. The activity in the kidneys gradually accumulated in the renal medulla as visualized in the mip image of Fig. 6 and the quantitative VOI-based results in Fig. 7.

The peak uptake of in the kidneys was 18%IA. The kidney radioactivity uptake ranged between 0.34 and 0.66 MBq (1.2 and 2.3 MBq/mL). These SPECT-based activity concentrations in the kidneys were found to be well above the 0.32 MBq/mL threshold for linear response.

The decay-corrected radioactivity accumulation in the urinary bladder followed a single-exponential build-up pattern with an 11 ± 2 min half-life. The non-decay corrected uptake data of the kidneys could be fitted with a single exponential curve with an effective clearance half-life of 52 min (95% confidence interval: 36–96 min). A horizontal line was the preferred fit through the decay corrected kidney data. The residence time for the ²¹³Bi-DTPA uptake in the kidneys was 11.7 ± 0.4 min, leading to an absorbed dose of 26 ± 2 Gy by 7.4 MBq. The largest part (94%) of this dose was delivered by the ²¹³Po α -particles.

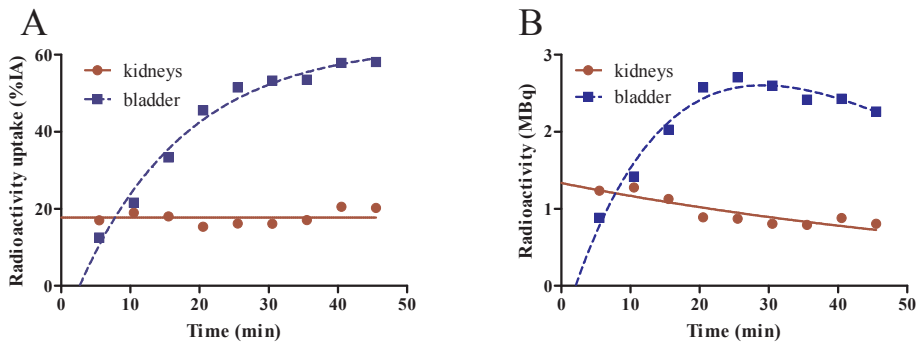


Figure 7, Kinetic modeling of ²¹³Bi-DTPA in the urinary bladder and the kidneys. In the decay-corrected data (A) the bladder activity is fit by a single exponential with a $T_{1/2} = 11 \pm 2$ min ($T_{eff} = 15$ min). The kidneys did not show clearance, whereas in the uncorrected data (B) the renal clearance proceeded with $T_{eff} = 52 \pm 10$ min half-life. Images were reconstructed from combined 79 keV/440 keV photo peaks.

DISCUSSION

Direct imaging of the 440 keV gamma-rays from ²¹³Bi is possible with dedicated high-energy SPECT, despite the low activity injected to avoid an undesirably high dose to the animal. We found that including the 440 keV setting in image reconstruction is essential; only using 79 keV X-rays has a strong negative effect on image quality. Generally, the results for the 440 keV and the combined 440 keV/79keV setting are close. Resolution and contrast-noise properties were slightly better for the combined setting which also showed better quantification properties for short time frames. However, on longer time frames 440

keV alone performed slightly better. We believe that for low-count studies the combined window performs better as it contains more counts, while for higher count levels the downscatter of 440 keV gammas in the 79 keV photo peak adversely affects quantification.

Quantification sensitivity of the camera in the 5-minute frame setting was high enough to allow kinetic modeling of the kidney uptake and bladder filling, which is apparent when comparing the results from the 5-minute phantom scan and the results of the *in vivo* ^{213}Bi -DTPA scan. Tumor and pancreas modeling should also be possible for most DOTA-conjugated somatostatin analogues as their uptake in mice is in the order of approximately 10%IA/mL [5] to even 225%IA/g for Exendin [21]. With an injected activity of 5–10 MBq this will lead to activities in these organs that enable 5-minute frame scanning, but results will become uncertain when the activity concentration will drop below 0.32 MBq/mL. In those cases, longer time frames should be used with the risk of missing essential fast kinetic effects.

The maximum resolution reported here was achieved with a static scan and relatively high activity compared to that injected in mice. This was done to test (maximum) system performance for ^{213}Bi imaging and to investigate optimal energy window settings which is easiest on almost noiseless data. As common in SPECT and shown in the supplemental data, the resolution that can be obtained depends on the number of detected counts and thus increasing system sensitivity may be very beneficial for ^{213}Bi imaging in mice. Such sensitivity improvements have already been realized in practice through increasing crystal thickness which makes the system 2.5 times more efficient. Furthermore, new high-energy collimators with larger sensitivity have been developed. The choice of collimator depends on the imaging task and these higher sensitivity collimators may be very suitable for ^{213}Bi imaging. The VECTor system used in this paper is a first-generation scanner and could not benefit yet from these improvements.

Ex-vivo and *in vivo* mouse experiments were performed as proof of principle, to investigate the feasibility to image the tumor and physiological uptake using ^{213}Bi . The reported kidney dose of 26 Gy by ^{213}Bi -DTPA is however high and most probably would lead to renal toxicity at a later stage. Renal toxicity has been observed after scanning ^{111}In labeled peptides with cumulative kidney doses of 20–40 Gy [20]. Considering the high LET nature of its radiation 26 Gy by ^{213}Bi will be at least as equitoxic as 20–40 Gy by ^{111}In .

In the biodistribution assay for [^{213}Bi -DOTA,Tyr³]-octreotate showed an absolute tumor uptake of 5.3%IA and in the kidney of 1.9%IA. The renal uptake was therefore too low to be detectable on SPECT. These uptake values are higher than found from the SPECT data. It is not clear what caused this discrepancy.

The uptake of ^{111}In -DTPA in rat kidneys has been reported to be $0.9 \pm 0.2\%$ /mL at 38 minutes after injection [21]. Initially (at 2–4 min) the peak activity in the renal cortex is 5–7 times higher by perfusion with radioactive blood. The uptake of ^{213}Bi -DTPA in the kidneys seems to be much higher than that observed with ^{111}In -DTPA. This may be the result of

the persistent uptake of ^{213}Bi in the kidneys, independent of the compound administered [22]. Species-specific differences in DTPA uptake by mice and rats could also cause this difference, but the reported renal uptake of ^{111}In -DTPA in dogs was found to be comparable to the rat values [23].

Using significantly higher injected activities of ^{213}Bi labeled peptides for better quantification is not ideal both for the consequentially higher amount of peptide needed, which might partially block receptor-mediated targeting, as well as for increased probability of radiation toxicity.

CONCLUSION

We have shown that it is possible to image ^{213}Bi at sub-mm resolution level with a SPECT system equipped with a dedicated high-energy collimator. We found that the use of the 440 keV gamma-ray peak is essential and produced significantly better images than the 79 keV X-ray peak. Quantification of the ^{213}Bi activity concentration was reliable above 0.240 MBq/mL with 30-minutes image time using the 440 keV energy window setting and above 0.320 MBq/mL with 5-minutes frames using the combined energy window setting. Uptake of [^{213}Bi -DOTA,Tyr³]-octreotate in a CA20948 tumor xenograft was well visualized. Dynamic *in vivo* imaging of the ^{213}Bi -DTPA distribution in a mouse showed distinct renal uptake patterns, enabling identification of sub-organ distributions (renal cortex). Quantification of the uptake data allowed kinetic modeling and estimation of the absorbed dose to the kidneys, albeit with uncertainties of around 20%.

SUPPLEMENTAL DATA

Quantification Calibration

For quantification calibration, radioactivity of ^{213}Bi was determined on the gamma-spectrum count rate measured with a high-purity germanium detector (Canberra Industries Inc.). The counting efficiency of the HPGe detector at 440 keV was determined using a known amount of ^{225}Ac activity provided and calibrated at the ITU with a high-resolution gamma spectrometer [1,2]. The measurements showed an accuracy of 10%.

For converting reconstructed images in Nifti index (Nii) values to MBq, a calibration factor (in MBq/nii) was determined [3]. To this end, a point source of 70 MBq ^{213}Bi (volume 0.6 mL) in an Eppendorf tube was placed in the center of VECTor and scanned in 30 minutes net measuring time. Calibration factors to convert the image NII values into MBq are indicated in Table 2.

Table 1, Radiation characteristics of ^{213}Bi and its decay-chain daughters. In this table the half-lives of the listed isotopes are shown, as well as the transition energy E for the emission of the listed particles, and the emission yield per transition Y_i . [4, 13, 14].

	Yield	Decay	α particles		β particles		γ -rays		X-rays	
	ratio	$T_{1/2}$	E (MeV)	Y_i (/nt)	\bar{E} (keV)	Y_i (/nt)	E (keV)	Y_i (/nt)	E (keV)	Y_i (/nt)
^{213}Bi		45.62 min	5.878	0.0214	435	0.9786	440.5	0.261	77.1	0.0121
									79.6	0.0202
^{213}Po	0.9786	3.708 μs	8.375	1.0						
^{209}Tl	0.0214	2.16 min			656	1.0	117.2	0.843	73.0	0.0635
							465.1	0.969	75.3	0.107
							1567	0.998	85	0.035
^{209}Pb		3.232 h			198	1.0				

Table 2, Calibration Factors (CF) using energy windows around the 79 keV X-ray peak, the 440 keV gamma ray peak, or the 79 keV and 440 keV peaks combined.

Energy window	79 keV		440 keV		79 keV + 440 keV	
Voxel size	0.8 mm	0.4 mm	0.8 mm	0.4 mm	0.8 mm	0.4 mm
CF (MBq/Nii)	16560	16440	2260	2220	1850	1820

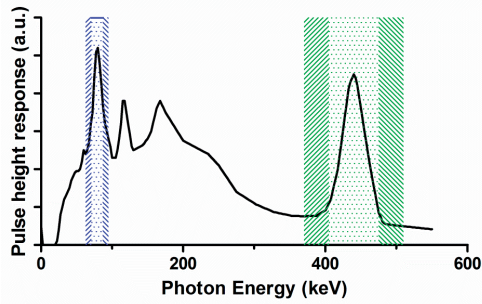


Figure S1, Measured pulse height distribution of ²¹³Bi. The 440 keV photo peak window setting (width 16%: 405–475 keV) is represented by the green dotted area. The adjacent green striped areas represent the background windows (width 35 keV: 307–405 and 475–510 keV) used for scatter correction. The dotted blue areas represent the 79 keV window (width: 20%: 71–87 keV) and the striped blue areas are the background windows (width 8 keV: 63–71 and 87–95 keV).

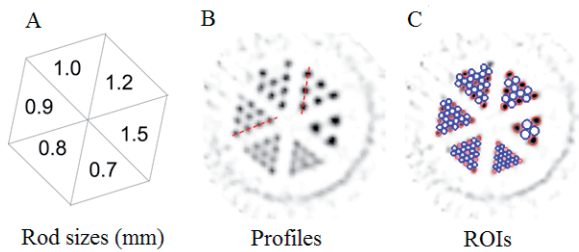


Figure S2, Resolution phantom images of ²¹³Bi SPECT. A) Phantom has 6 segments containing capillary diameters of 1.5, 1.2, 1.0, 0.9, 0.8 and 0.7 mm. B) Across 0.9 and 1.2 mm diameter rods profiles were drawn. C) Position of the ROI's to obtain contrast and contrast-to-noise ratios.

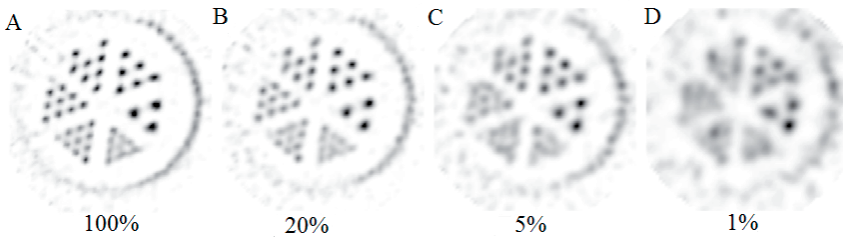


Figure S3, Resolution phantom images for the same phantom as shown in figure 3 for various count levels. Reconstructions were based on (A) all listmode data or (B) 20%, (C) 5%, (D) 1% of all detected counts. The combined 79 keV/440 keV photo peak window setting was used. Post-reconstruction 3D Gaussian filters with 0.4, 0.6, 0.9 and 1.0 mm FWHM were applied to (A-D).

REFERENCES

1. Essler, M., et al., *Therapeutic efficacy and toxicity of 225Ac-labelled vs. 213Bi-labelled tumour-homing peptides in a preclinical mouse model of peritoneal carcinomatosis*. Eur J Nucl Med Mol Imaging, 2012. 39(4): p. 602-12.
2. Wild, D., et al., *Alpha-versus beta-particle radiopeptide therapy in a human prostate cancer model (213Bi-DOTA-PESIN and 213Bi-AMBA versus 177Lu-DOTA-PESIN)*. Cancer Res, 2011. 71(3): p. 1009-18.
3. Morgenstern, A., F. Bruchertseifer, and C. Apostolidis, *Targeted alpha therapy with 213Bi*. Curr Radiopharm, 2011. 4(4): p. 295-305.
4. Jaggi, J.S., et al., *Renal tubulointerstitial changes after internal irradiation with alpha-particle-emitting actinium daughters*. J Am Soc Nephrol, 2005. 16(9): p. 2677-89.
5. Norenberg, J.P., et al., *213Bi-[DOTA0, Tyr3]octreotide peptide receptor radionuclide therapy of pancreatic tumors in a preclinical animal model*. Clin Cancer Res, 2006. 12(3 Pt 1): p. 897-903.
6. Eckerman, K.F., A. Endo, and . *Medical Internal Radiation Dose Committee : MIRD radionuclide data and decay schemes*. 2nd ed. 2007, Reston, VA: Society of Nuclear Medicine. viii, 671 p.
7. Sgouros, G., et al., *Pharmacokinetics and dosimetry of an alpha-particle emitter labeled antibody: 213Bi-HuM195 (anti-CD33) in patients with leukemia*. J Nucl Med, 1999. 40(11): p. 1935-46.
8. Rosenblat, T.L., et al., *Sequential cytarabine and alpha-particle immunotherapy with bismuth-213-lintuzumab (HuM195) for acute myeloid leukemia*. Clin Cancer Res, 2010. 16(21): p. 5303-11.
9. Kratochwil, C., et al., *213Bi-DOTATOC receptor-targeted alpha-radionuclide therapy induces remission in neuroendocrine tumours refractory to beta radiation: a first-in-human experience*. Eur J Nucl Med Mol Imaging, 2014. 41(11): p. 2106-19.
10. Goorden, M.C., van der Have F., and Beekman, F. J. , *Optimizing image reconstruction for simultaneous sub-mm clustered pinhole PET-SPECT*. . Proceedings of the 12th International Meeting on Fully 3D Image Reconstruction in Radiology and Nuclear Medicine. , 2013: p. 126-129.
11. Goorden, M.C., et al., *VECTor: a preclinical imaging system for simultaneous submillimeter SPECT and PET*. J Nucl Med, 2013. 54(2): p. 306-12.
12. Chan, H.S., et al., *Optimizing labeling conditions of 213Bi-somatostatin analogs for receptor-mediated processes in preclinical models*. J NUCL MED MEETING ABSTRACTS, 2014. 55(1_MeetingAbstracts): p. 1179-.
13. Vaissier, P.E., et al., *Fast spiral SPECT with stationary gamma-cameras and focusing pinholes*. J Nucl Med, 2012. 53(8): p. 1292-9.
14. Vastenhouw, B. and F. Beekman, *Submillimeter total-body murine imaging with U-SPECT-I*. J Nucl Med, 2007. 48(3): p. 487-93.
15. Branderhorst, W., B. Vastenhouw, and F.J. Beekman, *Pixel-based subsets for rapid multi-pinhole SPECT reconstruction*. Phys Med Biol, 2010. 55(7): p. 2023-34.
16. Ogawa, K., et al., *A practical method for position-dependent Compton-scatter correction in single photon emission CT*. IEEE Trans Med Imaging, 1991. 10(3): p. 408-12.
17. van der Have, F., et al., *System calibration and statistical image reconstruction for ultra-high resolution stationary pinhole SPECT*. IEEE Trans Med Imaging, 2008. 27(7): p. 960-71.
18. Walker, M.D., et al., *Performance Assessment of a Preclinical PET Scanner with Pinhole Collimation by Comparison to a Coincidence-Based Small-Animal PET Scanner*. J Nucl Med, 2014. 55(8): p. 1368-74.

19. Konijnenberg, M.W., et al., *Therapeutic application of CCK2R-targeting PP-F11: influence of particle range, activity and peptide amount*. EJNMMI Res, 2014. 4(1): p. 47.
20. Melis, M., et al., *Nephrotoxicity in mice after repeated imaging using ¹¹¹In-labeled peptides*. J Nucl Med, 2010. 51(6): p. 973-7.
21. Melis, M., et al., *Dynamic and static small-animal SPECT in rats for monitoring renal function after ¹⁷⁷Lu-labeled Tyr³-octreotate radionuclide therapy*. J Nucl Med, 2010. 51(12): p. 1962-8.
22. Slikkerveer, A. and F.A. de Wolff, *Pharmacokinetics and toxicity of bismuth compounds*. Med Toxicol Adverse Drug Exp, 1989. 4(5): p. 303-23.
23. McAfee, J.G., et al., *Biological distribution and excretion of DTPA labeled with Tc-99m and In-111*. J Nucl Med, 1979. 20(12): p. 1273-8.



Chapter 7

Summary and Concluding Remarks, Samenvatting

SUMMARY

Over the past decades ^{177}Lu -DOTA-Tyr³-octreotate (^{177}Lu -DOTATATE) has been applied to treat patients with metastatic neuroendocrine tumours (NETs) in our institute. Most favorable results have been obtained regarding anti-tumour responses and improved quality of life, complete cure in these patients is rarely reached however. Therefore, the search for better treatment for patients with metastasized NETs continues. The use of α -emitting radionuclides in targeted alpha therapy (TAT) has become very attractive, since α -emitting particles such as ^{213}Bi shows greater cytotoxic effects than β -emitting radionuclides. In this thesis we investigated ^{213}Bi -DOTATATE for applications in preclinical models, with the ultimate aim to improve TAT for patients suffering from metastatic NETs.

In **Chapter 1** of this thesis, a general introduction on NETs, the concept of targeted radionuclide imaging and radionuclide therapy, and TAT is given. Furthermore, in this chapter we have introduced the use of the α -emitter ^{213}Bi as a potential radionuclide for labelling of DOTATATE and application in TAT. General requirements and limitations of targeted radionuclide therapy for (pre)clinical applications are given in this chapter as well.

Due to the low radioactivity $^{225}\text{Ac}/^{213}\text{Bi}$ generator (< 222 MBq) available and used in our preclinical studies, adjustments of the labelling procedure were required to meet the criteria for preclinical studies, e.g. highly stable labelled peptide with high molar activity (MA). Furthermore, a small injection volume at physiological conditions is required in mice to maintain the homeostasis of the animal. Therefore, the labelling conditions of ^{213}Bi -DOTATATE were optimized in stepwise fashion as described in **Chapter 2** for preclinical applications. The optimized labelling procedure resulted in high incorporation yield, high radiochemical purity and high stability up to 2 hours after labelling. The addition of quenchers such as ascorbic acid during radiolabelling appeared to be essential for the protection of the peptide from radiolysis, since the absorbed dose rate within the reaction vial was high, > 165 mGy.s⁻¹ with 100 MBq of ^{213}Bi . However, at high concentrations ascorbic acid also appeared to be cytotoxic to the CA20948 cells, pancreatic rat carcinoma cells with high expression of somatostatin receptor subtype 2 (SSTR₂). The ascorbic acid concentration used for labelling was therefore optimized as well. An $^{225}\text{Ac}/^{213}\text{Bi}$ generator containing higher radioactivity is recommended to fully overcome the limitations encountered.

Investigations on pharmacokinetics and pharmacodynamics of ^{213}Bi -DOTATATE *in vivo* in mice were described in **Chapter 3**. The tumour model used was the rat pancreatic tumour cell line AR42J with well-characterized overexpression of SSTR₂. The optimal amount of peptide was determined in mice using ^{111}In -DOTATATE as a model radiopeptide to obtain biodistribution data and estimates of the radiation absorbed dose to the tumour and other organs. Tumour uptake appeared similar for ^{111}In -DOTATATE and ^{213}Bi -DOTATATE, but renal activity of ^{213}Bi -DOTATATE was significantly higher than that of ^{111}In -DOTATATE. The optimal amount of peptide injected was 0.3 nmol; this amount was therefore used for all

following *in vivo* studies. The calculated mean radiation absorbed dose was approximately 0.5 Gy/MBq for tumour. Next, the maximum tolerated dose (MTD) of ^{213}Bi -DOTATATE was determined. ^{213}Bi -labelled compounds tend to accumulate in the kidneys, resulting in a high radiation absorbed dose to the kidney and potential nephrotoxicity. In this study, the high renal uptake could be reduced with 50% by pretreatment with L-lysine, a renal protectant applied for peptide receptor radionuclide therapy. Acute radiation nephrotoxicity occurred at a mean renal radiation absorbed dose > 20 Gy (LD_{50}). A correlation was found between the amount of injected radioactivity and Neutrophil Gelatinase-Associated Lipocalin (NGAL) levels. The therapeutic potential of ^{213}Bi -DOTATATE was illustrated by significantly improved overall survival. Renal protection with L-lysine immediately prior to TAT with ^{213}Bi -DOTATATE prolonged survival. The MTD was found to be 22 MBq with L-lysine for renal protection and without L-lysine this was < 13 MBq.

As described elsewhere, α -emitters are thought to be mainly suitable for treatment of small tumour clusters and metastases. Reduction of larger tumour volumes was however also observed in patients after TAT with ^{213}Bi -DOTA-Tyr³-octreotide. In **Chapter 4** we compared the efficacy of ^{213}Bi -DOTATATE between large and small tumour volumes (50 and 200 mm³), for two different tumour models showing low and high SSTR₂ expression levels in mice; a rat pancreatic tumour (CA20948) and human small cell lung carcinoma (H69). The amount of radioactivity injected was below the MTD without L-lysine. Anti-tumour effects following TAT with ^{213}Bi -DOTATATE were observed in all tumour-bearing animals. The effects were more pronounced in H69 tumour-bearing animals; their survival rate was higher. The response to the therapy was similar for both tumour sizes with no significant differences observed, indicating that ^{213}Bi -DOTATATE was suitable for TAT in small and in larger tumours. Renal function was evaluated using *in vivo* SPECT imaging with $^{99\text{m}}\text{Tc}$ -DMSA; no renal dysfunction was observed after TAT in ^{213}Bi -DOTATATE-treated mice using the doses applied in this study.

In **Chapter 5**, cell survival assays were performed to compare the relative biological effect (RBE) *in vitro* of ^{213}Bi -ligand with that of the gold standard ^{137}Cs (external radiation) and ^{177}Lu -ligand. Two cell lines (CA20948, a rat pancreatic tumour and BON, a human carcinoma) with different radio-sensitivity and different expression levels of SSTR₂ were used. The radiation absorbed doses were calculated using a small-scale dosimetry model, this enabled comparison of different radiation types to determine the RBE. ^{111}In -DOTATATE was used to mimic the cellular uptake of ^{213}Bi -DOTATATE and ^{177}Lu -DOTATATE, since ^{111}In -DOTATATE, ^{213}Bi -DOTATATE and ^{177}Lu -DOTATATE have similar receptor affinities (in the low nM range) for SSTR₂. Survival curves of both cell lines after exposure to ^{137}Cs as function of dose fitted the linear quadratic model, showing the typical curvature for low LET irradiation. BON cells have very low expression of SSTR₂ and cellular uptake could therefore be neglected. ^{177}Lu -DTPA (^{177}Lu -diethylenetriaminepentaacetic acid) and ^{177}Lu -DOTATATE showed no effect on cellular survival with increased radioactivity in

these cells. In CA20948 cells on the other hand, with high expression of SSTR₂, no effect on survival was observed with increased amounts of ¹⁷⁷Lu-DTPA. However, survival decreased with increasing amounts of ¹⁷⁷Lu-DOTATATE. Linear exponential decline in cell survival was observed in both BON and CA20948 cells after exposure to increased activities of both ²¹³Bi-DTPA and ²¹³Bi-DOTATATE, indicating both the high LET nature of this exposure and the radiation absorbed dose from the incubation medium to be higher than the radiation absorbed dose from cellular uptake. Both ²¹³Bi-DTPA and ²¹³Bi-DOTATATE showed a 6-fold advantage in cell killing compared to ¹⁷⁷Lu-DOTATATE in CA20948 cells. The RBE of ²¹³Bi-ligand ranged from 1.5–2.0 compared to ¹³⁷Cs in both cell models.

In **Chapter 6**, the feasibility of ²¹³Bi imaging by Single Photon Emission Computed Tomography (SPECT) was investigated. ²¹³Bi emits γ -radiation of 440 keV that could be used to follow the pharmacokinetics of ²¹³Bi-DOTATATE *in vivo*. A phantom study was performed to determine the lowest detectable radioactivity concentration using a multiple pinhole small-animal SPECT camera, followed by imaging *in vivo* in mice as well as ex-vivo. A spatial resolution of 0.75 mm was obtained. In non tumour-bearing mice, ²¹³Bi-DTPA showed renal uptake and urinary clearance *in vivo*, allowing visualization of the renal excretion pathway from cortex to ureter to be visualized. In ex-vivo studies, tumour uptake of ²¹³Bi-DOTATATE could still be visualized at one hour post-mortem.

CONCLUDING REMARKS

α -Emitters offer enhanced possibilities to treat tumours, due to their high ionization energy deposition, resulting in high cell-killing abilities [1–4]. Therefore, the interest to use α -emitters for TAT is continuously growing. As discussed in this thesis and elsewhere, ²¹³Bi is a widely used α -emitter for preclinical research, due to the availability of an ²²⁵Ac/²¹³Bi generator. Confounding issues regarding ²¹³Bi include its short half-life of 45.9 min and the limited availability of the mother radionuclide ²²⁵Ac. Despite this relatively short half-life of ²¹³Bi, a reliable labelling protocol with DOTA-biomolecules could be successfully achieved, which can be easily transferred to clinical targeted therapy [5]. Furthermore, the limited availability of ²²⁵Ac may be overcome by the development of accelerator-driven production processes of ²²⁵Ac, this would enable unrestricted production of high activity ²²⁵Ac/²¹³Bi generators for preclinical (> 370 MBq) and clinical applications (> 2 GBq) [5–7]. The use of receptor antagonistic peptides could be another approach to obtain higher radioactivity delivered at the target, as several studies demonstrated higher tumour uptake could be achieved with antagonists compared to that obtained with a receptor agonistic peptide with similar receptor affinity [8–10].

Actinium-225 (²²⁵Ac) is a very attractive radionuclide for TAT because of its longer half-life and the emission of four α -particles in its decay and that of its four α -emitting daughters.

The challenge of working with ^{225}Ac is the recoil effect of the four daughters, which might lead to off-targeting when released from the chelator. Kratochwil et al. demonstrated that ^{225}Ac -PSMA-617 can be applied as salvage therapy for end-stage mCRPC patients. The tolerated dose was 100 kBq/kg and the treatment was safe and could be repeated with 8 weeks interval [11]. Concerns for late toxicity by ^{225}Ac -PSMA-617 prevent currently its use in an earlier phase of the disease. Besides ^{213}Bi and ^{225}Ac , Astatine-211 (^{211}At) is also considered to be an attractive radionuclide for TAT because of its 7.2 h half-life and the possibility to produce ^{211}At by a particle accelerator [12]. These radionuclides emit γ -rays with low abundance, like ^{213}Bi . Terbium-149 (^{149}Tb) is also highly appealing for radiotheranostic applications in future clinical applications, since ^{149}Tb is an α -emitter as well as a β^+ -emitter [3, 13].

Caution must be made for dosimetry calculation for α -emitters, since it is different from that for β or γ -radiation. Inhomogeneous activity distribution is often seen in targeted radionuclide therapy as not all tumour cells show equal receptor-density. Inhomogeneous activity distribution over the tumour cells in combination with the short path length of α -emitters leads to a wrong estimation of overall effects when using the macrodosimetric approach for TAT. Macrodosimetry assumes that all cells receive the same absorbed dose with the assumption of a uniform energy distribution over the target mass. Microdosimetry can also be used to determine the probability for radiation damage. Microdosimetry includes the absorbed specific energy deposited to the target mass and the stochastic effect at cellular level. It is, however, not possible to perform a full microdosimetry model for complete tumours and whole organs at risk. Small-scale dosimetry for representative geometries at the cellular level makes use of the same macrodosimetry concept and could serve as a bridge between macrodosimetry and microdosimetry [14]. Information from small-scale dosimetry might be used to correct the mean absorbed dose for α -emitters [14]. In general small-scale dosimetry models like MIRDcell can be used to estimate the cellular absorbed dose, which will resemble the total macroscopic dose in most therapeutic settings with high amounts of activity which is homogeneously distributed [15].

To summarize, in this thesis ^{213}Bi -DOTATATE showed therapeutic efficacy *in vitro* as well *in vivo* in mice with different tumour models as well as in tumours of different size, even in tumours with low SSTR₂ expression. An MTD of 22 MBq was found in mice corresponding to a renal LD₅₀ of 20 Gy. High renal uptake and α -particle induced toxicity could be managed by renal protectants [16], such as L-lysine. The relative biological effect of ^{213}Bi -DOTATATE was 6 times higher with than that of ^{177}Lu -DOTATATE *in vitro*, making ^{213}Bi -DOTATATE a suitable candidate radionuclide for treatment of patients with metastatic NETs in larger patient studies. However, the short half-life of ^{213}Bi makes the therapy logistically too demanding for routine clinical use; α -emitters with a longer half-life (like ^{225}Ac) are therefore considered to be more suitable for clinical applications.

SAMENVATTING

Sinds jaren wordt ^{177}Lu -DOTA-Tyr³-octreotate (^{177}Lu -DOTATATE) in ons ziekenhuis toegepast voor behandeling van patiënten met gemetastaseerde neuroendocriene tumoren (NET). Indrukwekkende anti-tumor resultaten zijn geboekt en de kwaliteit van leven wordt verbeterd in deze patiënten, maar totale genezing wordt helaas niet vaak bereikt. De zoektocht naar betere behandeling voor deze patiënten is daarom volop gaande. Het gebruik van α -emitters voor doelgerichte alfa-therapie (TAT) is zeer aantrekkelijk, omdat α -emitters, zoals bijvoorbeeld ^{213}Bi , meer cytotoxisch zijn dan β -emitters. In dit proefschrift beschrijven we de applicatie van ^{213}Bi -DOTATATE in preklinische modellen, dit onderzoek had als uiteindelijk doel om TAT veilig en effectief te kunnen toepassen voor behandeling van patiënten met gemetastaseerde NET.

In **Hoofdstuk 1** van dit proefschrift wordt een algemene introductie gegeven over NET en het concept van doelgerichte beeldvorming en therapie met behulp van radioactief gelabelde peptiden. Verder worden in dit hoofdstuk het gebruik van ^{213}Bi als potentieel radionuclide voor het labelen van DOTATATE en de toepassing van TAT geïntroduceerd. De algemene voorwaarden en beperkingen van doelgerichte alfa-radionuclidetherapie voor klinische en preklinische applicaties worden hierin ook behandeld.

Doordat er in ons onderzoek gebruikt is gemaakt van een laag actieve $^{225}\text{Ac}/^{213}\text{Bi}$ generator (< 222 MBq) voor preklinische doeleinden was het noodzakelijk om de labelingsprocedure van ^{213}Bi -DOTATATE aan te passen om onder andere een stabiel en met hoge specifieke activiteit gelabeld peptide te verkrijgen. Dit was nodig, omdat er met een klein injectievolumen gewerkt moet worden in de kleine proefdieren. In **Hoofdstuk 2** wordt de optimalisatie van de labelingsprocedure van ^{213}Bi -DOTATATE voor preklinische doeleinden beschreven, hierdoor was het mogelijk om ^{213}Bi -DOTATATE te labelen met een hoge incorporatie en een hoge radiochemische zuiverheid. Het product bleef stabiel gedurende meer dan 2 uur na labeling. Toevoeging van ascorbinezuur gedurende labeling bleek zeer essentieel te zijn om radiolyse te voorkomen, het absorbeerde dosistempo in de labeling was namelijk hoog: > 165 mGy.s⁻¹ bij 100 MBq ^{213}Bi . Een te hoge concentratie van ascorbinezuur bleek echter cytotoxisch voor CA20948 tumorcellen, een pancreas rat carcinoom met hoge expressie van de somatostatine receptor subtype 2 (SSTR₂). De toegevoegde hoeveelheid ascorbinezuur gedurende de labeling is daarop aangepast. Een $^{225}\text{Ac}/^{213}\text{Bi}$ generator met hogere radioactiviteit is echter sterk aan te raden om deze beperkingen te voorkomen.

Onderzoek betreffende de farmacokinetiek en farmacodynamiek van ^{213}Bi -DOTATATE *in vivo* is uiteengezet in **Hoofdstuk 3**. Als tumormodel werd gebruik gemaakt van AR42J tumorcellen, pancreas tumorcellen met een hoge SSTR₂ expressie. De peptidemassa-afhankelijke tumoropname in muizen werd bepaald met behulp van verschillende hoeveelheden ^{111}In -DOTATATE. Ook de biodistributie en de optimale geabsorbeerde dosis in tumoren en verschillende organen werd bestudeerd. De tumoropnames van ^{111}In -DOTATATE en

^{213}Bi -DOTATATE bleken goed vergelijkbaar, maar de nieropnames verschilden significant. De optimale hoeveelheid geïnjecteerd peptide bleek 0.3 nmol, deze hoeveelheid is daarom in alle verdere *in vivo* studies gebruikt. De berekende geabsorbeerde dosis in de tumor was circa 0.5 Gy/MBq. Daarnaast is de maximaal toelaatbare dosis (MTD) van ^{213}Bi -DOTATATE in de muizen bepaald. Het is bekend dat ^{213}Bi -complexen zich ophopen in de nieren, dit heeft een hoge nieropname met mogelijk ook nierschade tot gevolg. Uit deze studie bleek dat de nieropname kon worden verminderd tot 50% door pre-injectie van L-lysine, een nierbeschermers die meer wordt toegepast in klinische peptide-receptor-radionuclidetherapie. Acute nierschade trad op bij een gemiddelde nierdosis > 20 Gy. Een correlatie tussen de hoeveelheid geïnjecteerde radioactiviteit en de marker Neutrophil Gelatinase-Associated Lipocalin (NGAL) werd ook gevonden. ^{213}Bi -DOTATATE zorgde voor een betere overleving, het overlevingspercentage was nog hoger bij toediening van L-lysine voor aanvang van de therapie; een MTD van 22 MBq met L-lysine en < 13 MBq zonder L-lysine werd gevonden.

Zoals eerder beschreven, wordt algemeen verondersteld dat α -emitters voornamelijk geschikt zijn voor de behandeling van kleine tumorclusters en metastasen. In bepaalde klinische onderzoeken werd echter ook een afname van tumorgrootte waargenomen in patiënten met grote tumoren na ^{213}Bi -DOTA-Tyr³-octreotide therapie. **Hoofdstuk 4** beschrijft de effectiviteit van ^{213}Bi -DOTATATE in muizen met tumoren van verschillende grootte, namelijk 50 en 200 mm³, we maakten gebruik van twee verschillende tumormodellen met verschillende expressie van SSTR₂ (CA20948 en H69 cellen, de laatste zijn humane kleincellige longkankercellen). De geïnjecteerde activiteit van ^{213}Bi -DOTATATE was onder de MTD zonder L-lysine. In alle behandelde muizen werd een afname van tumorgrootte waargenomen. Sterkere anti-tumoreffecten werden waargenomen in H69-tumordragende muizen; de overlevingskans was ook hoger in deze dieren. Wat betreft de behandeling van dieren met verschillende tumorgrootte werden geen significante verschillen gevonden, ^{213}Bi -DOTATATE bleek dus geschikt voor behandeling van zowel grotere als kleine tumoren. De nierfunctie is onderzocht door middel van een $^{99\text{m}}\text{Tc}$ -DMSA-scan; geen nierafwijkingen werden waargenomen na therapie met de toegepaste hoeveelheid ^{213}Bi -DOTATATE. In **Hoofdstuk 5** is de bepaling van het relatieve biologische effect (RBE) van ^{213}Bi -ligand beschreven. Dit onderzoek is gedaan met behulp van kolonievormingsexperimenten met tumorcellen. De vorming van kolonies na externe bestraling van ^{137}Cs en na bestralen met ^{177}Lu -liganden of ^{213}Bi -liganden is met elkaar vergeleken. Twee cellijnen werden in dit experiment gebruikt; CA20948 cellen en BON cellen, deze laatste zijn humane carcinoïdcellen. Deze cellijnen verschillen met betrekking tot SSTR₂ expressie en stralingsgevoeligheid. De geabsorbeerde dosis in de cellen werd berekend met een microdosimetrisch model, hierdoor was het mogelijk om de RBE-waarden te bepalen na bestraling met verschillende bronnen en konden ze onderling vergeleken worden. ^{111}In -DOTATATE is gebruikt om de celopname van ^{177}Lu -DOTATATE en ^{213}Bi -DOTATATE te simuleren. Dit was mogelijk,

omdat ^{111}In -DOTATATE dezelfde affiniteit voor SSTR_2 heeft als ^{177}Lu -DOTATATE en ^{213}Bi -DOTATATE. De overlevingscurves na bestraling met ^{137}Cs verliepen volgens het lineair kwadratisch model bij toenemende bestralingsdosis, dit gold voor beide cellijnen. Het lineair kwadratisch model is typerend voor β - en γ -bestraling. Een lineaire afname van celoverleving werd waargenomen in beide cellijnen na het bestralen met toenemende hoeveelheden ^{213}Bi -DTPA of ^{213}Bi -DOTATATE. ^{213}Bi -DTPA en ^{213}Bi -DOTATATE waren 6x meer toxisch dan ^{177}Lu -DOTATATE in CA20948 cellen. De RBE verkregen na bestraling van ^{213}Bi -liganden varieerde van 1.5–2 in vergelijking met externe bestraling met ^{137}Cs in beide cellijnen.

In **Hoofdstuk 6** is het onderzoek naar ^{213}Bi beeldvorming door middel van Single Photon Emission Computed Tomography (SPECT) beschreven. ^{213}Bi zendt 440 keV γ -straling uit waarmee het mogelijk zou kunnen zijn de farmacokinetiek van ^{213}Bi -DOTATATE te volgen *in vivo* met behulp van SPECT. Klassieke fantoomstudies werden uitgevoerd om de laagst detecteerbare hoeveelheid radioactiviteit te bepalen met een pinhole SPECT camera geschikt voor kleine dieren, gevolgd door *in vivo* en *ex-vivo* beeldopnames in muizen. Een resolutie van 0.75 mm werd gevonden in de fantoomstudie; in muizen kon de nieropname en klaring van ^{213}Bi -DTPA goed waargenomen worden. In *ex-vivo* studies in dieren met een CA20948 tumor was de tumoropname van ^{213}Bi -DOTATATE een uur na euthanasie nog steeds waar te nemen.

REFERENCES

1. Jurcic, J.G., et al., *Radiolabeled anti-CD33 monoclonal antibody M195 for myeloid leukemias*. *Cancer Res*, 1995. 55(23 Suppl): p. 5908s-5910s.
2. Kratochwil, C., et al., *225Ac-PSMA-617 for PSMA-Targeted alpha-Radiation Therapy of Metastatic Castration-Resistant Prostate Cancer*. *J Nucl Med*, 2016. 57(12): p. 1941-1944.
3. Muller, C., et al., *A unique matched quadruplet of terbium radioisotopes for PET and SPECT and for alpha- and beta- radionuclide therapy: an in vivo proof-of-concept study with a new receptor-targeted folate derivative*. *J Nucl Med*, 2012. 53(12): p. 1951-9.
4. Andersson, H., et al., *Intraperitoneal alpha-particle radioimmunotherapy of ovarian cancer patients: pharmacokinetics and dosimetry of (211)At-MX35 F(ab')₂—a phase I study*. *J Nucl Med*, 2009. 50(7): p. 1153-60.
5. Kratochwil, C., et al., *(2)(1)(3)Bi-DOTATOC receptor-targeted alpha-radionuclide therapy induces remission in neuroendocrine tumours refractory to beta radiation: a first-in-human experience*. *Eur J Nucl Med Mol Imaging*, 2014. 41(11): p. 2106-19.
6. Apostolidis, C., et al., *Cyclotron production of Ac-225 for targeted alpha therapy*. *Appl Radiat Isot*, 2005. 62(3): p. 383-7.
7. Weidner, J.W., et al., *225Ac and 223Ra production via 800 MeV proton irradiation of natural thorium targets*. *Appl Radiat Isot*, 2012. 70(11): p. 2590-5.
8. Cescato, R., et al., *Evaluation of 177Lu-DOTA-sst2 antagonist versus 177Lu-DOTA-sst2 agonist binding in human cancers in vitro*. *J Nucl Med*, 2011. 52(12): p. 1886-90.
9. Nicolas, G.P., et al., *Biodistribution, pharmacokinetics and dosimetry of 177Lu-, 90Y- and 111In-labeled somatostatin receptor antagonist OPS201 in comparison to the agonist 177Lu-DOTA-TATE: the mass effect*. *J Nucl Med*, 2017.
10. Wild, D., et al., *Comparison of somatostatin receptor agonist and antagonist for peptide receptor radionuclide therapy: a pilot study*. *J Nucl Med*, 2014. 55(8): p. 1248-52.
11. Kratochwil, C., et al., *Targeted Alpha Therapy of mCRPC with 225Actinium-PSMA-617: Dosimetry estimate and empirical dose finding*. *J Nucl Med*, 2017.
12. Vaidyanathan, G. and M.R. Zalutsky, *Applications of 211At and 223Ra in targeted alpha-particle radiotherapy*. *Curr Radiopharm*, 2011. 4(4): p. 283-94.
13. Muller, C., et al., *Future prospects for SPECT imaging using the radiolanthanide terbium-155 - production and preclinical evaluation in tumor-bearing mice*. *Nucl Med Biol*, 2014. 41 Suppl: p. e58-65.
14. Roeske, J.C., et al., *Small-scale dosimetry: challenges and future directions*. *Semin Nucl Med*, 2008. 38(5): p. 367-83.
15. Vaziri, B., et al., *MIRD pamphlet No. 25: MIRDcell V2.0 software tool for dosimetric analysis of biologic response of multicellular populations*. *J Nucl Med*, 2014. 55(9): p. 1557-64.
16. Rolleman, E.J., et al., *Molecular imaging of reduced renal uptake of radiolabelled [DOTA⁰,Tyr³] octreotate by the combination of lysine and Gelofusine in rats*. *Nuklearmedizin*, 2008. 47(3): p. 110-5.

LIST OF PUBLICATIONS

***In vitro* comparison of ^{213}Bi - and ^{177}Lu -radiation for peptide receptor radionuclide therapy.**

Ho Sze Chan, Erik de Blois, Alfred Morgenstern, Frank Bruchertseifer, Marion de Jong, Wouter A. Breeman, Mark W. Konijnenberg

PLoS One. 2017 Jul 21;12(7)

Improved safety and efficacy of ^{213}Bi -DOTATATE-targeted alpha therapy of somatostatin receptor-expressing neuroendocrine tumors in mice pre-treated with L-lysine.

Ho Sze Chan, Mark W. Konijnenberg, Tamara Daniels, Monique Nysus, Mehran Makvandi, Erik de Blois, Wouter A. Breeman, Robert W. Atcher, Marion de Jong and Jeffrey P. Norenberg

EJNMMI Res, 2016, 6:83

Optimizing labelling conditions of ^{213}Bi -DOTATATE for preclinical applications of peptide receptor targeted alpha therapy.

Ho Sze Chan, Erik de Blois, Mark W. Konijnenberg, Alfred Morgenstern, Frank Bruchertseifer, Jeffrey P. Norenberg, Fred J. Verzijlbergen, Marion de Jong, Wouter A. Breeman

EJNMMI Radiopharmacy and Chemistry, May 2016, 1:9

Influence of tumour size on the efficacy of targeted alpha therapy with ^{213}Bi -[DOTA⁰,Tyr³]-octreotate.

Ho Sze Chan, Mark W. Konijnenberg, Erik de Blois, Stuart Koelewijn, Richard P. Baum, Alfred Morgenstern, Frank Bruchertseifer, Wouter A. Breeman, Marion de Jong

EJNMMI Res, January 2016, 6:6

Utilizing high-energy gamma photons for high-resolution ^{213}Bi SPECT in mice.

Jan de Swart, **Ho Sze Chan**, Marlies C Goorden, Alfred Morgenstern, Frank Bruchertseifer, Freek J Beekman, Marion de Jong, Mark Konijnenberg

JNM. 2016; 57, 3, 486–492

Alternative method to determine Specific Activity of (^{177}Lu) by HPLC.

Breeman W.A., de Zanger R.M., **Chan H.S.**, de Blois E

Curr Top Med Chem. 2015; 8(2):119–22

Therapeutic application of CCK2R-targeting PP-F11: Influence of particle range, activity and peptide amount.

M.W.Konijnenberg, W.A.P.Breeman, E.de Blois, **H.S.Chan**, O.C. Boerman, P.Laverman, P.Kolenc-Peitzl, M.Melis, M.de Jong

EJNMMI Res 2014 Dec 30;4(1):47

Application of single-vial ready-for-use formulation of ^{111}In - or ^{177}Lu -labelled somatostatin analogs.

De Blois E, Chan H.S., de Zanger R., Konijnenberg M., Breeman W.A.
Appl Radiat Isot. 2014 Feb;85:28–33

Determination of peptide content and purity of DOTA-peptides by metal ion titration and UPLC: an alternative method to monitor quality of DOTA-peptides.

W.A.P.Breeman, H.S.Chan, E. de Blois
Journal of Radioanalytical and Nuclear Chemistry, 2014, 302:825–830

Effectiveness of quenchers to reduce radiolysis of (111)In- or (177)Lu-labelled methionine-containing regulatory peptides. Maintaining radiochemical purity as measured by HPLC.

de Blois E, Chan HS, Konijnenberg M, de Zanger R, Breeman WA.
Curr Top Med Chem. 2012;12(23):2677–85

Iodination and stability of somatostatin analogues: comparison of iodination techniques. A practical overview.

de Blois E, Chan HS, Breeman WA.
Curr Top Med Chem. 2012;12(23):2668–76

(68)Ga-labeled DOTA-peptides and (68)Ga-labeled radiopharmaceuticals for positron emission tomography: current status of research, clinical applications, and future perspectives.

Breeman WA, de Blois E, Sze Chan H, Konijnenberg M, Kwekkeboom DJ, Krenning EP.
Semin Nucl Med. 2011 Jul;41(4):314–21

Reduction of ^{68}Ge activity containing liquid waste from ^{68}Ga PET chemistry in nuclear medicine and radiopharmacy by solidification.

Erik de Blois, Ho Sze Chan, Kamalika Roy, Eric P. Krenning and Wouter A. P. Breeman
J Radioanal Nucl Chem. 2011; 288(1): 303–306

Characteristics of SnO_2 -based $^{68}\text{Ge}/^{68}\text{Ga}$ generator and aspects of radiolabelling DOTA-peptides.

de Blois E, Sze Chan H, Naidoo C, Prince D, Krenning EP, Breeman WA.
Appl Radiat Isot. 2011 Feb;69(2):308–15

PhD PORTFOLIO

Summary of PhD training and teaching

Erasmus MC Department:	Department of Radiology and Nuclear Medicine
Promotor:	Prof.dr. M. de Jong
Co-promotors:	Dr. W.A.P. Breeman Dr. M.W. Konijnenberg

Courses and training	Year	ECTS
Biomedical English Writing and Communication	2014	0.5
Research Integrity	2014	0.3
Laboratory animal science (art.9)	2012	3.0
Health physics level 3	2011	5.3
Translational Imaging	2011	1.1
Excel Basic	2014	0.3
Excel Advanced	2014	0.3
Molecular Medicine	2014	0.7
Attendance to (Inter)national conferences		
7th Symposium on Targeted alpha therapy, Germany	2011	0.9
MINI-SYMPOSIUM 25 years of Radiopeptide Research at the Department of Nuclear Medicine (ErasmusMC)	2011	0.3
NKRV (Delft)	2012	0.3
SNM, St Louis, USA	2014	1.25
EANM, Gothenburg, Sweden	2014	1.25
9th Symposium on Targeted alpha therapy, Poland	2015	0.9
ISRS, Missouri, USA	2015	1.25
SNM, Baltimore, USA	2015	1.25
EANM, Hamburg, Germany	2015	1.25
Teaching activities		
Supervising trainees	2011–2015	10
Journal clubs Nuclear Medicine	2013	0.3
Invited lectures		
NKRV (Delft, The Netherlands)	2016	0.3
Freiburg University (Freiburg, Germany)	2016	0.3
Basel University (Basel, Switzerland)	2016	0.3
Total		31.35

Courses and training

Presentations/Posters at national/international congresses

SNM 2014, June, St Louis, USA (3 poster presentations)

EANM 2014, October, Gothenburg, Sweden (2 oral presentations)

ISRS 2015, May, Missouri, USA (1 oral presentation)

TAT 2015, May, Warsaw, Poland (1 oral presentation and 2 poster presentations)

SNM 2015, June, Baltimore, USA (1 oral presentation)

EANM 2015, October, Hamburg, Germany (1 oral presentation)

ACKNOWLEDGEMENTS

It has been a long and stressful journey with its fair share of ups and downs, long hours and late nights. Nevertheless, it has been wonderful and lots of fun with experiences and opportunities for personal development. I would like to take this opportunity to thank everyone for their help and support.

First of all, I would like to thank my promotor Prof. dr. Marion de Jong and my co-promotors Dr. Wouter Breeman and Dr. Mark Konijnenberg for their amazing support and effort; thank you for believing in me.

Dear Wout, thank you so much for everything. Without you, I would not be standing here in the first place. You have always been really patient with me and encouraged me to continue my career in science. You are someone who I can always rely on to discuss work and personal matters. You have taught me so much, ranging from radiochemistry to your passions in life such as: nature (Africa & India), birds (although for me a bird is still a bird), good wines and off course my favorite, food. You will always be someone I look up to.

Dear Mark, thank you for all the time you spent to help me with data analysis and discussions relating to my research. It is always wonderful to talk to you about the planning and set up of the experiments, because we share lots of similar perspectives about certain subjects. You taught me about dosimetry and I apologize for all the headaches I gave you. You also gave me the opportunity to explore science outside the academic world, for which I am very thankful. Because of that I was able to experience life in Schoorl and meet your lovely family. Thank you for always being so nice to me Mark.

Dear Marion, thank you for the opportunity to be part of this project and your advise with writing and presentations. You always work hard, stand up for all PhD students and help them find their way. Besides being a great scientist, you are a caring and understanding person. I enjoyed the conversations we had, and thank you for sharing your personal and scientific experiences with me. Thank you so much Marion, I really appreciate it all.

Dear Jan van Overeem and Phillipe van Overeem from IDB Holland bv, thank you so much for your support, advice and opportunity you provided me to be able to perform my studies. The little time we spent together is precious to me. Dear Jan, you are missed.

Special thanks to Prof. dr. Jeffrey Norenberg and his amazing group (UNM, New Mexico), for the opportunity to perform part of my research there and also for the introduction of green chiles. Dear Jeff, Tamara, Monique, Chelsea, Dr. Robert Atcher, Jay and students, thank you, I had a great time in Albuquerque. The crazy and productive hours I spent in the lab were lots of fun and a joyful experience. I would also like to thank Jim, Piccolo, Shelby, Alaina, Ryan, Kelli, Terry, Mercedes and Mom (Jennifer) for your wonderful friendship and for showing me around in Albuquerque. God bless you all.

Dear Dr. Alfred Morgenstern and Dr. Frank Bruchertseifer, thank you so much for the great collaboration and your guidance to work with ²¹³Bismuth. I had a great time in Karlsruhe and enjoyed watching soccer with you.

I would like to thank the former department heads of Nuclear Medicine Prof. dr. Eric Krenning and Prof. dr. Fred Verzijlbergen, as well as the current head of the department Radiology and Nuclear Medicine Prof. dr. Gabriel Krestin for their support of this project.

Dear Prof. dr. Fred Verzijlbergen, next to your already busy schedule, you always found the time to help me with my PhD process. You have no idea how grateful I am for your support.

I would also like to thank all my colleagues of department of Radiology and Nuclear Medicine.

To Prof. dr. Leo Hofland and Peter van Koetsveld, thank you for your expertise, knowledge and help in cell biology.

Dear Lieneke, Marieke, Nicolette, Big Foot, Peter, Toon (MetorX), Emar, Sarai, Asha, Ronald, Tuki, Paul and Ambroos, thank you for always being so nice and supportive to me in many ways. I really appreciate your friendship.

To Marcel, Monique, Marleen, Gaby, Jan, ex-colleagues; Harald, Linda, Saskia, Stuart and other (former) PhD students (Sandra, Sander, Joost, Ingrid, Costanza, Kristell, Simone, Tessa, Wouter and Hendrik), thank you for your mental support. I really enjoyed the conversations and the laughter we had.

Dear Stuart, thank you for helping me out with the animal studies and your artistic talent which you can find on the cover of this thesis. Beside of your great work, I am also grateful for your friendship.

To all my students (John, Ries, Jolanda, Martin, Jim, Shing Fei, Eugenie) and other former interns (Madi, Gabrielle, Louann, Martijn, Eldert and Jeffrey), thank you all for your hard work in support of me.

Dear Linda, I'm grateful that we have been friends since HRO, I finally made it, yeah.

My special thanks to my paranymphs/bodyguards; Erik and Rory. Dear Erik, besides being a colleague, you are one of my best buddies. You have been really supportive in many ways. I will still call and bother you in the future, just like I always do :). Zo makkelijk kom je niet van mij af. Dear Rory, my teddy bear. You are one of the sweetest people I know, you are always so thoughtful and I am really grateful to know you. No matter where I go, we will keep in touch.

To all my dear friends over the world, I love you guys. Your friendship and support is precious to me.

At last and but certainly not the least I want to take this opportunity to thank my lovely family Chan and family Leung for all their support and love.

To my parents: Pa and Ma, you are the best parents in the world. Your love and support are unlimited and unconditional. Suk Sze, my only big sis, I am very grateful to have a big sis like you. No matter what choices I make in life, you guys are my number one support. Pa, ma and Suki, I love you with all my heart. And I would like take this great opportunity to say: THANK YOU XOXO.

CURRICULUM VITAE

Ho Sze was born on 27 April 1982 in Hong Kong. She moved with her family to the Netherlands at the age of 9 and stayed there for 2 years. At the age of 11, the family decided to move to the happy island of Aruba, where she graduated in 2002 from high school at Colegio Arubano. Afterwards the family moved to the Netherlands again, where she studied Analytical and Physical Chemistry at Hogeschool Rotterdam. During this period Ho Sze started her first internship at the department of Nuclear Medicine at Erasmus MC in Rotterdam, she focused on certain aspects of radiochemistry, her second internship was at the department of Biocatalyse and Organic Chemistry at Technical University of Delft. After obtaining her bachelor degree in science in 2006, she studied at University of Leiden in the track Physical of and Theoretical Chemistry. During her master degree, Ho Sze started her major internship at the department of Soft Advanced Matter at the University of Leiden. For her minor internship, she went back to the department of Nuclear Medicine at Erasmus MC. After she obtained her Master Degree in 2010, she started her PhD research project focusing on targeted alpha therapy for neuroendocrine tumours at the department of Radiology and Nuclear Medicine at Erasmus MC, Rotterdam, under supervision of Prof. dr. M. de Jong, Dr. W.A.P. Breeman and Dr. M.W. Konijnenberg. During this period, she travelled several times to Albuquerque, the United States, to the department of Radiopharmaceutical Sciences Program College of Pharmacy at the University of New Mexico Health Sciences Center, under supervision of Prof. Pharm.D. dr. J.P. Norenberg, to perform part of her research there. The research performed during the complete research period is presented in this thesis.

